Crystal Plasticity Modelling
of Large Strain Deformation in Single Crystals
# of Magnesium

by

Adel Izadbakhsh

A thesis

presented to the University of Waterloo

in fulfillment of the

thesis requirement for the degree of

Doctor of Philosophy

in

Mechanical Engineering

Waterloo, Ontario, Canada, 2010

Author's Declaration

I hereby declare that I am the sole author of this thesis. This is a true copy of the thesis, including any required final revisions, as accepted by my examiners.

I understand that my thesis may be made electronically available to the public.

Adel Izadbakhsh

Abstract

Magnesium, with a Hexagonal Close-Packed (HCP) structure, is the eighth most abundant element in the earth's crust and the third most plentiful element dissolved in the seawater. Magnesium alloys exhibit the attractive characteristics of low densities and high strength-to-weight ratios along with good castability, recyclability, and machinability.

Replacing the steel and/or aluminum sheet parts with magnesium sheet parts in vehicles is a great way of reducing the vehicles weight, which results in great savings on fuel consumption. The lack of magnesium sheet components in vehicle assemblies is due to magnesium's poor room-temperature formability. In order to successfully form the sheets of magnesium at room temperature, it is necessary to understand the formability of magnesium at room temperature controlled by various plastic deformation mechanisms.

The plastic deformation mechanisms in pure magnesium and some of its alloys at room temperature are crystallographic slip and deformation twinning. The slip systems in magnesium at room temperature are classified into primary (first generation), secondary (second generation), and tertiary (third generation) slip systems. The twinning systems in magnesium at room temperature are classified into primary (first generation) and secondary (second generation, or double) twinning systems. A new comprehensive rate-dependent elastic-viscoplastic Crystal Plasticity Constitutive Model (CPCM) that accounts for all these plastic deformation mechanisms in magnesium was proposed. The proposed model individually simulates slip-induced shear in the parent as well as in the primary and secondary twinned regions, and twinning-induced shear in the primary and secondary twinned regions. The model also tracks the texture evolution in the parent, primary and secondary twinned regions. Separate resistance evolution functions for the primary, secondary, and tertiary slip systems, as well as primary and secondary twinning systems were considered in the formulation. In the resistance evolution functions, the interactions between various slip and twinning systems were accounted for.

The CPCM was calibrated using the experimental data reported in the literature for pure magnesium single crystals at room temperature, but needs further experimental data for full calibration. The partially calibrated model was used to assess the contributions of various plastic deformation mechanisms in the material stress-strain response. The results showed that neglecting secondary slip and secondary twinning while simulating plastic deformation of magnesium alloys by crystal plasticity approach can lead to erroneous results. This indicates that all the plastic deformation mechanisms have to be accounted for when modelling the plastic deformation in magnesium alloys.

Also, the CPCM in conjunction with the Marciniak–Kuczynski (M–K) framework were used to assess the formability of a magnesium single crystal sheet at room temperature by predicting the Forming

Limit Diagrams (FLDs). Sheet necking was initiated from an initial imperfection in terms of a narrow band. A homogeneous deformation field was assumed inside and outside the band, and conditions of compatibility and equilibrium were enforced across the band interfaces. Thus, the CPCM only needs to be applied to two regions, one inside and one outside the band. The FLDs were simulated under two conditions: a) the plastic deformation mechanisms are primary slip systems alone, and b) the plastic deformation mechanisms are primary slip and primary twinning systems. The FLDs were computed for two grain orientations. In the first orientation, primary extension twinning systems had favourable orientation for activation. In the second orientation, primary contraction twinning systems had favourable orientation for activation. The effects of shear strain outside the necking band, rate sensitivity, and c/a ratio on the simulated FLDs in the two grain orientations were individually explored.

Acknowledgments

I would like to especially thank my supervisors professor Kaan Inal and professor Sanjeev Bedi, for granting me the opportunity to work on this fantastic project.

The constant support of my family members (Saki, Abbas, Ali, Elham, and Emad) has been a key element in keeping me inspired throughout my PhD program, and I am extremely grateful for that. I also thank Nasi for being a very kind friend.

Many people have been helpful in various ways toward the accomplishment of this work, and I would like to name some of them (in alphabetical order): Hossein Ahari, professor Aria Alasty, Rajnish Bassi, Dragos Besliu, Dr. Glen Chabi, Morteza Dashtizadeh, Hamidreza Faramarzi, Houshang Haji Hassanpour, Dr. Ramin Khorasany, Mohsen Morshedi, Saeid Rostami Bookani, and Gerardo Salas.

To Saki, Abbas, Ali, Elham, Emad, and Nasi with plenty of love

Table of Contents

List of Figures

List of Tables

Nomenclature

s	Slip or twinning system shear direction
m	Slip or twinning system plane normal
F	Total deformation gradient
F^*	Elastic part of the deformation gradient
F^p	Plastic part of the deformation gradient
F^{tw1}	Deformation gradient associated with a primary twinning system [50-52]
F^{tw2}	Deformation gradient associated with a secondary twinning system [50-52]
σ	Cauchy stress
$\overset{\triangledown}{\sigma}{}^*$	Lattice Jaumann rate of Cauchy stress
$\overset{\triangledown}{\sigma}$	Material Jaumann rate of Cauchy stress
$\overset{\circ}{C}$	Elastic moduli
L	Velocity gradient
L^p	Plastic part of the velocity gradient
L^*	Elastic part of the velocity gradient
D	Strain rate
D^p	Plastic part of the strain rate
D^*	Elastic part of the strain rate
Ω	Spin
Ω^p	Plastic part of the spin

Ω^{*}	Elastic part of the spin
$\varphi_1, \varphi, \varphi_2$	Bunge angles [59]
γ	Shear strain on the slip systems
f	Volume fraction of the twinning systems
g	Resistance of slip or twinning systems
H	Thickness of the sheet outside or inside the groove
ψ	Groove angle
t	Time
c_1, c_2, c_3	Constant parameters

Superscripts and subscripts:

p	Plastic part
$*$	Elastic part
αp	Primary slip system
αs	Secondary slip system
αt	Tertiary slip system
βp	Primary twinning system
βs	Secondary twinning system
mat	Parent (matrix) region
$tw1$	Primary twinned region
$tw2$	Secondary twinned region
ip	This parameter represents 1 and 2, representing outside and inside the band regions in the FLD calculations, respectively; e.g. $\gamma_{(n)}^{(ip)\alpha} = \gamma_{(n)}^{(1)\alpha}$ and $\gamma_{(n)}^{(2)\alpha}$
n	Time step

Chapter 1

Introduction and contributions

1.1 Introduction

Magnesium, with a Hexagonal Close-Packed (HCP) structure presented in Figure 1-1, is the eighth most abundant element in the earth's crust and the third most plentiful element dissolved in the seawater [1].
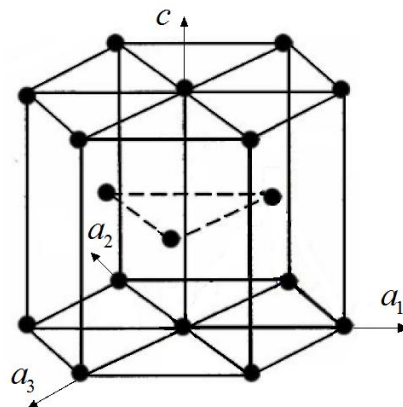
Figure 1-1 An HCP unit cell

The four-index Miller-Bravais coordinate system $\{a_1, a_2, a_3, c\}$, shown in Figure 1-1, is the most convenient way to present the orientations in an HCP structure. The angle between the three axes a_1, a_2, and a_3 is $120°$ (i.e. $a_1 + a_2 + a_3 = 0$), and the c-axis is perpendicular to all of them. For numerical

computation, however, an orthonormal coordinate system (Miller coordinate system) is required (transformation between the Miller-Bravais and Miller coordinate systems is outlined in Appendix C). The c/a ratio in pure magnesium is 1.624 which is close to the ratio in an ideal HCP structure (c/a=1.633) [2]. A thorough crystallography of HCP metals is discussed in [2].

The plastic deformation mechanisms in magnesium are crystallographic slip and deformation twinning. Crystallographic slip is caused by the movement of atoms with respect to one another, on certain planes of material in certain directions. With deformation twinning, the lattice orientation of a part of the material changes with respect to a plane in the material called *twinning plane*. This process is illustrated in Figure 1-2 [3]. As shown in this figure, after shear is applied to the lattice of the material in the noted direction, atoms on plane 1 undergo a certain shear with respect to the atoms on plane 0, atoms on plane 2 undergo the same amount of shear with respect to the atoms on plane 1, atoms on plane 3 with respect to the atoms on plane 2, etc. The result is the reproduction of the lattice with a new orientation, which is the mirror image of the lattice in the untwinned part of the material.
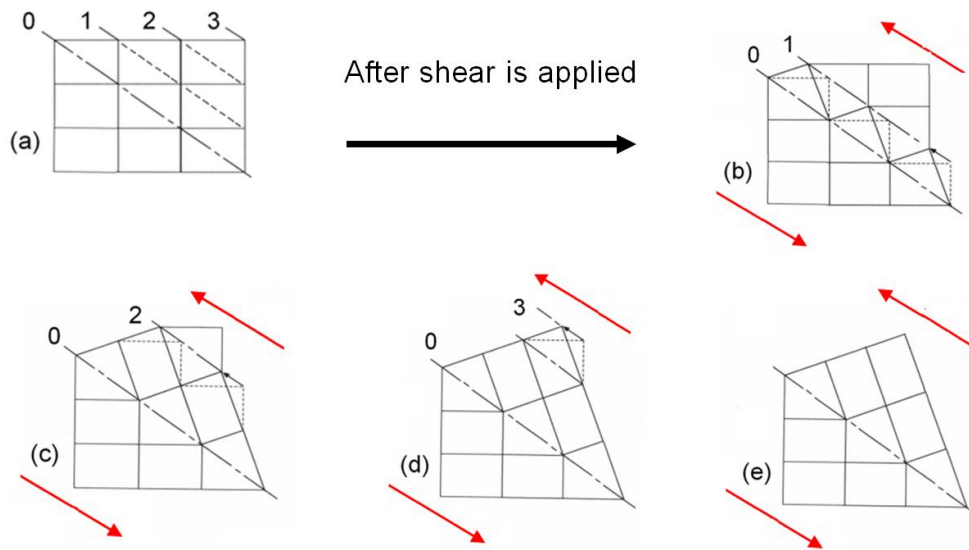
Figure 1-2 The deformation twinning process [3]

The important differences between the crystallographic slip and deformation twinning are as follows [3]:

1. With crystallographic slip, the amount of shear displacement is an integral number of the interatomic repeat distance of the material (i.e. an integer number multiplied by the length of the slip dislocation burger vector) whereas with deformation twinning it is a fraction of the interatomic repeat distance.

2. Slip occurs on a few parallel planes of the material, but in twinning shear occurs on every successive layer of the material.

3. Twinning is polar; meaning on a twinning plane deformation can happen in one direction only. This limitation does not exist in the case of slip, where on a slip plane shear can happen in two opposite directions.

4. While deformation twinning changes the lattice orientation of the material abruptly, the change in the lattice orientation of the material caused by slip is gradual.
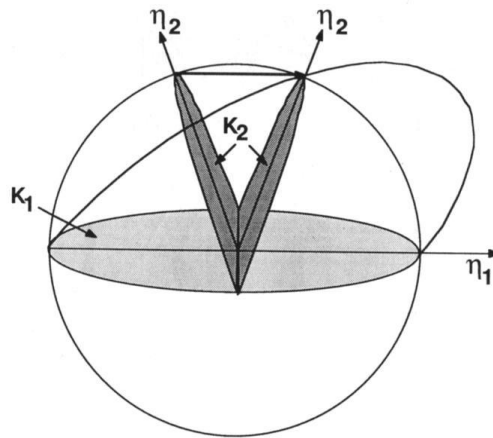
Figure 1-3 A sphere of a material with the top part of it twinned [3]

Figure 1-3 shows a sphere of a material where the top part of it undergone twinning. In this figure, K_1 is the twinning plane (the lattice in the twinned region is the mirror image of the lattice in the untwinned region with respect to this plane) which remains undistorted during deformation twinning. K_2 is another plane in the material that remains undistorted during deformation twinning. η_1 is the direction of twinning shear. η_2 lies in the K_2 plane and is perpendicular to the intersection of the K_1 and K_2 planes. Twinning systems are classified into type I, type II, and compound twins [3-5]. In type I twins, the lattice of the twinned region results from rotation of the parent lattice by $180°$ around the normal to the K_1 plane. In type II twins, the lattice of the twinned region results from rotation of the parent lattice around η_1. In FCC and BCC crystals all four twinning elements K_1, K_2, η_1, and η_2 are rational, however, in HCP crystals some of the twinning elements might be irrational [3]. The type I twins in which all the four twinning elements are rational are called compound twins. The twinning systems for magnesium reported in Table C-1 in Appendix C are compound twins [6].

Some important planes in magnesium are presented in Figure 1-4 (more details are available in [1,2]).
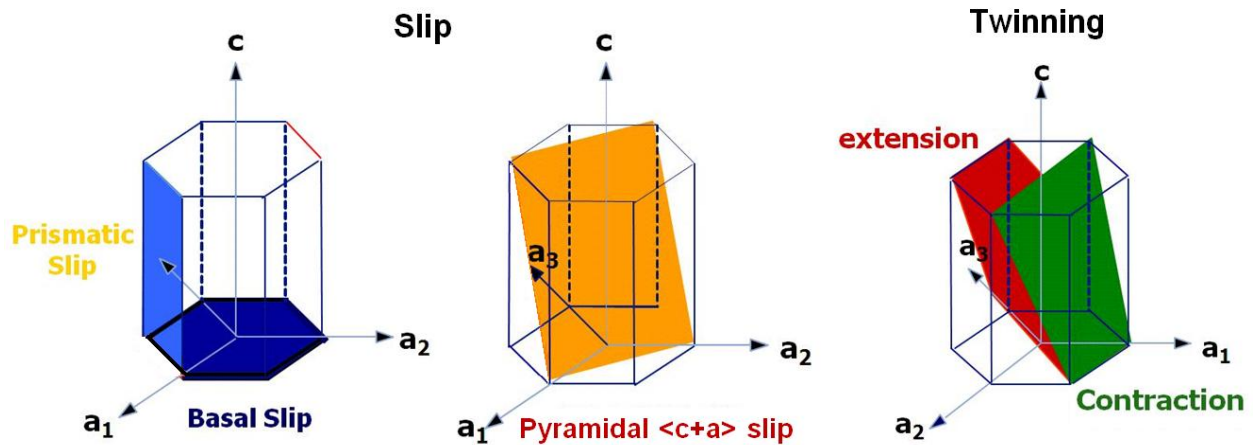
Figure 1-4 Some important planes in magnesium at room temperature [1,2]

Based on the Von Mises criterion [7,8], activity of five independent plastic deformation mechanisms were required to accommodate an arbitrary plastic deformation in a given material. Basal, prismatic, and pyramidal $\langle a \rangle$ slip systems provide four independent plastic deformation mechanisms. Pyramidal $\langle c+a \rangle$ slip system, which can be the fifth independent plastic deformation mechanism, is difficult to activate at room temperature, since it has a high Critical Resolved Shear Stress (CRSS) [9,10]. At room temperature, deformation twinning has a lower CRSS than the pyramidal $\langle c+a \rangle$ slip system, and it can provide the fifth independent plastic deformation mechanism to satisfy the Von Mises criterion. At elevated temperature, the CRSS of pyramidal $\langle c+a \rangle$ slip and other non-basal slip systems decreases [11], and they can provide the fifth independent plastic deformation mechanism.

Magnesium alloys exhibit the attractive combination of low densities (e.g. the lowest density of structural materials) and high strength-to-weight ratios as well as good castability, recyclability, and machinability [12,13]. Due to high fuel prices, automotive companies are investigating new light metal alloys and among the most promising are various magnesium alloys. Replacing the steel and/or aluminum sheet parts with magnesium sheet parts in vehicles is a great way of reducing vehicle weight if it can be cost-competitive. The lack of magnesium sheet components in vehicle assemblies is due to magnesium's poor room-temperature formability [13,14]. In order to successfully form the sheets of magnesium at room temperature it is necessary to understand the formability of magnesium alloys at room temperature controlled by various plastic deformation mechanisms.

Due to the complicated behaviour of plastic deformation mechanisms in magnesium at room temperature, which is a function of initial texture and strain rate, the macroscopic plastic behaviour of magnesium and its alloys is quite anisotropic. As a result, researchers were not able to capture this behaviour by phenomenological continuum plasticity models with great success. Therefore, developing a physics-based model such as crystal plasticity that can consider the crystallographic slip and deformation twinning as the deformation mechanisms, as well as material initial texture and its evolution is inevitable.

The plastic deformation mechanisms in pure magnesium [15,16] and some of its alloys [16-19] at room temperature are crystallographic slip and deformation twinning. The slip systems are classified into primary (first generation), secondary (second generation), and tertiary (third generation) slip systems. The twinning systems are classified into primary (first generation) and secondary (second generation, or double) twinning systems. Here a primary slip system refers to a slip system that is active inside an untwinned region of the grain (parent grain or matrix). A primary twinned region lies inside the matrix. A secondary slip system is active inside a primary twinned region. A secondary twinned region lies inside a primary twinned region. A tertiary slip system is active inside a secondary twinned region. Jiang et al. [17,18] reported an average volume fraction of nearly 50% for the combined volume fraction of the primary contraction and double twins during uniaxial tension experiments on the extruded AM30 tubes at room temperature at a loading rate of 0.1/s. For the extruded AZ31 tubes under the same loading condition this average volume fraction was reported to be 24%. This suggests that the contribution of the additional shear from these twinning systems in the macroscopic plastic strain of the loaded specimen must be accounted when modelling the plastic deformation of magnesium. The inclusion of primary and secondary twinning systems in a model necessitates the inclusion of secondary and tertiary slip systems, especially for large deformation simulations. There is a requirement to develop models to account for all the intragranular plastic deformation mechanisms in magnesium, and this thesis describes a comprehensive model to capture these deformation mechanisms.

1.2 Literature review

Here, the main models in the literature that have considered both crystallographic slip and deformation twinning for simulating the plastic deformation in metals are presented. All of them treat the deformation twinning as a pseudo-slip deformation mechanism, meaning if γ_t, f, and γ_{tw} are the shear strain, volume fraction, and specific shear strain (Appendix D) associated with a twinning system, respectively, then $\gamma_t = f \cdot \gamma_{tw}$ (more details in [20]). Explanation of the models are as follows:

a) Predominant twin reorientation (PTR) method with Taylor [8] assumptions: this method was proposed by Van Houtte [20], and was then improved by Tomé et al. [21]. The growth of the volume

fractions of the twinned regions is carefully tracked in each grain, however, using a statistical criterion (based on the volume fraction of the twinned regions in the grain and entire polycrystal aggregate) the entire grain is reoriented into a dominant twin orientation, and the orientations of the twinned regions are not changed at the end of each simulation time step. The total number of grain orientations remains constant, and from the computational point of view this is a major advantage. Two major weaknesses were pointed out by Kalidindi for this method [22]. First, for the statistical criterion to be meaningful a large number of grain orientations are required. Second, the grain is re-oriented based on the increments of the volume fractions of the twinned regions in a given time-step, independent of the previous deformation history, and therefore the orientation at which a grain may be twinned may not be the most dominant one. In this method, primary and secondary slip systems, as well as primary twinning systems were considered as the plastic deformation mechanisms.

b) Volume fraction transfer (VFT) scheme with Taylor [8] assumptions: this approach was proposed by Tomé et al. [21], to overcome the second limitation of van Houtte's approach [20] mentioned above. It employs weighted grain orientations to work around the problem of tracking the large number of new orientations created by deformation twinning [22]. In this scheme, the twinned parts of the grains are re-oriented at the end of each time step. Weighted grain orientations are used in the model, and by suitably modifying them, the orientation changes caused by deformation twinning were computed (more details were available in [22]). The plastic deformation mechanisms considered in this method were primary and secondary slip systems as well as primary twinning systems.

c) Total Lagrangian approach with Taylor [8] assumptions: there is a fundamental drawback to both models a and b. In these two models, the twinned regions are treated as new grains which can undergo further slip and twinning similar to an untwinned grain. It is well-known that the deformation characteristics of the twinned regions are not similar to the untwinned grains [22]. Kalidindi [22] proposed a model to address this shortcoming. He modified the available rate-dependent Crystal Plasticity Constitutive Model (CPCM) that was formulated for materials that exhibit only crystallographic slip to consider deformation twinning [23]. In this work deformation twinning is included as an additional mode of deformation into the evolution equation of the plastic part of the deformation gradient. An advantage of this method is that it allows the deployment of the crystal plasticity theory with deformation twinning while taking full advantage of an efficient fully implicit time integration scheme that was previously developed [23]. The difficultly of using this formulation is determining the resistance evolution functions for various plastic deformation mechanisms from the experimental data for a given material. In this model, only primary slip and primary twinning systems were considered as the plastic deformation mechanisms.

Salem et al. [24] employed this crystal plasticity framework with separate resistance evolution functions for primary slip and primary twinning systems to simulate the plastic deformation in $\alpha -$ Titanium which deforms predominantly by twinning up to a compressive strain of 0.3 and by slip and twinning in the fragmented grain structure at higher strains. The model captured the plastic deformation behaviour of $\alpha -$ Titanium quite well. This model was still further improved by Wu et al. [25] who considered secondary slip (with same resistance functions as primary slip) and introduced a grain fragmentation technique to improve the accuracy of the simulation of $\alpha -$ Titanium. In these models, the lattice orientations in the matrix and primary twinned regions can be tracked throughout the deformation, although with the deployed computational procedure this is not necessary at each simulation time step. The integration was carried out between the initial undeformed and final deformed configurations (total Lagrangian approach).

d) Crystal plasticity constitutive model implemented in a finite element code: Staroselsky and Anand [26] proposed a rate-independent CPCM incorporated in a User-defined MATerial subroutine (VUMAT) in ABAQUS/Explicit [27] finite element software to simulate the plastic deformation of the AZ31B magnesium alloy. In their CPCM the resistances of the primary slip and primary twinning systems were constant. They modified the evolution of the plastic part of the deformation gradient to approximately account for the grain-boundary sliding effect reported by Hauser et al. [28]. They employed Van Houtte's method (PTR) [20] to account for the twinning shear as well as the lattice reorientation due to twinning deformation. The prediction of the macroscopic stress-strain curves for the AZ31B by this model in some loading paths was not satisfactory when compared with the experimental data [26].

e) Updated Lagrangian approach with Taylor [8] assumptions: Lévesque et al. [29] proposed a rate-dependent CPCM for the AM30 magnesium alloy. They modified the CPCM of Peirce et al. [30] proposed for the materials that undergo plastic deformation by crystallographic slip alone to account for the deformation twinning, as well. In their CPCM they considered the primary slip and primary twinning as the plastic deformation mechanisms. The proposed model was successful in predicting the stress-strain curves as well as texture evolution for AM30 in a number of loading paths. The integration was carried out between every two successive deformed configurations (updated Lagrangian approach).

f) Viscoplastic self-consistent (VPSC) polycrystal approach: self-consistent models allow for different strain response in each grain, depending upon the relative stiffness between the grain and surrounding homogeneous equivalent medium with consistency conditions requiring that the averaged behaviour over all the grains must be the same as the macroscopically imposed one. A number of studies have used VPSC scheme to simulate large strain behaviour and texture evolution of HCP polycrystalline magnesium under various deformations [11,31-36]. Recently, attempts to develop a finite strain Elastic-

Viscoplastic Self-Consistent (EVPSC) model for polycrystalline materials were also made [37]. The results tend to be extremely sensitive to the stiffness of the grain-matrix interaction associated with the Self-Consistent Schemes. Proust et al. [34] combined a Composite Grain (CG) model with the VPSC polycrystal approach. Their proposed model accounted for volume fractions of the matrix, primary, and secondary twinned regions, as well as the activity of primary and secondary slip systems. Proust et al. [34] successfully applied this model to predict the stress-strain curves as well as texture evolution of hexagonal Zr deformed in compression at 76 K for monotonic and non-monotonic loading paths.

In a single crystal of magnesium, the resistance evolution of a given slip system depends, in a complex manner, on the interactions that exist between this slip system and other slip and twinning systems. The same holds true for a given twinning system (for a review of these effects, see [34,35]). For instance, it is well-known that twin boundaries can act as obstacles to further slip (Hall-Petch effect [38,39]). Also, the resistance of the slip systems inside the twins is different from the resistance of the slip systems inside the parent due to the Basinski-hardening mechanism [40]. The models by Van Houtte [20], Tomé et al. [21], and Staroselsky and Anand [26] (a, b, and d, respectively) did not account for these effects, and the other models (i.e. c, e, and f) accounted for these interactions in a phenomenological way (not at dislocation level). There were efforts in understanding these effects [4,41,42], and quantitative data on these interactions are becoming available for accurate numerical modelling.

This thesis describes a model incorporating the plastic deformation mechanisms of primary, secondary, and tertiary slip systems, as well as primary and secondary twinning systems in a comprehensive CPCM for the hexagonal magnesium. Crystallographic slip in the parent, primary, and secondary twinned regions, as well as different twinning modes in magnesium are considered. The interactions between various slip and twinning systems are incorporated in a phenomenological way.

1.3 Contributions and outline of the thesis

This thesis offers two major contributions. The first contribution is that upon calibration and validation of the proposed CPCM with experimental data at room temperature, the model can be used to simulate and understand the plastic deformation of magnesium under different loading conditions. The CPCM contains a number of parameters corresponding to different plastic deformation mechanisms. Some of them have been calibrated using limited experimental data reported in literature for pure magnesium single crystals at room temperature. More experimental data are required to completely calibrate and take advantage of the proposed CPCM. The influences of the parameters that could not be calibrated due to lack of experimental data were investigated through a numerical study (assessing the relative contributions of different plastic deformation mechanisms in the material stress-strain response) to highlight the strength of the new model with all the plastic deformation mechanisms included in it. The results show that

neglecting secondary twinning and secondary slip while simulating deformation of magnesium alloys by crystal plasticity approach can lead to erroneous results. From this, it is concluded that accounting for all not just a few of the plastic deformation mechanisms to model the plastic deformation in magnesium alloys is necessary. While the model by Proust et al. [34] and the one proposed in this thesis account for the same number of intragranular plastic deformation mechanisms in magnesium, there are differences between them. The model by Proust et al. [34] does not account for the material elasticity. To simulate the unloading and strain path changes in the material by the VPSC approach, accounting for material elasticity is necessary (as pointed out by Wang et al. [37]). In the VPSC polycrystal approach, each grain is not in direct interaction with the neighbor grains (each grain is in interaction with the entire aggregate as an equivalent medium), and the conditions of equilibrium and compatibility are not completely satisfied between neighbor grains. The grain geometric shape is also restricted to be an ellipsoid. The proposed model in this thesis accounts for material elasticity. It can be applied to polycrystals through finite element, as well (this technique is called Crystal Plasticity Finite Element Method (CPFEM)). In the CPFEM each grain is in direct interaction with the neighbor grains, and the conditions of equilibrium and compatibility are imultaneously satisfied between them (more details are available in [43]). With CPFEM the grains can have any arbitrary geometric shape.

The second contribution is that the proposed CPCM in conjunction with the Marciniak–Kuczynski (M–K) approach were used to assess the formability of a magnesium single crystal sheet by simulating the Forming Limit Diagrams (FLDs). Sheet necking was initiated from an initial imperfection in terms of a narrow band. A homogeneous deformation field was assumed inside and outside the band, and conditions of compatibility and equilibrium were enforced across the band interfaces. Thus, the CPCM only needed to be applied to two regions, one inside and one outside the band. The FLDs were simulated under two conditions: a) the plastic deformation mechanisms are primary slip systems alone, and b) the plastic deformation mechanisms are primary slip and twinning systems. The FLDs were computed for two grain orientations. In the first orientation, primary extension twinning systems have favourable orientation for activation. In the second orientation, primary contraction twinning systems have favourable orientation for activation. The effects of shear strain outside the necking band, rate sensitivity, and c/a ratio on the simulated FLDs for the two orientations were individually explored.

In Chapter 2 the proposed CPCM for magnesium single crystals, its formulation, and integration procedure are outlined. The calibration of the CPCM is presented in Chapter 3. There, by an illustrative example, the importance of accounting for the kinematics of various plastic deformation mechanisms in the CPCM is also emphasized. In Chapter 4, the formulation for simulating the FLDs using the proposed CPCM within the M–K framework, as well as the FLDs' simulation results for two grain orientations

under various conditions are presented. Chapter 5 contains the conclusions and proposed research for the future.

The equations related to the calculation of plastic work in the parent and primary twinned regions, number of state variables, conversion of the Miller-Bravais coordinate system into an orthonormal one, and some metallurgical information about magnesium are all presented in the appendices.

Chapter 2

A new crystal plasticity constitutive model for magnesium single crystals, formulation, and integration procedure

2.1 A new crystal plasticity constitutive model for magnesium single crystals

In this work, the rate-dependent elastic-viscoplastic Crystal Plasticity Constitutive Model (CPCM) laid out by Peirce et al. [30] for materials in which primary slip systems are the only plastic deformation mechanism, was modified to include the secondary and tertiary slip systems as well as primary and secondary twinning systems as additional plastic deformation mechanisms. Deformation twinning was treated as a pseudo-slip mechanism (i.e. $\gamma_t = f \cdot \gamma_{tw}$ [20]). Following the Taylor [8] assumptions, a homogeneous deformation field was assumed in the entire grain. This means that the parent, primary, and secondary twinned regions undergo the same total deformation gradient, and there is a single decomposition of the total deformation gradient tensor into the elastic and plastic parts (similar to the works in [22,24,25,29]).

It was demonstrated that in order to activate twinning, twinning dislocations have to nucleate first (see e.g. [44]). In the case of single crystals, it is believed that twinning dislocations originate from the elements of the dislocations substructure produced before twinning by the activity of slip systems. The plastic work is a good indicator to describe slip system activity in the material (the calculation method of plastic work in the matrix and primary twinned regions is presented in Appendix A). Because of this fact, in the proposed model, a plastic work-based criterion was employed to activate the twinning systems. In

this approach, the nucleation of a primary twinning system does not occur before the plastic work due to slip-induced deformation inside the parent has reached a certain threshold value. Similarly, a double twin will not nucleate before the plastic work due to the slip-induced deformation inside the primary twinned region has reached a certain threshold value. This approach is similar to the approach of using a threshold stress to invoke the activation of a new mechanism for plastic deformation of magnesium polycrystal employed by Staroselsky and Anand [26]. The plastic work based nucleation criterion for twinning in magnesium single crystals is the simplest criterion at the meso-scale level modelling. This criterion should be improved as the understanding of twin nucleation mechanisms in magnesium single crystals advances. For magnesium polycrystals, recent results reveal that twinning nucleation depends strongly on the grain boundary misorientation angle and defect structure of the grain boundaries [45-47]. Therefore, when the proposed model is applied to magnesium polycrystals (with an appropriate homogenization scheme), the twinning nucleation criterion has to account for these effects.

The proposed model works in a sequential manner as follows; each step has its own set of equations:

1. When a single crystal of magnesium is loaded, at the initial stage of deformation, the proposed model considers the primary slip systems inside the untwinned crystal as the only plastic deformation mechanisms that can accommodate the macroscopic plastic deformation.

2. When the plastic work due to primary slip systems has reached a certain value (c_1), nucleation of the primary extension or contraction twinning systems is allowed in the code. Provided that the Resolved Shear Stress (RSS) for the primary extension (Figure 2-1a) or contraction (Figure 2-1b) twinning systems is non-zero, they can grow.

3. Nucleation of the secondary slip systems inside the primary extension twinned region is allowed in the code. Provided that the RSS for the secondary slip systems is non-zero, they can take up shear.

4. Nucleation of the secondary slip systems inside the primary contraction twinned region is allowed in the code. Provided that the RSS for the secondary slip systems is non-zero, they can take up shear.

5. When the plastic work due to the slip-induced deformation inside a primary contraction twinned region has reached a certain value (c_2), nucleation of secondary extension twinning systems inside the primary contraction twinned region (double twin) is allowed. Provided that the RSS for the secondary extension twinning systems is non-zero, they can grow (Figure 2-1b).

6. Nucleation of the tertiary slip systems inside the secondary extension twinned region is allowed. Provided that the RSS for the tertiary slip systems is non-zero, they can take up shear.

It is worth mentioning that the proposed CPCM can be used for modelling the plastic deformation in titanium alloys where the primary slip, primary twinning, and secondary slip systems are the plastic deformation mechanisms [25] (i.e. the first four steps of the proposed model can be used to model the plastic deformation in titanium alloys). The corresponding formulation for each step of the above algorithm is described in the following section.
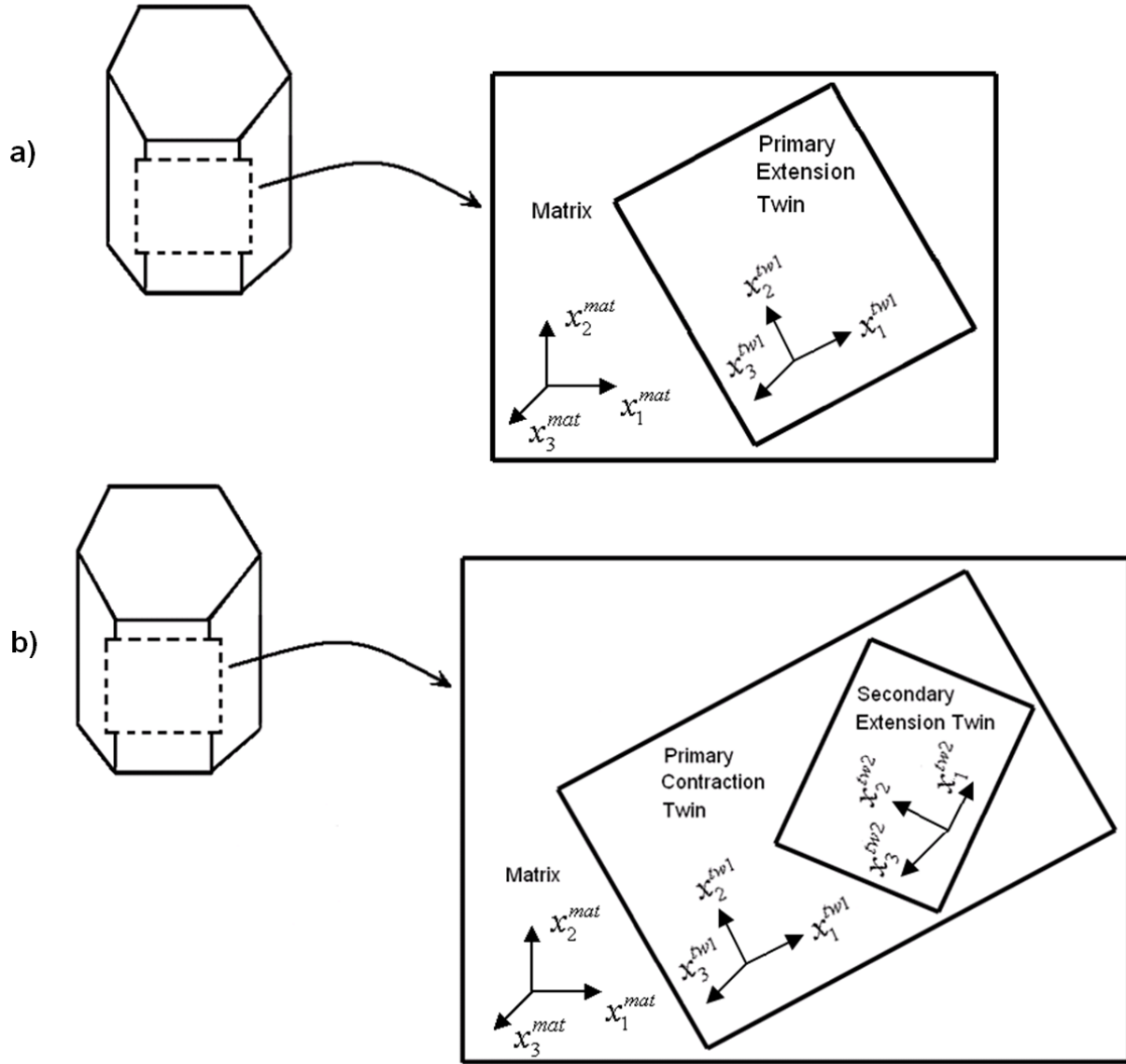
Figure 2-1 Twinned regions types in magnesium. a) a primary extension twinned region, and b) a primary contraction twinned region with a secondary extension twinned region inside

2.2 Formulation of the proposed crystal plasticity constitutive model

The equations corresponding to each step of the CPCM are outlined in the following subsections.

2.2.1 Equations corresponding to step 1 of the crystal plasticity constitutive model

In step 1 of the CPCM, primary slip systems are the only plastic deformation mechanisms. The equations for this step of the model are identical to the ones outlined by Peirce et al. [30] which are presented here.

Similar to the work by Peirce et al. [30], the deformation gradient is decomposed into the elastic and plastic parts as follows:

$$F = F^* F^p \tag{2-1}$$

F^* includes the elastic stretch and rigid body rotation effects, and F^p includes the plastic deformation resultant from the primary slip systems.

The Eulerian velocity gradient, L, can be written as:

$$L = \dot{F} F^{-1} = L^* + L^p \tag{2-2}$$

where,

$$L^* = \dot{F}^* F^{*-1}, \ L^p = \dot{F} F^{-1} - \dot{F}^* F^{*-1} = F^* \left(\dot{F}^p F^{p-1} \right) F^{*-1} \tag{2-3}$$

L^* and L^p are the elastic and plastic parts of the velocity gradient, respectively.

The deformation rate and spin are decomposed into the elastic and plastic parts as follows:

$$D = D^* + D^p \tag{2-4}$$

$$\Omega = \Omega^* + \Omega^p \tag{2-5}$$

The total deformation rate and spin are related to the velocity gradient according to the following equations:

$$D = sym(L) \tag{2-6}$$

$$\Omega = asym(L) \tag{2-7}$$

The plastic part of the deformation rate and spin are related to the plastic part of the velocity gradient as shown below:

$$D^p = sym(L^p) \tag{2-8}$$

$$\Omega^p = asym(L^p) \tag{2-9}$$

The orientation matrix of the grain, Q, defined later by Equations (2-178)-(2-187), is updated by Ω^*. This is valid for all the six steps of the model.

Consider $s^{(\alpha p)}$ and $m^{(\alpha p)}$ as the shear direction and plane normal of a primary slip system (αp), and $s^{(\beta p)}$ and $m^{(\beta p)}$ as the shear direction and plane normal of a primary twinning system (βp). The following equations govern the change in their orientation after the deformation:

$$s^{*(\alpha p)} = F^* s^{(\alpha p)} \tag{2-10}$$

$$m^{*(\alpha p)} = m^{(\alpha p)} F^{*-1} \tag{2-11}$$

$$s^{*(\beta p)} = F^* s^{(\beta p)} \tag{2-12}$$

$$m^{*(\beta p)} = m^{(\beta p)} F^{*-1} \tag{2-13}$$

From Equations (2-10)-(2-13), at any given stage of deformation, $s^{(\alpha p)}$ and $m^{(\alpha p)}$, as well as $s^{(\beta p)}$ and $m^{(\beta p)}$ remain mutually perpendicular.

L^P has contributions from the primary slip systems and is defined as follows:

$$L^p = \sum_{\alpha p} s^{*(\alpha p)} \otimes m^{*(\alpha p)} \dot{\gamma}^{(\alpha p)} \tag{2-14}$$

For each primary slip system (αp), the symmetric tensor, $P^{(\alpha p)}$, and antisymmetric tensor, $W^{(\alpha p)}$, are defined by:

$$P^{(\alpha p)} = \frac{1}{2}(s^{*(\alpha p)} \otimes m^{*(\alpha p)} + m^{*(\alpha p)} \otimes s^{*(\alpha p)}) \tag{2-15}$$

$$W^{(\alpha p)} = \frac{1}{2}(s^{*(\alpha p)} \otimes m^{*(\alpha p)} - m^{*(\alpha p)} \otimes s^{*(\alpha p)}) \tag{2-16}$$

The plastic part of the deformation rate and spin are related to the plastic part of the velocity gradient as follows:

$$D^p = sym(L^p) = \sum_{\alpha p} P^{(\alpha p)} \dot{\gamma}^{(\alpha p)} \tag{2-17}$$

$$\Omega^p = asym(L^p) = \sum_{\alpha p} W^{(\alpha p)} \dot{\gamma}^{(\alpha p)} \tag{2-18}$$

The constitutive law is given by:

$$\overset{\triangledown (mat)}{\sigma} = \dot{\sigma}^{mat} - \Omega \sigma^{mat} + \sigma^{mat} \Omega = C_{mat} D - \sum_{\alpha p} \left(C_{mat} P^{(\alpha p)} + W^{(\alpha p)} \sigma^{mat} - \sigma^{mat} W^{(\alpha p)} \right) \dot{\gamma}^{(\alpha p)}$$
$$- \sigma^{mat} \left(D_{11} + D_{22} + D_{33} \right)$$
$$\tag{2-19}$$

where C_{mat} is defined by:

$$C_{mat} = QQ\overset{\circ}{C} Q^T Q^T \tag{2-20}$$

15

$\overset{\circ}{C}$ is the Elastic moduli for magnesium single crystal defined in Appendix D.

Pan and Rice [48] and Hutchinson [49] assumed a simple power law relation between the slip rate on a primary slip system and the ratio of RSS to the resistance of the primary slip system as follows:

$$\dot{\gamma}^{(\alpha p)} = \dot{a}^{(\alpha p)} \left[\frac{\sigma^{(\alpha p)}}{g^{(\alpha p)}} \right] \left[\left| \frac{\sigma^{(\alpha p)}}{g^{(\alpha p)}} \right| \right]^{\left(\frac{1}{m}\right) - 1} \tag{2-21}$$

where,

$$\sigma^{(\alpha p)} = P^{(\alpha p)} : \sigma^{mat} \tag{2-22}$$

$\sigma^{(\alpha p)}$ is the RSS on the primary slip systems, and $\dot{a}^{(\alpha p)}$ represents a reference shear rate. Equation (2-21) is used for calculating the shear strain rate on the primary slip systems in the next steps of the model, as well.

The evolution of resistance of the primary slip systems is given by:

$$\dot{g}^{(\alpha p)} = \sum_{\alpha p} h_{\alpha p}^{1A} \left| \dot{\gamma}^{(\alpha p)} \right| \tag{2-23}$$

$$h_{\alpha p}^{1A} = h_{\alpha p}^{1A}(\gamma_1) \tag{2-24}$$

$$\gamma_1 = \sum_{\alpha p} \gamma^{(\alpha p)} \tag{2-25}$$

$h_{\alpha p}^{1A}$ is the resistance evolution matrix, and, in general, converges to zero as γ_1 increases. This holds true for the similar functions used in the resistance evolution of the other plastic deformation mechanisms in the next steps of the model. The diagonal terms of this matrix represent the slip systems, self-hardening, and off-diagonal terms, latent hardening.

Since there is no twinned region at this step of the model, the total stress in the grain is equal to the stress in the parent as follows:

$$\sigma_{tot} = \sigma^{mat} \tag{2-26}$$

Equations (2-1) through (2-9) are valid for all six steps of the model and are not repeated in steps 2-6 of the model. It should be noted that:

- In step 2: L^p has contributions from the primary slip and primary twinning systems (Equations (2-37))

- In steps 3-4: L^p has contributions from the primary and secondary slip, and primary twinning systems (Equation (2-56))

- In step 5: L^p has contributions from the primary and secondary slip, and primary and secondary twinning systems (Equation (2-82))

- In step 6: L^p has contributions from the primary, secondary, and tertiary slip, as well as the primary and secondary twinning systems (Equation (2-112))

This is the generalization of what Kalidindi [22] did in his model, where only primary slip and twinning systems were considered as the plastic deformation mechanisms.

2.2.2 Equations corresponding to step 2 of the crystal plasticity constitutive model

In step 2 of the proposed CPCM nucleation of the primary twinning systems is allowed. The same deformation field is assumed to exist over the parent and primary twinned regions (Taylor [8] assumptions). In addition, Equations (2-1)-(2-13), (2-15)-(2-16), (2-20)-(2-22), and (2-25) are valid for step 2 of the model. An interaction between the resistances of the primary slip and primary twinning systems enforced and is highlighted later in Equations (2-46) and (2-51).

At the very beginning of this stage, the initial lattice orientation of the primary twinned region as well as crystallographic planes and directions of the secondary slip and twinning systems inside of it are calculated.

For type I twins, the transformation between the lattice orientations in the parent and a primary twinned region (Q_{tw1}^{mat}) with the plane normal, n, and shear direction, b, is [5,6,50]:

$$Q_{tw1}^{mat} = X^{-1}RX \tag{2-27}$$

$$X = \begin{bmatrix} b_1 & b_2 & b_3 \\ b_3 n_2 - b_2 n_3 & b_1 n_3 - b_3 n_1 & b_2 n_1 - b_1 n_2 \\ n_1 & n_2 & n_3 \end{bmatrix} \tag{2-28}$$

$$R = \begin{bmatrix} -1 & 0 & 0 \\ 0 & -1 & 0 \\ 0 & 0 & 1 \end{bmatrix} \tag{2-29}$$

R is the rotation matrix, involving $180°$ rotation of a parent lattice around the normal to the twinning plane [5,6,50][1]. The transformation from the lattice orientation in a primary twinned region to the lattice orientation in a secondary twinned region is defined in a similar manner in Subsection 2.2.4.

Let us consider m and s as the crystallographic plane normal and shear direction of an arbitrary slip or twinning systems in the parent. Also, m' and s' as the crystallographic plane normal and shear direction of the same slip or twinning systems in a type I twinned region in the same material. If n and b are plane normal and shear direction of that type I twinned region, then the following equations relate the m' and s' to m and s, respectively [5,50-52]:

$$F^{tw1} = \begin{bmatrix} 1+\gamma_{tw}b_1n_1 & \gamma_{tw}b_1n_2 & \gamma_{tw}b_1n_3 \\ \gamma_{tw}b_2n_1 & 1+\gamma_{tw}b_2n_2 & \gamma_{tw}b_2n_3 \\ \gamma_{tw}b_3n_1 & \gamma_{tw}b_3n_2 & 1+\gamma_{tw}b_3n_3 \end{bmatrix} \tag{2-30}$$

$$m' = m\left(F^{tw1}\right)^{-1} \tag{2-31}$$

$$s' = F^{tw1}s \tag{2-32}$$

F^{tw1} and γ_{tw} are the deformation gradient and specific shear strain associated with a primary twinning system, respectively. For extension and compression twins, the value of γ_{tw} is given in Appendix D. m' and s' are the plane normal and shear direction in the primary twinned region. The components of m, s, n, b, m', and s' are all expressed in the same coordinate system attached to the parent. Following the same procedure, the crystallographic plane normal and shear direction of the slip systems in a secondary twinned region is calculated (using F^{tw2}, in Subsection 2.2.4) from the corresponding crystallographic plane normal and shear direction of the slip systems in the primary twinned region (in which the secondary twinned region lies).

If $s^{(\alpha s)}$ and $m^{(\alpha s)}$ represent the shear direction and plane normal of a secondary slip system, and $s^{(\beta s)}$ and $m^{(\beta s)}$ represent the shear direction and plane normal of a secondary twinning system, the following equations govern their updated orientation in the deformed configuration [5,50,51]:

$$s^{*(\alpha s)} = F^{tw1}s^{*(\alpha p)} \tag{2-33}$$

$$m^{*(\alpha s)} = m^{*(\alpha p)}\left(F^{tw1}\right)^{-1} \tag{2-34}$$

$$s^{*(\beta s)} = F^{tw1}s^{*(\beta p)} \tag{2-35}$$

---

[1] The transformation between the lattice orientation in the matrix to the lattice orientation in a primary twinned region defined by Van Houtte [10] is not applicable to type I twins.

$$m^{*(\beta s)} = m^{*(\beta p)} \left(F^{tw1} \right)^{-1} \tag{2-36}$$

where F^{tw1} is defined in Equation (2-30). It is obvious from Equations (2-33)-(2-36) that at any given stage of deformation, $s^{(\alpha s)}$ and $m^{(\alpha s)}$, as well as $s^{(\beta s)}$ and $m^{(\beta s)}$ remain mutually perpendicular.

L^P has contributions from the primary slip and twinning systems, and is defined as follows:

$$L^p = \sum_{\alpha p} s^{*(\alpha p)} \otimes m^{*(\alpha p)} \dot{\gamma}^{(\alpha p)} + \sum_{\beta p} s^{*(\beta p)} \otimes m^{*(\beta p)} (\dot{f}^{(\beta p)} \gamma_{tw}^{(\beta p)}) \tag{2-37}$$

For each primary twinning system (βp), the symmetric tensor, $P^{(\beta p)}$, and antisymmetric tensor, $W^{(\beta p)}$, are defined as follows:

$$P^{(\beta p)} = \frac{1}{2} (s^{*(\beta p)} \otimes m^{*(\beta p)} + m^{*(\beta p)} \otimes s^{*(\beta p)}) \tag{2-38}$$

$$W^{(\beta p)} = \frac{1}{2} (s^{*(\beta p)} \otimes m^{*(\beta p)} - m^{*(\beta p)} \otimes s^{*(\beta p)}) \tag{2-39}$$

The plastic part of the deformation rate and spin are related to the plastic part of the velocity gradient as follows:

$$D^p = sym(L^p) = \sum_{\alpha p} P^{(\alpha p)} \dot{\gamma}^{(\alpha p)} + \sum_{\beta p} P^{(\beta p)} (\dot{f}^{(\beta p)} \gamma_{tw}^{(\beta p)}) \tag{2-40}$$

$$\Omega^p = asym(L^p) = \sum_{\alpha p} W^{(\alpha p)} \dot{\gamma}^{(\alpha p)} + \sum_{\beta p} W^{(\beta p)} (\dot{f}^{(\beta p)} \gamma_{tw}^{(\beta p)}) \tag{2-41}$$

The constitutive laws are given by:

$$\overset{\nabla}{\sigma}^{(mat)} = \dot{\sigma}^{mat} - \Omega \sigma^{mat} + \sigma^{mat} \Omega = C_{mat} D - \sum_{\alpha p} \left(C_{mat} P^{(\alpha p)} + W^{(\alpha p)} \sigma^{mat} - \sigma^{mat} W^{(\alpha p)} \right) \dot{\gamma}^{(\alpha p)}$$
$$- \sum_{\beta p} \left(C_{mat} P^{(\beta p)} + W^{(\beta p)} \sigma^{mat} - \sigma^{mat} W^{(\beta p)} \right) \dot{f}^{(\beta p)} \gamma_{tw}^{(\beta p)} - \sigma^{mat} (D_{11} + D_{22} + D_{33})$$

$$\tag{2-42}$$

$$\overset{\nabla}{\sigma}^{(tw1)} = \dot{\sigma}^{tw1} - \Omega \sigma^{tw1} + \sigma^{tw1} \Omega = C_{tw1} D - \sum_{\alpha p} \left(C_{tw1} P^{(\alpha p)} + W^{(\alpha p)} \sigma^{tw1} - \sigma^{tw1} W^{(\alpha p)} \right) \dot{\gamma}^{(\alpha p)}$$
$$- \sum_{\beta p} \left(C_{tw1} P^{(\beta p)} + W^{(\beta p)} \sigma^{tw1} - \sigma^{tw1} W^{(\beta p)} \right) \dot{f}^{(\beta p)} \gamma_{tw}^{(\beta p)} - \sigma^{tw1} (D_{11} + D_{22} + D_{33})$$

$$\tag{2-43}$$

where C_{mat} is given by Equation (2-20), and C_{tw1} is defined by:

$$C_{tw1} = Q^{tw1} Q^{tw1} \overset{\circ}{C} Q^{tw1^T} Q^{tw1^T} \qquad (2\text{-}44)$$

Q^{tw1}, the transformation matrix that expresses the lattice orientation in a primary twinned region with the normal plane, n, and shear direction, b, with respect to the global coordinate system is defined as follows:

$$Q^{tw1} = Q \times Q_{tw1}^{mat^{-1}} \qquad (2\text{-}45)$$

Q_{tw1}^{mat} is given in Equation (2-27).

The evolution of the resistance functions for the primary slip systems is defined by:

$$\dot{g}^{(\alpha p)} = \sum_{\alpha p} h_{\alpha p}^{2A} \left| \dot{\gamma}^{(\alpha p)} \right| + \sum_{\beta p} h_{\beta p}'^{2A} \left| \dot{f}^{(\beta p)} \right| \qquad (2\text{-}46)$$

$$h_{\alpha p}^{2A} = h_{\alpha p}^{2A}(\gamma_1) \qquad (2\text{-}47)$$

$$h_{\beta p}'^{2A} = h_{\beta p}'^{2A}(f_1) \qquad (2\text{-}48)$$

The diagonal terms of $h_{\alpha p}^{2A}$ matrix represent the slip systems, self-hardening, and off-diagonal terms, latent hardening. $h_{\beta p}'^{2A}$ accounts for the interaction between the primary slip and twinning systems.

Following Neil and Agnew [33] and Lévesque et al. [29], Equation (2-49) was used to calculate the growth rate of the volume fraction of primary twinned regions as follows:

$$\dot{f}^{(\beta p)} = \frac{\dot{a}^{(\beta p)}}{\gamma_{tw}} \left[\frac{\sigma^{(\beta p)}}{g^{(\beta p)}} \right] \left| \left[\frac{\sigma^{(\beta p)}}{g^{(\beta p)}} \right] \right|^{\left(\frac{1}{m}\right)-1} \qquad (2\text{-}49)$$

$$\sigma^{(\beta p)} = P^{(\beta p)} : \sigma^{ave(mat,\beta p)} \qquad (2\text{-}50)$$

where $\sigma^{ave(mat,\beta p)}$ is the volumetric average of the stresses in the parent and primary twinned regions (two regions that lie on the two sides of the twinning plane) used to calculate the RSS $\sigma^{(\beta p)}$ on the twinning plane. Equation (2-49) is used to calculate the volume fraction rate of the primary twinning systems in the next steps of the model.

The evolution of the resistance of the primary twinning systems is given by:

$$\dot{g}^{(\beta p)} = \sum_{\alpha p} h_{\alpha p}^{2B} \left| \dot{\gamma}^{(\alpha p)} \right| + \sum_{\beta p} h_{\beta p}'^{2B} \left| \dot{f}^{(\beta p)} \right|$$

(2-51)

$$h_{\alpha p}^{2B} = h_{\alpha p}^{2B}(\gamma_1)$$

(2-52)

$$h_{\beta p}'^{2B} = h_{\beta p}'^{2B}(f_1)$$

(2-53)

where $h_{\alpha p}^{2B}$ accounts for the interaction between the primary slip and twinning systems, γ_1 is defined by Equation (2-25), and f_1 is:

$$f_1 = \sum_{\beta p} f^{(\beta p)}$$

(2-54)

Following Kalidindi's approach [22], the total stress in the grain is equal to the volumetric average of the stresses in the parent and primary twinned regions:

$$\sigma_{tot} = \left(1 - \sum_{\beta p} f^{\beta p}\right)\sigma^{mat} + \sum_{\beta p} f^{\beta p}\sigma^{\beta p}$$

(2-55)

2.2.3 Equations corresponding to steps 3-4 of the crystal plasticity constitutive model

In steps 3-4 of the proposed CPCM, nucleation of the secondary slip systems inside the primary twinned regions is allowed. Like step 2, the same deformation field is assumed to exist over the parent and primary twinned regions. Also, Equations (2-1)-(2-13), (2-15), (2-16), (2-20)-(2-22), (2-25), (2-27)-(2-36), (2-38), (2-39), (2-44), (2-49), (2-50), (2-54), and (2-55) are valid for steps 3-4 of the model. Interactions between the resistances of the primary slip, primary twinning, and secondary slip systems enforced and are highlighted later in Equations (2-63), (2-66), and (2-73).

L^P has contributions from the primary and secondary slip, and primary twinning systems, and is defined as follows:

$$L^P = \sum_{\alpha p} s^{*(\alpha p)} \otimes m^{*(\alpha p)} \dot{\gamma}^{(\alpha p)} + \sum_{\beta p} s^{*(\beta p)} \otimes m^{*(\beta p)}(\dot{f}^{(\beta p)}\gamma_{tw}^{(\beta p)}) + \sum_{\beta p} f^{(\beta p)}\left(\sum_{\alpha s} s^{*(\alpha s)} \otimes m^{*(\alpha s)}(\dot{\gamma}^{(\alpha s)})\right)$$

(2-56)

For each secondary slip system (αs), the symmetric tensor, $P^{(\alpha s)}$, and anti-symmetric tensor, $W^{(\alpha s)}$, are defined as follows:

$$P^{(\alpha s)} = \frac{1}{2}(s^{*(\alpha s)} \otimes m^{*(\alpha s)} + m^{*(\alpha s)} \otimes s^{*(\alpha s)}) \tag{2-57}$$

$$W^{(\alpha s)} = \frac{1}{2}(s^{*(\alpha s)} \otimes m^{*(\alpha s)} - m^{*(\alpha s)} \otimes s^{*(\alpha s)}) \tag{2-58}$$

The plastic part of the deformation rate and spin are related to the plastic part of the velocity gradient as follows:

$$D^p = sym(L^p) = \sum_{\alpha p} P^{(\alpha p)} \dot{\gamma}^{(\alpha p)} + \sum_{\beta p} P^{(\beta p)}(\dot{f}^{(\beta p)} \gamma_{tw}^{(\beta p)}) + \sum_{\beta p} f^{(\beta p)}\left(\sum_{\alpha s} P^{(\alpha s)}(\dot{\gamma}^{(\alpha s)})\right) \tag{2-59}$$

$$\Omega^p = asym(L^p) = \sum_{\alpha p} W^{(\alpha p)} \dot{\gamma}^{(\alpha p)} + \sum_{\beta p} W^{(\beta p)}(\dot{f}^{(\beta p)} \gamma_{tw}^{(\beta p)}) + \sum_{\beta p} f^{(\beta p)}\left(\sum_{\alpha s} W^{(\alpha s)}(\dot{\gamma}^{(\alpha s)})\right) \tag{2-60}$$

The constitutive laws are given by:

$$\overset{\triangledown}{\sigma}{}^{(mat)} = \dot{\sigma}^{mat} - \Omega\sigma^{mat} + \sigma^{mat}\Omega = C_{mat}D - \sum_{\alpha p}\left(C_{mat}P^{(\alpha p)} + W^{(\alpha p)}\sigma^{mat} - \sigma^{mat}W^{(\alpha p)}\right)\dot{\gamma}^{(\alpha p)}$$

$$- \sum_{\beta p}\left(C_{mat}P^{(\beta p)} + W^{(\beta p)}\sigma^{mat} - \sigma^{mat}W^{(\beta p)}\right)\dot{f}^{(\beta p)}\gamma_{tw}^{(\beta p)}$$

$$- \sum_{\beta p} f^{(\beta p)}\left(\sum_{\alpha s}\left(C_{mat}P^{(\alpha s)} + W^{(\alpha s)}\sigma^{mat} - \sigma^{mat}W^{(\alpha s)}\right)\dot{\gamma}^{(\alpha s)}\right)$$

$$- \sigma^{mat}\left(D_{11} + D_{22} + D_{33}\right)$$

$$\tag{2-61}$$

$$\overset{\triangledown}{\sigma}{}^{(tw1)} = \dot{\sigma}^{tw1} - \Omega\sigma^{tw1} + \sigma^{tw1}\Omega = C_{tw1}D - \sum_{\alpha p}\left(C_{tw1}P^{(\alpha p)} + W^{(\alpha p)}\sigma^{tw1} - \sigma^{tw1}W^{(\alpha p)}\right)\dot{\gamma}^{(\alpha p)}$$

$$- \sum_{\beta p}\left(C_{tw1}P^{(\beta p)} + W^{(\beta p)}\sigma^{tw1} - \sigma^{tw1}W^{(\beta p)}\right)\dot{f}^{(\beta p)}\gamma_{tw}^{(\beta p)}$$

$$- \sum_{\beta p} f^{(\beta p)}\left(\sum_{\alpha s}\left(C_{tw1}P^{(\alpha s)} + W^{(\alpha s)}\sigma^{tw1} - \sigma^{tw1}W^{(\alpha s)}\right)\dot{\gamma}^{(\alpha s)}\right) - \sigma^{tw1}\left(D_{11} + D_{22} + D_{33}\right)$$

$$\tag{2-62}$$

where C_{mat} and C_{tw1} are given in Equations (2-20) and (2-44), respectively.

The evolution of the resistance functions for the primary slip systems is defined by:

$$\dot{g}^{(\alpha p)} = \sum_{\alpha p} h_{\alpha p}^{3-4A} \left| \dot{\gamma}^{(\alpha p)} \right| + \sum_{\beta p} h_{\beta p}'^{3-4A} \left| \dot{f}^{(\beta p)} \right| \tag{2-63}$$

$$h_{\alpha p}^{3-4A} = h_{\alpha p}^{3-4A}(\gamma_1) \tag{2-64}$$

$$h_{\beta p}'^{3-4A} = h_{\beta p}'^{3-4A}(f_1) \tag{2-65}$$

The diagonal terms of, $h_{\alpha p}^{3-4A}$ matrix represent the slip systems, self-hardening, and off-diagonal terms, latent hardening. $h_{\beta p}'^{3-4A}$ accounts for the interaction between the primary slip and twinning systems.

The evolution of the resistance of the primary twinning systems is given by:

$$\dot{g}^{(\beta p)} = \sum_{\alpha p} h_{\alpha p}^{3-4B} \left| \dot{\gamma}^{(\alpha p)} \right| + \sum_{\beta p} h_{\beta p}'^{3-4B} \left| \dot{f}^{(\beta p)} \right| + \sum_{\alpha s} h_{\alpha s}''^{3-4B} \left| \dot{\gamma}^{(\alpha s)} \right| \tag{2-66}$$

$$h_{\alpha p}^{3-4B} = h_{\alpha p}^{3-4B}(\gamma_1) \tag{2-67}$$

$$h_{\beta p}'^{3-4B} = h_{\beta p}'^{3-4B}(f_1) \tag{2-68}$$

$$h_{\alpha s}''^{3-4B} = h_{\alpha s}''^{3-4B}(\gamma_2) \tag{2-69}$$

$h_{\alpha p}^{3-4B}$ accounts for the interaction between the primary twinning and primary slip systems, and $h_{\alpha s}''^{3-4B}$ accounts for the interaction between the primary twinning and secondary slip systems. γ_1 and f_1 are defined by Equations (2-25) and (2-54), respectively, and:

$$\gamma_2 = \sum_{\alpha s} \gamma^{(\alpha s)} \tag{2-70}$$

The evolution of the shear strain on the secondary slip systems is calculated as follows (similar to the primary slip systems in Equation (2-21)):

$$\dot{\gamma}^{(\alpha s)} = \dot{a}^{(\alpha s)} \left[\frac{\sigma^{(\alpha s)}}{g^{(\alpha s)}} \right] \left| \frac{\sigma^{(\alpha s)}}{g^{(\alpha s)}} \right|^{\left(\frac{1}{m}\right)-1} \tag{2-71}$$

$$\sigma^{(\alpha s)} = P^{(\alpha s)} : \sigma^{tw1} \tag{2-72}$$

Equation (2-71) is used to calculate the shear strain rate on the secondary slip systems in the next steps of the model as well. The evolution of the resistance of the secondary slip systems is given by:

$$\dot{g}^{(\alpha s)} = h_{\beta p}^{3-4C} \left| \dot{f}^{(\beta p)} \right| + \sum_{\alpha s} h_{\alpha s}^{\prime 3-4C} \left| \dot{\gamma}^{(\alpha s)} \right| \tag{2-73}$$

$$h_{\beta p}^{3-4C} = h_{\beta p}^{3-4C}(f_1) \tag{2-74}$$

$$h_{\alpha s}^{\prime 3-4C} = h_{\alpha s}^{\prime 3-4C}(\gamma_2) \tag{2-75}$$

The diagonal terms of the $h_{\alpha s}^{\prime 3-4C}$ matrix represent the slip systems, self-hardening, and off-diagonal terms, latent hardening. $h_{\beta p}^{3-4C}$ accounts for the interaction between the secondary slip and primary twinning systems.

Finally, similar to step 2, the total stress in the grain is calculated by Equation (2-55).

2.2.4 Equations corresponding to step 5 of the crystal plasticity constitutive model

In step 5 of the proposed CPCM, nucleation of the secondary twinning systems inside the primary twinned regions is allowed. The same deformation field is assumed to exist over the parent, primary and secondary twinned regions. Equations (2-1)-(2-13), (2-15), (2-16), (2-20)-(2-22), (2-25), (2-27)-(2-36), (2-38), (2-39), (2-44), (2-49), (2-50), (2-54), (2-57), (2-58), and (2-70)-(2-72) are valid for step 5 of the model. Interactions between the resistances of the primary slip, primary twinning, secondary slip, and secondary twinning systems enforced and are highlighted later in Equations (2-92), (2-95), (2-100), and (2-106).

At the very beginning of this stage, the initial lattice orientation of the nucleated secondary twinned region as well as crystallographic planes and directions of the tertiary slip systems inside of it are calculated.

The transformation between the lattice orientations in a primary twinned region and a secondary twinned region (Q_{tw2}^{tw1}) inside of it with the plane normal, n, and shear direction, b, is derived as below [5,6,50]:

$$Q_{tw2}^{tw1} = X^{-1}RX \tag{2-76}$$

The matrices X and R are defined in Equations (2-28) and (2-29), respectively.

Let us consider m and s as the crystallographic plane normal and shear direction of an arbitrary slip system in a primary twinned region. Also, m' and s' as the crystallographic plane normal and shear direction of the same slip system in a type I secondary twinned region (that lies inside the primary twinned region). If n and b are the plane normal and shear direction of that primary twinned region, then the following equations relate the m' and s' to m and s, respectively [5,50-52]:

$$F^{tw2} = \begin{bmatrix} 1+\gamma_{tw}b_1n_1 & \gamma_{tw}b_1n_2 & \gamma_{tw}b_1n_3 \\ \gamma_{tw}b_2n_1 & 1+\gamma_{tw}b_2n_2 & \gamma_{tw}b_2n_3 \\ \gamma_{tw}b_3n_1 & \gamma_{tw}b_3n_2 & 1+\gamma_{tw}b_3n_3 \end{bmatrix} \tag{2-77}$$

$$m' = m\left(F^{tw2}\right)^{-1} \tag{2-78}$$

$$s' = F^{tw2}s \tag{2-79}$$

F^{tw2} and γ_{tw} are the deformation gradient and specific shear strain associated with a secondary twinning system, respectively. The components of m, s, n, b, m', and s' are all expressed in the same coordinate system attached to the parent.

If $s^{(\alpha t)}$ and $m^{(\alpha t)}$ represent the shear direction and plane normal of a tertiary slip system, the following equations govern their updated orientation in the deformed configuration [5,50-52]:

$$s^{*(\alpha t)} = F^{tw2}s^{*(\alpha s)} \tag{2-80}$$

$$m^{*(\alpha t)} = m^{*(\alpha s)}\left(F^{tw2}\right)^{-1} \tag{2-81}$$

It is obvious from Equations (2-80) and (2-81) that at any given stage of deformation $s^{(\alpha t)}$ and $m^{(\alpha t)}$ remain mutually perpendicular.

L^P has contributions from the primary and secondary slip, as well as the primary and secondary twinning systems, and is defined as follows:

$$L^p = \sum_{\alpha p} s^{*(\alpha p)} \otimes m^{*(\alpha p)} \dot{\gamma}^{(\alpha p)} + \sum_{\beta p} s^{*(\beta p)} \otimes m^{*(\beta p)} (\dot{f}^{(\beta p)} \gamma_{tw}^{(\beta p)}) + \sum_{\beta p} f^{(\beta p)} \left(\sum_{\alpha s} s^{*(\alpha s)} \otimes m^{*(\alpha s)} (\dot{\gamma}^{(\alpha s)}) \right)$$

$$+ \sum_{\beta p} f^{(\beta p)} \left(\sum_{\beta s} s^{*(\beta s)} \otimes m^{*(\beta s)} (\dot{f}^{(\beta s)} \gamma_{tw}^{(\beta s)}) \right)$$

(2-82)

For each secondary twinning system (βs), the symmetric tensor, $P^{(\beta s)}$, and antisymmetric tensor, $W^{(\beta s)}$, are defined as follows:

$$P^{(\beta s)} = \frac{1}{2} (s^{*(\beta s)} \otimes m^{*(\beta s)} + m^{*(\beta s)} \otimes s^{*(\beta s)})$$

(2-83)

$$W^{(\beta s)} = \frac{1}{2} (s^{*(\beta s)} \otimes m^{*(\beta s)} - m^{*(\beta s)} \otimes s^{*(\beta s)})$$

(2-84)

The plastic part of the deformation rate and spin are related to the plastic part of the velocity gradient as follows:

$$D^p = sym(L^p) = \sum_{\alpha p} P^{(\alpha p)} \dot{\gamma}^{(\alpha p)} + \sum_{\beta p} P^{(\beta p)} (\dot{f}^{(\beta p)} \gamma_{tw}^{(\beta p)}) + \sum_{\beta p} f^{(\beta p)} \left(\sum_{\alpha s} P^{(\alpha s)} (\dot{\gamma}^{(\alpha s)}) \right) +$$

$$\sum_{\beta p} f^{(\beta p)} \left(\sum_{\beta s} P^{(\beta s)} (\dot{f}^{(\beta s)} \gamma_{tw}^{(\beta s)}) \right)$$

(2-85)

$$\Omega^p = asym(L^p) = \sum_{\alpha p} W^{(\alpha p)} \dot{\gamma}^{(\alpha p)} + \sum_{\beta p} W^{(\beta p)} (\dot{f}^{(\beta p)} \gamma_{tw}^{(\beta p)}) + \sum_{\beta p} f^{(\beta p)} \left(\sum_{\alpha s} W^{(\alpha s)} (\dot{\gamma}^{(\alpha s)}) \right) +$$

$$\sum_{\beta p} f^{(\beta p)} \left(\sum_{\beta s} W^{(\beta s)} (\dot{f}^{(\beta s)} \gamma_{tw}^{(\beta s)}) \right)$$

(2-86)

The constitutive laws are given by:

$$\overset{\nabla\ (mat)}{\sigma} = \dot{\sigma}^{mat} - \Omega\sigma^{mat} + \sigma^{mat}\Omega = C_{mat}D - \sum_{\alpha p}\left(C_{mat}P^{(\alpha p)} + W^{(\alpha p)}\sigma^{mat} - \sigma^{mat}W^{(\alpha p)}\right)\dot{\gamma}^{(\alpha p)}$$

$$- \sum_{\beta p}\left(C_{mat}P^{(\beta p)} + W^{(\beta p)}\sigma^{mat} - \sigma^{mat}W^{(\beta p)}\right)\dot{f}^{(\beta p)}\gamma_{tw}^{(\beta p)}$$

$$- \sum_{\beta p}f^{(\beta p)}\left(\sum_{\alpha s}\left(C_{mat}P^{(\alpha s)} + W^{(\alpha s)}\sigma^{mat} - \sigma^{mat}W^{(\alpha s)}\right)\dot{\gamma}^{(\alpha s)}\right)$$

$$- \sum_{\beta p}f^{(\beta p)}\left(\sum_{\beta s}\left(C_{mat}P^{(\beta s)} + W^{(\beta s)}\sigma^{mat} - \sigma^{mat}W^{(\beta s)}\right)\dot{f}^{(\beta s)}\gamma_{tw}^{(\beta s)}\right)$$

$$- \sigma^{mat}\left(D_{11} + D_{22} + D_{33}\right)$$

$$(2\text{-}87)$$

$$\overset{\nabla\ (tw1)}{\sigma} = \dot{\sigma}^{tw1} - \Omega\sigma^{tw1} + \sigma^{tw1}\Omega = C_{tw1}D - \sum_{\alpha p}\left(C_{tw1}P^{(\alpha p)} + W^{(\alpha p)}\sigma^{tw1} - \sigma^{tw1}W^{(\alpha p)}\right)\dot{\gamma}^{(\alpha p)}$$

$$- \sum_{\beta p}\left(C_{tw1}P^{(\beta p)} + W^{(\beta p)}\sigma^{tw1} - \sigma^{tw1}W^{(\beta p)}\right)\dot{f}^{(\beta p)}\gamma_{tw}^{(\beta p)}$$

$$- \sum_{\beta p}f^{(\beta p)}\left(\sum_{\alpha s}\left(C_{tw1}P^{(\alpha s)} + W^{(\alpha s)}\sigma^{tw1} - \sigma^{tw1}W^{(\alpha s)}\right)\dot{\gamma}^{(\alpha s)}\right)$$

$$- \sum_{\beta p}f^{(\beta p)}\left(\sum_{\beta s}\left(C_{tw1}P^{(\beta s)} + W^{(\beta s)}\sigma^{tw1} - \sigma^{tw1}W^{(\beta s)}\right)\dot{f}^{(\beta s)}\gamma_{tw}^{(\beta s)}\right)$$

$$- \sigma^{tw1}\left(D_{11} + D_{22} + D_{33}\right)$$

$$(2\text{-}88)$$

$$\overset{\nabla\ (tw2)}{\sigma} = \dot{\sigma}^{tw2} - \Omega\sigma^{tw2} + \sigma^{tw2}\Omega = C_{tw2}D - \sum_{\alpha p}\left(C_{tw2}P^{(\alpha p)} + W^{(\alpha p)}\sigma^{tw2} - \sigma^{tw2}W^{(\alpha p)}\right)\dot{\gamma}^{(\alpha p)}$$

$$- \sum_{\beta p}\left(C_{tw2}P^{(\beta p)} + W^{(\beta p)}\sigma^{tw2} - \sigma^{tw2}W^{(\beta p)}\right)\dot{f}^{(\beta p)}\gamma_{tw}^{(\beta p)}$$

$$- \sum_{\beta p}f^{(\beta p)}\left(\sum_{\alpha s}\left(C_{tw2}P^{(\alpha s)} + W^{(\alpha s)}\sigma^{tw2} - \sigma^{tw2}W^{(\alpha s)}\right)\dot{\gamma}^{(\alpha s)}\right)$$

$$- \sum_{\beta p}f^{(\beta p)}\left(\sum_{\beta s}\left(C_{tw2}P^{(\beta s)} + W^{(\beta s)}\sigma^{tw2} - \sigma^{tw2}W^{(\beta s)}\right)\dot{f}^{(\beta s)}\gamma_{tw}^{(\beta s)}\right)$$

$$- \sigma^{tw2}\left(D_{11} + D_{22} + D_{33}\right)$$

$$(2\text{-}89)$$

where C_{mat} and C_{tw1} are given in Equation (2-20) and (2-44). C_{tw2} is defined by:

$$C_{tw2} = Q^{tw2}Q^{tw2}\overset{\circ}{C}Q^{tw2^T}Q^{tw2^T}$$

(2-90)

Q^{tw2}, the transformation matrix that expresses the lattice orientation in a secondary twinned region with the normal plane, n, and shear direction ,b , respectively, with respect to the global coordinate system is defined as follows:

$$Q^{tw2} = Q \times Q_{tw1}^{mat^{-1}} \times Q_{tw2}^{tw1^{-1}}$$

(2-91)

where Q_{tw1}^{mat} and Q_{tw2}^{tw1} are given in Equations (2-27) and (2-76), respectively.

The evolution of the resistance functions for the primary slip systems is defined by:

$$\dot{g}^{(\alpha p)} = \sum_{\alpha p} h_{\alpha p}^{5A} \left| \dot{\gamma}^{(\alpha p)} \right| + \sum_{\beta p} h_{\beta p}'^{5A} \left| \dot{f}^{(\beta p)} \right|$$

(2-92)

$$h_{\alpha p}^{5A} = h_{\alpha p}^{5A}(\gamma_1)$$

(2-93)

$$h_{\beta p}'^{5A} = h_{\beta p}'^{5A}(f_1)$$

(2-94)

The diagonal terms of the $h_{\alpha p}^{5A}$ matrix represent the slip systems, self-hardening, and off-diagonal terms, latent hardening. $h_{\beta p}'^{5A}$ accounts for the interaction between the primary slip and twinning systems.

The evolution of the resistance of the primary twinning systems is given by:

$$\dot{g}^{(\beta p)} = \sum_{\alpha p} h_{\alpha p}^{5B} \left| \dot{\gamma}^{(\alpha p)} \right| + \sum_{\beta p} h_{\beta p}'^{5B} \left| \dot{f}^{(\beta p)} \right| + \sum_{\alpha s} h_{\alpha s}''^{5B} \left| \dot{\gamma}^{(\alpha s)} \right| + \sum_{\beta s} h_{\beta s}'''^{5B} \left| \dot{f}^{(\beta s)} \right|$$

(2-95)

$$h_{\alpha p}^{5B} = h_{\alpha p}^{5B}(\gamma_1)$$

(2-96)

$$h_{\beta p}'^{5B} = h_{\beta p}'^{5B}(f_1)$$

(2-97)

$$h_{\alpha s}''^{5B} = h_{\alpha s}''^{5B}(\gamma_2)$$

(2-98)

$$h_{\beta s}'''^{5B} = h_{\beta s}'''^{5B}(f_2)$$

(2-99)

$h_{\alpha p}^{5B}$ accounts for the interaction between the primary twinning and primary slip systems, $h_{\alpha s}^{\prime\prime 5B}$ accounts for the interaction between the primary twinning and secondary slip systems, and $h_{\beta s}^{\prime\prime\prime 5B}$ accounts for the interaction between the primary and secondary twinning systems.

The evolution of the resistance functions for the secondary slip systems is defined by:

$$\dot{g}^{(\alpha s)} = \sum_{\beta p} h_{\beta p}^{5C} \left| \dot{f}^{(\beta p)} \right| + \sum_{\alpha s} h_{\alpha s}^{\prime 5C} \left| \dot{\gamma}^{(\alpha s)} \right| + \sum_{\beta s} h_{\beta s}^{\prime\prime 5C} \left| \dot{f}^{(\beta s)} \right| \tag{2-100}$$

$$h_{\beta p}^{5C} = h_{\beta p}^{5C}\left(f_1\right) \tag{2-101}$$

$$h_{\alpha s}^{\prime 5C} = h_{\alpha s}^{\prime 5C}\left(\gamma_2\right) \tag{2-102}$$

$$h_{\beta s}^{\prime\prime 5C} = h_{\beta s}^{\prime\prime 5C}\left(f_2\right) \tag{2-103}$$

The diagonal terms of the $h_{\alpha s}^{\prime 5C}$ matrix represent the slip systems self-hardening, and off-diagonal terms, latent hardening. $h_{\beta p}^{5C}$ accounts for the interaction between the secondary slip and primary twinning systems, and $h_{\beta s}^{\prime\prime 5C}$ accounts for the interaction between the secondary slip and secondary twinning systems.

The growth rate of the volume fraction of the secondary twinned regions is calculated as follows (similar to the primary twinning systems in Equation (2-49)):

$$\dot{f}^{(\beta s)} = \frac{\dot{a}^{(\beta s)}}{\gamma_{tw}} \left[\frac{\sigma^{(\beta s)}}{g^{(\beta s)}} \right] \left[\left| \frac{\sigma^{(\beta s)}}{g^{(\beta s)}} \right| \right]^{\left(\frac{1}{m}\right)-1} \tag{2-104}$$

$$\sigma^{(\beta s)} = P^{(\beta s)} : \sigma^{ave(\beta p, \beta s)} \tag{2-105}$$

where $\sigma^{ave(\beta p, \beta s)}$ is the volumetric average of the stresses in the primary and secondary twinned regions (two regions that lie on the two sides of the twinning plane) used to calculate the RSS $\sigma^{(\beta s)}$ on the twinning plane. Equation (2-104) is used to calculate the volume fraction rate of the secondary twinning systems in the next step of the model as well.

The evolution of the resistance of the secondary twinning systems is given by:

$$\dot{g}^{(\beta s)} = \sum_{\beta p} h_{\beta p}^{5D} \left| \dot{f}^{(\beta p)} \right| + \sum_{\alpha s} h_{\alpha s}'^{5D} \left| \dot{\gamma}^{(\alpha s)} \right| + \sum_{\beta s} h_{\beta s}''^{5D} \left| \dot{f}^{(\beta s)} \right| \qquad (2\text{-}106)$$

$$h_{\beta p}^{5D} = h_{\beta p}^{5D} \left(f_1 \right) \qquad (2\text{-}107)$$

$$h_{\alpha s}'^{5D} = h_{\alpha s}'^{5D} \left(\gamma_2 \right) \qquad (2\text{-}108)$$

$$h_{\beta s}''^{5D} = h_{\beta s}''^{5D} \left(f_2 \right) \qquad (2\text{-}109)$$

$h_{\beta p}^{5D}$ accounts for the interaction between the secondary twinning and primary twinning systems and $h_{\alpha s}'^{5D}$ accounts for the interaction between the secondary twinning and secondary slip systems. γ_1 is defined by Equation (2-25), f_1 by Equation (2-54), γ_2 by Equation (2-70), and f_2 by:

$$f_2 = \sum_{\beta s} f^{(\beta s)} \qquad (2\text{-}110)$$

Following Kalidindi's approach [22], the total stress in the grain is equal to the volumetric average of the stresses in the parent, primary and secondary twinned regions:

$$\tau_{tot} = \left(1 - \sum_{\beta p} f^{\beta p} \right) \sigma^{mat} + \sum_{\beta p} f^{\beta p} \left(\left(1 - \sum_{\beta s} f^{\beta s} \right) \sigma^{\beta p} + \sum_{\beta s} \left(f^{\beta s} \sigma^{\beta s} \right) \right) \qquad (2\text{-}111)$$

2.2.5 Equations corresponding to step 6 of the crystal plasticity constitutive model

In step 6 of the proposed CPCM, nucleation of the tertiary slip systems inside the secondary twinned regions is allowed. The same deformation field is assumed to exist over the parent, primary and secondary twinned regions. Also, Equations (2-1)-(2-13), (2-15), (2-16), (2-20)-(2-22), (2-25), (2-27)-(2-36), (2-38),(2-39), (2-44), (2-49),(2-50), (2-54), (2-57),(2-58), (2-70)-(2-72), (2-76)-(2-81), (2-83), (2-84), (2-90), (2-104), (2-105), (2-110), and (2-111) are valid for step 6 of the model. Interactions between the resistances of the primary slip, primary twinning, secondary slip, secondary twinning, and tertiary slip systems were enforced and are highlighted later in the Equations (2-120), (2-123), (2-128), (2-132), and (2-139).

L^P has contributions from the primary, secondary, and tertiary slip systems, as well as the primary and secondary twinning systems, and is defined as follows:

$$L^p = \sum_{\alpha p} s^{*(\alpha p)} \otimes m^{*(\alpha p)} \dot{\gamma}^{(\alpha p)} + \sum_{\beta p} s^{*(\beta p)} \otimes m^{*(\beta p)} (\dot{f}^{(\beta p)} \gamma_{tw}^{(\beta p)}) + \sum_{\beta p} f^{(\beta p)} \left(\sum_{\alpha s} s^{*(\alpha s)} \otimes m^{*(\alpha s)} (\dot{\gamma}^{(\alpha s)}) \right)$$

$$+ \sum_{\beta p} f^{(\beta p)} \left(\sum_{\beta s} s^{*(\beta s)} \otimes m^{*(\beta s)} (\dot{f}^{(\beta s)} \gamma_{tw}^{(\beta s)}) \right) + \sum_{\beta p} f^{(\beta p)} \left(\sum_{\beta s} f^{(\beta s)} \left(\sum_{\alpha t} s^{*(\alpha t)} \otimes m^{*(\alpha t)} (\dot{\gamma}^{(\alpha t)}) \right) \right)$$

$$(2\text{-}112)$$

For each tertiary slip system (αt), the symmetric tensor, $P^{(\alpha t)}$, and antisymmetric tensor, $W^{(\alpha t)}$, are defined as follows:

$$P^{(\alpha t)} = \frac{1}{2} (s^{*(\alpha t)} \otimes m^{*(\alpha t)} + m^{*(\alpha t)} \otimes s^{*(\alpha t)}) \tag{2-113}$$

$$W^{(\alpha t)} = \frac{1}{2} (s^{*(\alpha t)} \otimes m^{*(\alpha t)} - m^{*(\alpha t)} \otimes s^{*(\alpha t)}) \tag{2-114}$$

The plastic part of the deformation rate and spin are related to the plastic part of the velocity gradient as follows:

$$D^p = sym(L^p) = \sum_{\alpha p} P^{(\alpha p)} \dot{\gamma}^{(\alpha p)} + \sum_{\beta p} P^{(\beta p)} (\dot{f}^{(\beta p)} \gamma_{tw}^{(\beta p)}) + \sum_{\beta p} f^{(\beta p)} \left(\sum_{\alpha s} P^{(\alpha s)} (\dot{\gamma}^{(\alpha s)}) \right)$$

$$+ \sum_{\beta p} f^{(\beta p)} \left(\sum_{\beta s} P^{(\beta s)} (\dot{f}^{(\beta s)} \gamma_{tw}^{(\beta s)}) \right) + \sum_{\beta p} f^{(\beta p)} \left(\sum_{\beta s} f^{(\beta s)} \left(\sum_{\alpha t} P^{(\alpha t)} (\dot{\gamma}^{(\alpha t)}) \right) \right)$$

$$(2\text{-}115)$$

$$\Omega^p = asym(L^p) = \sum_{\alpha p} W^{(\alpha p)} \dot{\gamma}^{(\alpha p)} + \sum_{\beta p} W^{(\beta p)} (\dot{f}^{(\beta p)} \gamma_{tw}^{(\beta p)}) + \sum_{\beta p} f^{(\beta p)} \left(\sum_{\alpha s} W^{(\alpha s)} (\dot{\gamma}^{(\alpha s)}) \right)$$

$$+ \sum_{\beta p} f^{(\beta p)} \left(\sum_{\beta s} W^{(\beta s)} (\dot{f}^{(\beta s)} \gamma_{tw}^{(\beta s)}) \right) + \sum_{\beta p} f^{(\beta p)} \left(\sum_{\beta s} f^{(\beta s)} \left(\sum_{\alpha t} W^{(\alpha t)} (\dot{\gamma}^{(\alpha t)}) \right) \right)$$

$$(2\text{-}116)$$

The constitutive laws are given by:

$$\overset{\triangledown\,(mat)}{\sigma} = \dot{\sigma}^{mat} - \Omega\sigma^{mat} + \sigma^{mat}\Omega = C_{mat}D - \sum_{\alpha p}\left(C_{mat}P^{(\alpha p)} + W^{(\alpha p)}\sigma^{mat} - \sigma^{mat}W^{(\alpha p)}\right)\dot{\gamma}^{(\alpha p)}$$

$$-\sum_{\beta p}\left(C_{mat}P^{(\beta p)} + W^{(\beta p)}\sigma^{mat} - \sigma^{mat}W^{(\beta p)}\right)\dot{f}^{(\beta p)}\gamma_{tw}^{(\beta p)}$$

$$-\sum_{\beta p}f^{(\beta p)}\left(\sum_{\alpha s}\left(C_{mat}P^{(\alpha s)} + W^{(\alpha s)}\sigma^{mat} - \sigma^{mat}W^{(\alpha s)}\right)\dot{\gamma}^{(\alpha s)}\right)$$

$$-\sum_{\beta p}f^{(\beta p)}\left(\sum_{\beta s}\left(C_{mat}P^{(\beta s)} + W^{(\beta s)}\sigma^{mat} - \sigma^{mat}W^{(\beta s)}\right)\dot{f}^{(\beta s)}\gamma_{tw}^{(\beta s)}\right)$$

$$-\sum_{\beta p}f^{(\beta p)}\left(\sum_{\beta s}f^{(\beta s)}\left(\sum_{\alpha t}\left(C_{mat}P^{(\alpha t)} + W^{(\alpha t)}\sigma^{mat} - \sigma^{mat}W^{(\alpha t)}\right)\dot{\gamma}^{(\alpha t)}\right)\right)$$

$$-\sigma^{mat}\left(D_{11} + D_{22} + D_{33}\right)$$

$$(2\text{-}117)$$

$$\overset{\triangledown\,(tw1)}{\sigma} = \dot{\sigma}^{tw1} - \Omega\sigma^{tw1} + \sigma^{tw1}\Omega = C_{tw1}D - \sum_{\alpha p}\left(C_{tw1}P^{(\alpha p)} + W^{(\alpha p)}\sigma^{tw1} - \sigma^{tw1}W^{(\alpha p)}\right)\dot{\gamma}^{(\alpha p)}$$

$$-\sum_{\beta p}\left(C_{tw1}P^{(\beta p)} + W^{(\beta p)}\sigma^{tw1} - \sigma^{tw1}W^{(\beta p)}\right)\dot{f}^{(\beta p)}\gamma_{tw}^{(\beta p)}$$

$$-\sum_{\beta p}f^{(\beta p)}\left(\sum_{\alpha s}\left(C_{tw1}P^{(\alpha s)} + W^{(\alpha s)}\sigma^{tw1} - \sigma^{tw1}W^{(\alpha s)}\right)\dot{\gamma}^{(\alpha s)}\right)$$

$$-\sum_{\beta p}f^{(\beta p)}\left(\sum_{\beta s}\left(C_{tw1}P^{(\beta s)} + W^{(\beta s)}\sigma^{tw1} - \sigma^{tw1}W^{(\beta s)}\right)\dot{f}^{(\beta s)}\gamma_{tw}^{(\beta s)}\right)$$

$$-\sum_{\beta p}f^{(\beta p)}\left(\sum_{\beta s}f^{(\beta s)}\left(\sum_{\alpha t}\left(C_{tw1}P^{(\alpha t)} + W^{(\alpha t)}\sigma^{tw1} - \sigma^{tw1}W^{(\alpha t)}\right)\dot{\gamma}^{(\alpha t)}\right)\right)$$

$$-\sigma^{tw1}\left(D_{11} + D_{22} + D_{33}\right)$$

$$(2\text{-}118)$$

$$\overset{\triangledown (tw2)}{\sigma} = \dot{\sigma}^{tw2} - \Omega\sigma^{tw2} + \sigma^{tw2}\Omega = C_{tw2}D - \sum_{\alpha p}\left(C_{tw2}P^{(\alpha p)} + W^{(\alpha p)}\sigma^{tw2} - \sigma^{tw2}W^{(\alpha p)}\right)\dot{\gamma}^{(\alpha p)}$$

$$- \sum_{\beta p}\left(C_{tw2}P^{(\beta p)} + W^{(\beta p)}\sigma^{tw2} - \sigma^{tw2}W^{(\beta p)}\right)\dot{f}^{(\beta p)}\gamma_{tw}^{(\beta p)}$$

$$- \sum_{\beta p}f^{(\beta p)}\left(\sum_{\alpha s}\left(C_{tw2}P^{(\alpha s)} + W^{(\alpha s)}\sigma^{tw2} - \sigma^{tw2}W^{(\alpha s)}\right)\dot{\gamma}^{(\alpha s)}\right)$$

$$- \sum_{\beta p}f^{(\beta p)}\left(\sum_{\beta s}\left(C_{tw2}P^{(\beta s)} + W^{(\beta s)}\sigma^{tw2} - \sigma^{tw2}W^{(\beta s)}\right)\dot{f}^{(\beta s)}\gamma_{tw}^{(\beta s)}\right)$$

$$- \sum_{\beta p}f^{(\beta p)}\left(\sum_{\beta s}f^{(\beta s)}\left(\sum_{\alpha t}\left(C_{tw2}P^{(\alpha t)} + W^{(\alpha t)}\sigma^{tw2} - \sigma^{tw2}W^{(\alpha t)}\right)\dot{\gamma}^{(\alpha t)}\right)\right)$$

$$- \sigma^{tw2}\left(D_{11} + D_{22} + D_{33}\right)$$

<div align="right">(2-119)</div>

where C_{mat}, C_{tw1}, and C_{tw2} are defined by Equations (2-20), (2-44), and (2-90), respectively.

The evolution of the resistance functions for the primary slip systems is defined by:

$$\dot{g}^{(\alpha p)} = \sum_{\alpha p}h_{\alpha p}^{6A}\left|\dot{\gamma}^{(\alpha p)}\right| + \sum_{\beta p}h_{\beta p}^{\prime 6A}\left|\dot{f}^{(\beta p)}\right| \tag{2-120}$$

$$h_{\alpha p}^{6A} = h_{\alpha p}^{6A}\left(\gamma_1\right) \tag{2-121}$$

$$h_{\beta p}^{\prime 6A} = h_{\beta p}^{\prime 6A}\left(f_1\right) \tag{2-122}$$

The diagonal terms of the $h_{\alpha p}^{6A}$ matrix represent the slip systems, self-hardening, and off-diagonal terms, latent hardening. $h_{\beta p}^{\prime 6A}$ accounts for the interaction between the primary slip and twinning systems.

The evolution of the resistance of the primary twinning systems is given by:

$$\dot{g}^{(\beta p)} = \sum_{\alpha p}h_{\alpha p}^{6B}\left|\dot{\gamma}^{(\alpha p)}\right| + \sum_{\beta p}h_{\beta p}^{\prime 6B}\left|\dot{f}^{(\beta p)}\right| + \sum_{\alpha s}h_{\alpha s}^{\prime\prime 6B}\left|\dot{\gamma}^{(\alpha s)}\right| + \sum_{\beta s}h_{\beta s}^{\prime\prime\prime 6B}\left|\dot{f}^{(\beta s)}\right| \tag{2-123}$$

$$h_{\alpha p}^{6B} = h_{\alpha p}^{6B}\left(\gamma_1\right) \tag{2-124}$$

$$h_{\beta p}^{\prime 6B} = h_{\beta p}^{\prime 6B}\left(f_1\right) \tag{2-125}$$

$$h_{\alpha s}^{\prime\prime 6B} = h_{\alpha s}^{\prime\prime 6B}\left(\gamma_2\right) \tag{2-126}$$

$$h_{\beta s}^{\prime\prime\prime 6B} = h_{\beta s}^{\prime\prime\prime 6B}\left(f_2\right) \tag{2-127}$$

$h_{\alpha p}^{6B}$ accounts for the interaction between the primary twinning and primary slip systems, $h_{\alpha s}^{\prime\prime 6B}$ accounts for the interaction between the primary twinning and secondary slip systems, and $h_{\beta s}^{\prime\prime\prime 6B}$ accounts for the interaction between the primary twinning and secondary twinning systems.

The evolution of the resistance of the secondary slip systems is given by:

$$\dot{g}^{(\alpha s)} = \sum_{\beta p} h_{\beta p}^{C}\left|\dot{f}^{(\beta p)}\right| + \sum_{\alpha s} h_{\alpha s}^{\prime C}\left|\dot{\gamma}^{(\alpha s)}\right| + \sum_{\beta s} h_{\beta s}^{\prime\prime C}\left|\dot{f}^{(\beta s)}\right| \tag{2-128}$$

$$h_{\beta p}^{6C} = h_{\beta p}^{6C}\left(f_1\right) \tag{2-129}$$

$$h_{\alpha s}^{\prime 6C} = h_{\alpha s}^{\prime 6C}\left(\gamma_2\right) \tag{2-130}$$

$$h_{\beta s}^{\prime\prime 6C} = h_{\beta s}^{\prime\prime 6C}\left(f_2\right) \tag{2-131}$$

The diagonal terms of the $h_{\alpha s}^{\prime 6C}$ matrix represent the slip systems, self-hardening, and off-diagonal terms, latent hardening. $h_{\beta p}^{6C}$ accounts for the interaction between the secondary slip and primary twinning systems, and $h_{\beta s}^{\prime\prime 6C}$ accounts for the interaction between the secondary slip and secondary twinning systems.

The evolution of the resistance of the secondary twinning systems is given by:

$$\dot{g}^{(\beta s)} = \sum_{\beta p} h_{\beta p}^{6D}\left|\dot{f}^{(\beta p)}\right| + \sum_{\alpha s} h_{\alpha s}^{\prime 6D}\left|\dot{\gamma}^{(\alpha s)}\right| + \sum_{\beta s} h_{\beta s}^{\prime\prime 6D}\left|\dot{f}^{(\beta s)}\right| + \sum_{\alpha t} h_{\alpha t}^{\prime\prime\prime 6D}\left|\dot{\gamma}^{(\alpha t)}\right| \tag{2-132}$$

$$h_{\beta p}^{6D} = h_{\beta p}^{6D}\left(f_1\right) \tag{2-133}$$

$$h_{\alpha s}^{\prime 6D} = h_{\alpha s}^{\prime 6D}\left(\gamma_2\right) \tag{2-134}$$

$$h_{\beta s}^{\prime\prime 6D} = h_{\beta s}^{\prime\prime 6D}\left(f_2\right) \tag{2-135}$$

$$h_{\alpha t}^{\prime\prime\prime 6D} = h_{\alpha t}^{\prime\prime\prime 6D}\left(\gamma_3\right) \tag{2-136}$$

$h_{\beta p}^{6D}$ accounts for the interaction between the secondary twinning and primary twinning systems, $h_{\alpha s}^{\prime 6D}$ accounts for the interaction between the secondary twinning and secondary slip systems, and $h_{\alpha t}^{\prime\prime 6D}$ accounts for the interaction between the secondary twinning and tertiary slip systems.

The evolution of the shear strain on the tertiary slip systems is calculated as follows (similar to the primary and secondary slip systems in Equations (2-21) and (2-71), respectively):

$$\dot{\gamma}^{(\alpha t)} = \dot{a}^{(\alpha t)} \left[\frac{\sigma^{(\alpha t)}}{g^{(\alpha t)}} \right] \left[\left| \frac{\sigma^{(\alpha t)}}{g^{(\alpha t)}} \right| \right]^{\left(\frac{1}{m}\right)-1} \tag{2-137}$$

$$\sigma^{(\alpha t)} = P^{(\alpha t)} : \sigma^{tw2} \tag{2-138}$$

The evolution of the resistance of the tertiary slip systems is given by:

$$\dot{g}^{(\alpha t)} = \sum_{\beta s} h_{\beta s}^{6E} \left| \dot{f}^{(\beta s)} \right| + \sum_{\alpha t} h_{\alpha t}^{\prime 6E} \left| \dot{\gamma}^{(\alpha t)} \right| \tag{2-139}$$

$$h_{\beta s}^{6E} = h_{\beta s}^{6E}(f_2) \tag{2-140}$$

$$h_{\alpha t}^{\prime 6E} = h_{\alpha t}^{\prime 6E}(\gamma_3) \tag{2-141}$$

The diagonal terms of the $h_{\alpha t}^{\prime 6E}$ matrix represent the slip systems, self-hardening, and off-diagonal terms, latent hardening. $h_{\beta s}^{6E}$ accounts for the interaction between the tertiary slip and secondary twinning systems. γ_1, f_1, γ_2, f_2 are defined by Equations (2-25), (2-54), (2-70), and (2-110), respectively. γ_3 is defined by:

$$\gamma_3 = \sum_{\alpha t} \gamma^{(\alpha t)} \tag{2-142}$$

The total stress in the grain is calculated by Equation (2-111).

2.2.6 Resistance evolution functions and their dependency on the rate of slip and twinning systems

Separate resistance evolution functions for the primary slip (for step 1 in Equation (2-23), step 2 in Equation (2-46), steps 3-4 in Equation (2-63), step 5 in Equation (2-92), and step 6 in Equation (2-120)), secondary slip (for steps 3-4 in Equation (2-73), step 5 in Equation (2-100), and step 6 in Equation (2-

128)), and tertiary slip systems (for step 6 in Equation (2-139)), as well as primary twinning (for step 2 in Equation (2-51), steps 3-4 in Equation (2-66), step 5 in Equation (2-95), and step 6 in Equation (2-123)) and secondary twinning systems (for step 5 in Equation (2-106) and step 6 in Equation (2-132)) were considered. The h_x^{ij} functions where $x = \alpha p, \alpha s, \alpha t, \beta p, \beta s$, $i = 1,\ldots,6$, and $j = A, B,\ldots,D, E$ (for example in (2-24), (2-107), and (2-140)) can, in general, be any function that approaches zero rather quickly. Examples of these functions are found in Peirce et al. [53]. In step 1, it is assumed that the rate of resistance of a primary slip system (Equation (2-23)) is a function of the rate of shear on the primary slip systems. In the step 2, it is assumed that the rate of resistance of a primary slip system (Equation (2-46)) is a function of the rate of shear on the primary slip systems, and rate of change of volume fractions of primary twinning systems. The same holds true for the rate of change of resistances of the primary twinning systems (Equation (2-51)). These assumptions allow for the modelling of the interaction between primary slip and twinning systems. The evolution of the resistance functions in steps 3-4 are given by Equations (2-63), (2-66), and (2-73), for step 5 by Equations (2-92), (2-95), (2-100), and (2-106), and for step 6 by Equations (2-120), (2-123), (2-128), (2-132), and (2-139). The goal behind all of these assumed rate of change of resistance functions in all of the six steps is to allow interaction between different slip and twinning systems in the simplest yet comprehensive mathematical form. It is noted that regardless of the choice of h_x^{ij} functions, this formulation provides reasonable relations between the rate of change of resistance functions and the rate of slip and twinning systems at different regions of the grain (parent and twinned).

2.2.7 Proof of the constitutive equations

The following constitutive equation is valid for the parent region [30,53]:

$$\overset{*\nabla(mat)}{\tau} = C_{mat}D^*$$
(2-143)

where the lattice Jaumann rate of Cauchy stress is related to the elastic part of the strain rate through the elastic moduli in the parent region.

Similarly, the following constitutive equations can be written for the primary and secondary twinned regions:

$$\overset{*\nabla(tw1)}{\tau} = C_{tw1}D^*$$
(2-144)

$$\overset{*\nabla(tw2)}{\tau} = C_{tw2}D^*$$
(2-145)

Peirce et al. [30] showed how Equation (2-19) can be obtained from the Equation (2-143) above.

Here, we show how Equations (2-42) and (2-43) (for the step 2 of the CPCM), can be obtained from Equations (2-144) and (2-145) above, respectively. The other constitutive equations in the other steps can be derived in a similar manner.

In the step 2 of the proposed CPCM, L^p is defined as (identical to what Kalidindi [22] considered):

$$L^p = \sum_{\alpha p} s^{*(\alpha p)} \otimes m^{*(\alpha p)} \dot{\gamma}^{(\alpha p)} + \sum_{\beta p} s^{*(\beta p)} \otimes m^{*(\beta p)} (\dot{f}^{(\beta p)} \gamma_{tw}^{(\beta p)}) \tag{2-146}$$

Based on this, the following can be written:

$$D^p = \sum_{\alpha p} P^{(\alpha p)} \dot{\gamma}^{(\alpha p)} + \sum_{\beta p} P^{(\beta p)} (\dot{f}^{(\beta p)} \gamma_{tw}^{(\beta p)}) \tag{2-147}$$

$$\Omega^p = \sum_{\alpha p} W^{(\alpha p)} \dot{\gamma}^{(\alpha p)} + \sum_{\beta p} W^{(\beta p)} (\dot{f}^{(\beta p)} \gamma_{tw}^{(\beta p)}) \tag{2-148}$$

And finally considering Equations (2-4) and (2-5), as well as the following general relationships:

$$\overset{*\nabla}{\sigma} = \dot{\sigma} - \Omega^* \sigma + \sigma \Omega^* \tag{2-149}$$

$$\overset{\nabla}{\sigma} = \dot{\sigma} - \Omega \sigma + \sigma \Omega \tag{2-150}$$

Equations (2-42) and (2-43) can be derived from Equations (2-144) and (2-145).

2.2.8 Constitutive model limitation

A more accurate constitutive model does not assume the same deformation gradient for the parent, primary and secondary twinned regions (Taylor [8] assumptions). However, it considers individual deformation gradients for each region. Such a constitutive model should be implemented in a finite element code where the parent, primary and secondary twinned regions are included in different elements (because each region has a separate deformation gradient). In order to develop such a model, metallurgical information on the twin's nucleation sites and their growth pattern would be necessary. Clearly, the number of equations and state variables, as well as computational time for such a model would be much more compared to the proposed model in this thesis.

2.3 Integration procedure of the proposed crystal plasticity constitutive model

The numerical integration of the proposed CPCM can be accomplished by an explicit or implicit integration method. A very good discussion about different integration approaches for crystal plasticity constitutive equations was presented by Ling et al. [54]. Li et al. [55] developed an efficient implicit integration method (Homotopy Continuation), however, its implementation is rather difficult. Raphanel et al. [56] used the Runge-Kutta integration method to explicitly integrate the CPCM. Kuchnicki et al. [57] recast an implicit integration algorithm into an explicit one (subcycling algorithm), and by this method, they accelerated the integration procedure. However, the higher computational speed of their method comes at the cost of more complex implementation.

After exploring the available integration methods, for the sake of simplicity, the explicit forward Euler integration procedure proposed in [58] was adopted in this work. The integration procedure is based on the updated Lagrangian crystal plasticity framework, and was developed to incorporate the CPCM in a VUMAT in an explicit finite element code. While their integration method considers slip as the only deformation mechanism, it can be easily extended to apply to the crystal plasticity formulation that considers both slip and twinning plastic deformation mechanisms. In their procedure, the forward Euler algorithm was used to integrate the equations. The basic idea behind this algorithm is to use the slip rates per slip system and the volume fraction rates per twinning system at time $t_{(n)}$ to compute quantities for time $t_{(n+1)}$.

The proposed CPCM in this thesis evolves in a sequential manner. In the case that the primary slip systems in the parent are the only deformation mechanisms (i.e. step 1), the integration procedure in [58] can be used directly without any modification to calculate the stresses in the grain. For steps 2-6, where deformation occurs due to twinning as well, the integration procedure in [58] were modified. The integration procedures for steps 2-6 are similar, and for the step 2, the integration procedure is outlined below.

- Subroutine passes $F_{(n+1)}$, $F_{(n)}$, $\Delta F_{(n)}^{*}$, $\gamma_{(n)}^{\alpha p}$, $g_{(n)}^{\alpha p}$, $f_{(n)}^{\beta p}$, $g_{(n)}^{\beta p}$, $\sigma_{(n)}^{mat}$, $\sigma_{(n)}^{tw1}$, $Q_{(n)}$, $\varphi_{(n)}^{1}$ $\varphi_{(n)}$ $\varphi_{(n)}^{2}$, Δt

- Computing deformation and spin variables for $t_{(n+\frac{1}{2})}$:

$$\dot{F}_{(n+\frac{1}{2})} = \left(\frac{F_{(n+1)} - F_{(n)}}{\Delta t} \right) \tag{2-151}$$

$$L_{(n+\frac{1}{2})} = \dot{F}_{(n+\frac{1}{2})} \left(\frac{F_{(n)} + F_{(n+1)}}{2} \right)^{-1} \tag{2-152}$$

38

$$D_{(n+\frac{1}{2})} = sym\left(L_{(n+\frac{1}{2})}\right) \tag{2-153}$$

$$\Omega_{(n+\frac{1}{2})} = asym\left(L_{(n+\frac{1}{2})}\right) \tag{2-154}$$

- Updating the lattice vectors and P and W:

$$s_{(n)}^{*(\alpha p)} = \Delta F_{(n)}^{*} Q_{(n)} s_{(1)}^{(\alpha p)} \tag{2-155}$$

$$s_{(n)}^{*(\beta p)} = \Delta F_{(n)}^{*} Q_{(n)} s_{(1)}^{(\beta p)} \tag{2-156}$$

$$m_{(n)}^{*(\alpha p)} = Q_{(n)} m_{(1)}^{(\alpha p)} \Delta F_{(n)}^{*-1} \tag{2-157}$$

$$m_{(n)}^{*(\beta p)} = Q_{(n)} m_{(1)}^{(\beta p)} \Delta F_{(n)}^{*-1} \tag{2-158}$$

$$P_{(n)}^{(\alpha p)} = \frac{1}{2}(s_{(n)}^{*(\alpha p)} \otimes m_{(n)}^{*(\alpha p)} + m_{(n)}^{*(\alpha p)} \otimes s_{(n)}^{*(\alpha p)}) \tag{2-159}$$

$$W_{(n)}^{(\alpha p)} = \frac{1}{2}(s_{(n)}^{*(\alpha p)} \otimes m_{(n)}^{*(\alpha p)} - m_{(n)}^{*(\alpha p)} \otimes s_{(n)}^{*(\alpha p)}) \tag{2-160}$$

$$P_{(n)}^{(\beta p)} = \frac{1}{2}(s_{(n)}^{*(\beta p)} \otimes m_{(n)}^{*(\beta p)} + m_{(n)}^{*(\beta p)} \otimes s_{(n)}^{*(\beta p)}) \tag{2-161}$$

$$W_{(n)}^{(\beta p)} = \frac{1}{2}(s_{(n)}^{*(\beta p)} \otimes m_{(n)}^{*(\beta p)} - m_{(n)}^{*(\beta p)} \otimes s_{(n)}^{*(\beta p)}) \tag{2-162}$$

- Calculating the slip shear strain rates at time $t_{(n)}$ using the stress state and $P_{(n)}^{\alpha p}$, and the volume fraction rates at time $t_{(n)}$ using the stress state and $P_{(n)}^{\beta p}$:

$$\sigma_{(n)}^{(\alpha p)} = P_{(n)}^{(\alpha p)} : \sigma_{(n)}^{mat} \tag{2-163}$$

$$\dot{\gamma}_{(n)}^{(\alpha p)} = \dot{\gamma}_{\circ} \, \mathrm{sgn}(\sigma_{(n)}^{(\alpha p)}) \left| \frac{\sigma_{(n)}^{(\alpha p)}}{g_{(n)}^{(\alpha p)}} \right|^{\left(\frac{1}{m}\right)-1} \tag{2-164}$$

$$\sigma_{(n)}^{ave(mat,tw1)} = \left(1 - \sum_{\beta p} f_{(n)}^{\beta p}\right) \sigma_{(n)}^{mat} + f_{(n)}^{tw1} \sigma_{(n)}^{tw1} \tag{2-165}$$

$$\sigma_{(n)}^{(\beta p)} = P_{(n)}^{(\beta p)} : \sigma_{(n)}^{ave(mat,\beta p)} \tag{2-166}$$

$$\dot{f}_{(n)}^{(\beta p)} = \frac{\dot{f}_{\circ}}{\gamma_{tw}^{(\beta p)}} \, \mathrm{sgn}(\sigma_{(n)}^{(\beta p)}) \left| \frac{\sigma_{(n)}^{(\beta p)}}{g_{(n)}^{(\beta p)}} \right|^{\left(\frac{1}{m}\right)-1} \tag{2-167}$$

- Computing the total shear strain on the slip systems, volume fraction of the twinned regions, and resistance of the slip and twinning systems all at time $t_{(n+1)}$:

$$\gamma_{(n+1)}^{(\alpha p)} = \gamma_{(n)}^{(\alpha p)} + \sum_{\alpha p} \left| \dot{\gamma}_{(n)}^{(\alpha p)} \right| \Delta t \tag{2-168}$$

$$f_{(n+1)}^{(\beta p)} = f_{(n)}^{(\beta p)} + \sum_{\beta p} \left| \dot{f}_{(n)}^{(\beta p)} \right| \Delta t \tag{2-169}$$

$$g_{(n+1)}^{(\alpha p)} = g_{(n)}^{(\alpha p)} + \sum_{\alpha p} h_{\alpha p(n)}^{2A} \left| \dot{\gamma}_{(n)}^{(\alpha p)} \right| \Delta t + \sum_{\beta p} h_{\beta p(n)}^{\prime 2A} \left| \dot{f}_{(n)}^{(\beta p)} \right| \Delta t \tag{2-170}$$

$$g_{(n+1)}^{(\beta p)} = g_{(n)}^{(\beta p)} + \sum_{\alpha p} h_{\alpha p(n)}^{2B} \left| \dot{\gamma}_{(n)}^{(\alpha p)} \right| \Delta t + \sum_{\beta p} h_{\beta p(n)}^{\prime 2B} \left| \dot{f}_{(n)}^{(\beta p)} \right| \Delta t \tag{2-171}$$

- Updating the elasticity modulus:

$$C_{mat(n)} = Q_{(n)} Q_{(n)} \overset{\circ}{C} Q_{(n)}^{T} Q_{(n)}^{T} \tag{2-172}$$

$$Q_{(n)}^{tw1} = Q_{(n)} \times (X^{-1} R X)^{-1} \tag{2-173}$$

$$C_{tw1(n)} = Q_{(n)}^{tw1} Q_{(n)}^{tw1} \overset{\circ}{C} Q_{(n)}^{tw1^T} Q_{(n)}^{tw1^T} \tag{2-174}$$

- Updating the orientation matrix, Q, and Bunge angles [59]:

$$\Omega_{(n)}^{p} = \sum_{\alpha p} W_{(n)}^{(\alpha p)} \dot{\gamma}_{(n)}^{(\alpha p)} + \sum_{\beta p} W_{(n)}^{(\beta p)} \dot{f}_{(n)}^{(\beta p)} \gamma_{tw}^{(\beta p)} \tag{2-175}$$

$$\Omega^{*}_{(n+\frac{1}{2})} = \Omega_{(n+\frac{1}{2})} - \Omega_{(n)}^{p} \tag{2-176}$$

$$Q_{(n+1)} = e^{\left(\Omega^{*}_{(n+\frac{1}{2})}.\Delta t\right)} Q_{(n)} \tag{2-177}$$

$$Q = \begin{bmatrix} Q_{11} & Q_{12} & Q_{13} \\ Q_{21} & Q_{22} & Q_{23} \\ Q_{31} & Q_{32} & Q_{33} \end{bmatrix} \tag{2-178}$$

where from Bunge [59]:

$$Q_{11} = \cos(\varphi_2)\cos(\varphi_1) - \sin(\varphi_2)\sin(\varphi_1)\cos(\varphi) \tag{2-179}$$

$$Q_{12} = -\sin(\varphi_2)\cos(\varphi_1) - \cos(\varphi_2)\sin(\varphi_1)\cos(\varphi) \tag{2-180}$$

$$Q_{13} = \sin(\varphi_1)\sin(\varphi) \tag{2-181}$$

$$Q_{21} = \cos(\varphi_2)\sin(\varphi_1) + \sin(\varphi_2)\cos(\varphi_1)\cos(\varphi) \tag{2-182}$$

$$Q_{22} = -\sin(\varphi_2)\sin(\varphi_1) + \cos(\varphi_2)\cos(\varphi_1)\cos(\varphi) \tag{2-183}$$

$$Q_{23} = -\cos(\varphi_1)\sin(\varphi) \tag{2-184}$$

$$Q_{31} = \sin(\varphi_2)\sin(\varphi) \tag{2-185}$$

$$Q_{32} = \cos(\varphi_2)\sin(\varphi) \tag{2-186}$$

$$Q_{33} = \cos(\varphi) \tag{2-187}$$

$$Q_{(n+1)} \rightarrow \varphi^1_{(n+1)}, \varphi_{(n+1)}, \varphi^2_{(n+1)} \tag{2-188}$$

- Updating the stress in the parent, primary twinned region, and the whole grain [60]:

$$\Lambda^{(n+1)}_{(n)} = e^{\left(\Omega_{(n+\frac{1}{2})} \cdot \Delta t \right)} \tag{2-189}$$

$$\Lambda^{(n+\frac{1}{2})}_{(n)} = e^{\left(\Omega_{(n+\frac{1}{2})} \cdot \left(\frac{\Delta t}{2} \right) \right)} \tag{2-190}$$

$$\overset{\nabla}{\sigma}^{(mat)}_{(n+\frac{1}{2})} = C_{mat(n)} D_{(n+\frac{1}{2})} - \sum_{\alpha p} \left(C_{mat(n)} P^{(\alpha p)}_{(n)} + W^{(\alpha p)}_{(n)} \sigma^{mat}_{(n)} - \sigma^{mat}_{(n)} W^{(\alpha p)}_{(n)} \right) \dot{\gamma}^{(\alpha p)}_{(n)}$$
$$- \sum_{\beta p} \left(C_{mat(n)} P^{(\beta p)}_{(n)} + W^{(\beta p)}_{(n)} \sigma^{mat}_{(n)} - \sigma^{mat}_{(n)} W^{(\beta p)}_{(n)} \right) \dot{f}^{(\beta p)}_{(n)} \gamma^{(\beta p)}_{tw}$$
$$- \sigma^{mat}_{(n)} (D_{11(n+\frac{1}{2})} + D_{22(n+\frac{1}{2})} + D_{33(n+\frac{1}{2})})$$

$$\tag{2-191}$$

$$\overset{\nabla}{\sigma}^{(tw1)}_{(n+\frac{1}{2})} = C_{tw1(n)} D_{(n+\frac{1}{2})} - \sum_{\alpha p} \left(C_{tw1(n)} P^{(\alpha p)}_{(n)} + W^{(\alpha p)}_{(n)} \sigma^{tw1}_{(n)} - \sigma^{tw1}_{(n)} W^{(\alpha p)}_{(n)} \right) \dot{\gamma}^{(\alpha p)}_{(n)}$$
$$- \sum_{\beta p} \left(C_{tw1(n)} P^{(\beta p)}_{(n)} + W^{(\beta p)}_{(n)} \sigma^{tw1}_{(n)} - \sigma^{tw1}_{(n)} W^{(\beta p)}_{(n)} \right) \dot{f}^{(\beta p)}_{(n)} \gamma^{(\beta p)}_{tw}$$
$$- \sigma^{tw1}_{(n)} (D_{11(n+\frac{1}{2})} + D_{22(n+\frac{1}{2})} + D_{33(n+\frac{1}{2})})$$

$$\tag{2-192}$$

$$\sigma^{mat}_{(n+1)} = \Lambda^{(n+1)}_{(n)} \sigma^{mat}_{(n)} \left(\Lambda^{(n+1)}_{(n)} \right)^T + \Lambda^{(n+1)}_{(n+\frac{1}{2})} \overset{\nabla}{\sigma}^{(mat)}_{(n+\frac{1}{2})} \cdot \Delta t \left(\Lambda^{(n+1)}_{(n+\frac{1}{2})} \right)^T \tag{2-193}$$

$$\sigma^{tw1}_{(n+1)} = \Lambda^{(n+1)}_{(n)} \sigma^{tw1}_{(n)} \left(\Lambda^{(n+1)}_{(n)} \right)^T + \Lambda^{(n+1)}_{(n+\frac{1}{2})} \overset{\nabla}{\sigma}^{(tw1)}_{(n+\frac{1}{2})} \cdot \Delta t \left(\Lambda^{(n+1)}_{(n+\frac{1}{2})} \right)^T \tag{2-194}$$

$$\sigma_{(n+1)}^{tot} = \left(1 - \sum_{\beta p} f_{(n+1)}^{\beta p}\right)\sigma_{(n+1)}^{mat} + \sum_{\beta p} f_{(n+1)}^{\beta p}\sigma_{(n+1)}^{\beta p}$$

(2-195)

- Calculating ΔF^* :

$$\Delta L_{(n)}^P = \left(\sum_{\alpha p} s_{(n)}^{*(\alpha p)} \otimes m_{(n)}^{*(\alpha p)} \dot{\gamma}_{(n)}^{(\alpha p)} + \sum_{\beta p} s_{(n)}^{*(\beta p)} \otimes m_{(n)}^{*(\beta p)} \dot{f}_{(n)}^{(\beta p)} \gamma_{tw}^{(\beta p)}\right)\Delta t$$

(2-196)

$$\Delta F_{(n+1)}^* = I + L_{(n+\frac{1}{2})}\Delta t - \Delta L_{(n)}^P$$

(2-197)

Chapter 3

Crystal plasticity constitutive model calibration and application: the importance of accounting for various plastic deformation mechanisms

3.1 The experimental data on single crystals of magnesium and its alloys

The proposed Crystal Plasticity Constitutive Model (CPCM) accounts for the intragranular plastic deformation mechanisms of primary, secondary, and tertiary slip systems, as well as the primary and secondary twinning systems in magnesium, and is intended to simulate the plastic deformation behavior of magnesium single crystals at room temperature. Before using this model as a predictive tool, reasonable resistance functions for various plastic deformation mechanisms needed to be considered, and then the parameters of these resistance functions needed to be calibrated with experimental data on plastic deformation of magnesium single crystals. A review of the available experimental data on plastic deformation of magnesium single crystals is presented as follows.

The first attempt to understand the plastic deformation mechanisms in magnesium was made by Wonsiewicz and Backofen [15]. They grew single crystals of pure magnesium using the Bridgman technique, and ran plane strain compression tests on the specimens in four different loading directions, at temperatures ranging from 20°C to 307°C (Figures 3-1 and 3-2). They identified the plastic

deformation mechanisms (slip and twinning) in each loading direction, under metallographic examination with polarized light.
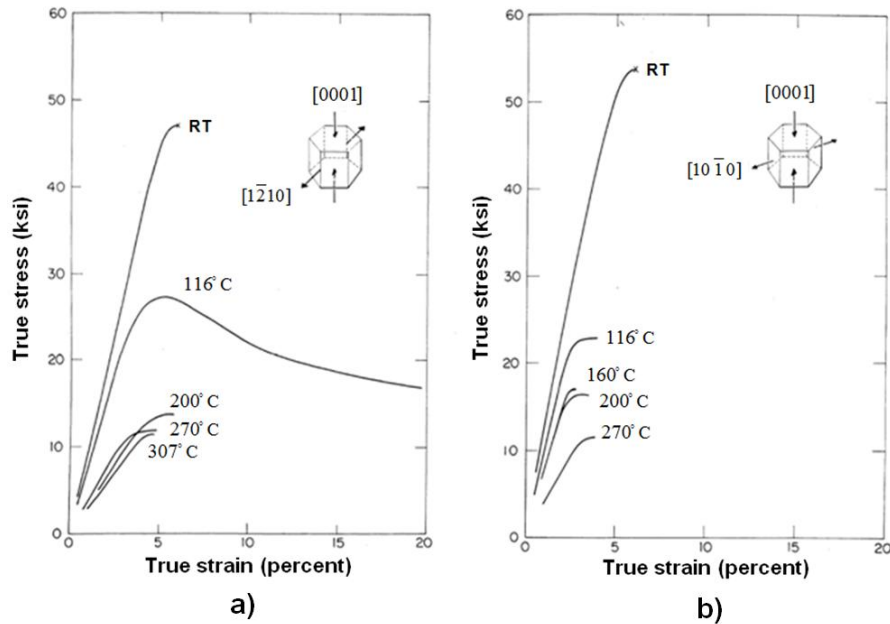

a)

b)

Figure 3-1 Stress-strain curves for magnesium single crystals compressed along a) the $[0001]$ c-axis with expansion limited to $[1\bar{2}10]$, and b) the $[0001]$ c-axis with expansion limited to $[10\bar{1}0]$ [15]
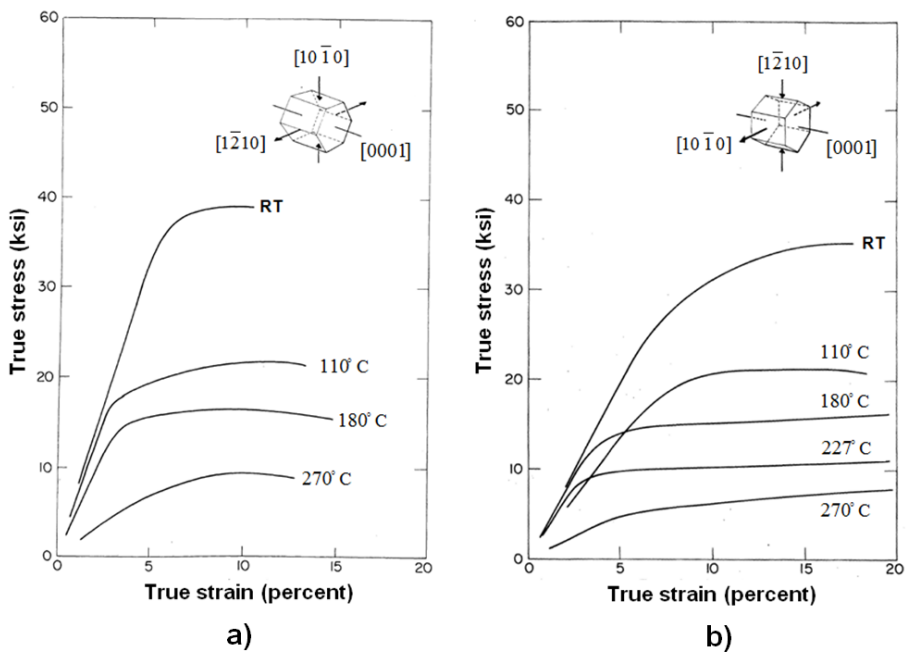

a)

b)

Figure 3-2 Stress-strain curves for magnesium single crystals compressed along a) the $[10\bar{1}0]$ with expansion limited to $[1\bar{2}10]$, and b) the $[1\bar{2}10]$ with expansion limited to $[10\bar{1}0]$ [15]

Kelley and Hosford [16] performed plane strain compression tests on single crystals of pure magnesium, magnesium with 0.5% thorium alloy, and magnesium with 4% lithium alloy in seven different loading directions, all at room temperature (Figures 3-3 through 3-6). They identified the plastic deformation mechanisms (slip and twinning) in each loading direction for the single crystals of pure and alloyed magnesium specimens. They have also investigated the effect of alloying in the activation energy of slip and twinning systems [16].
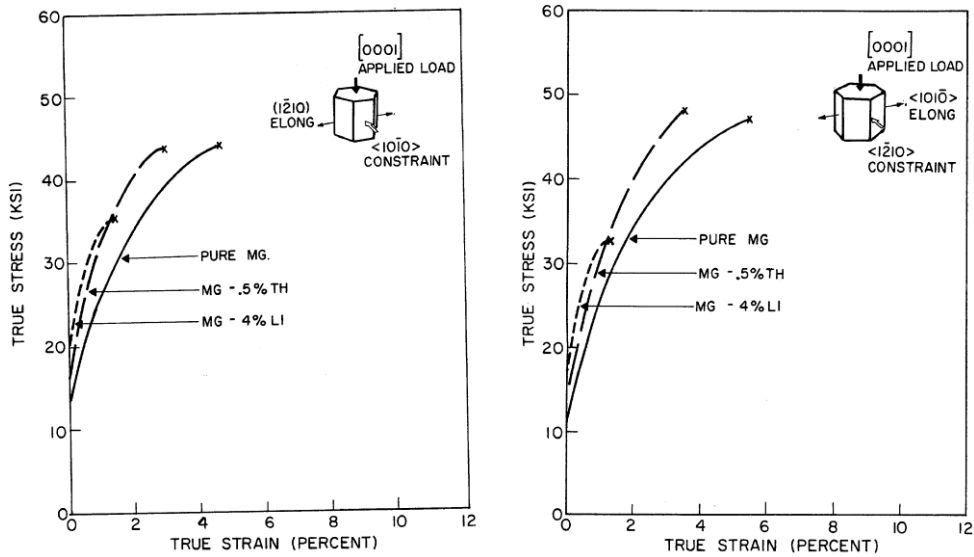

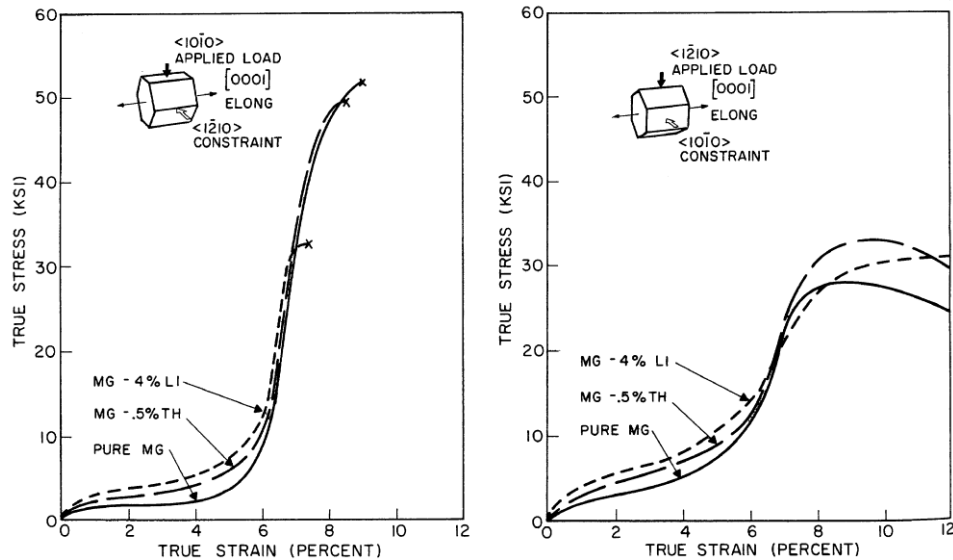Figure 3-3 Stress-strain curves in different loading conditions for pure/alloyed Mg single crystals [16]

Figure 3-4 Stress-strain curves in different loading conditions for pure/alloyed Mg single crystals [16]
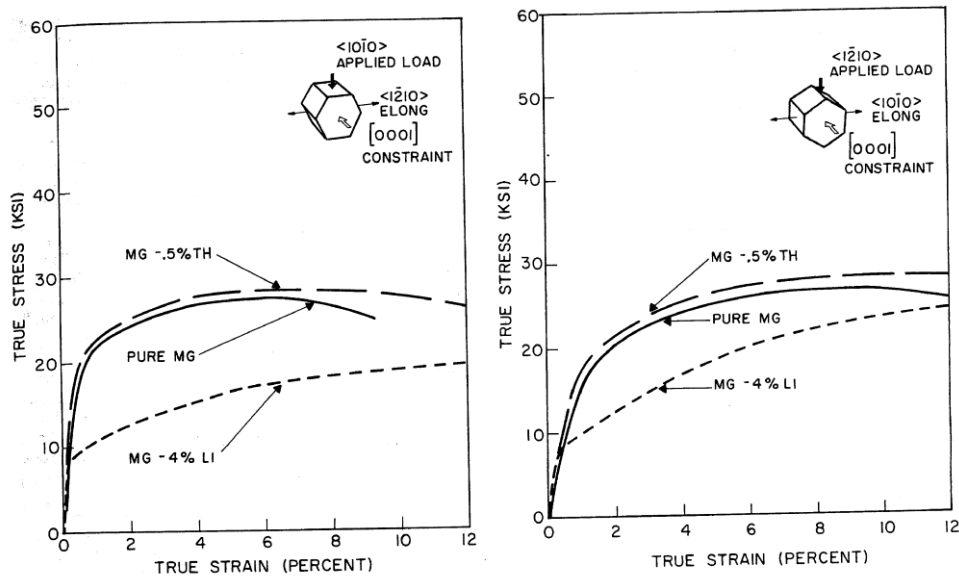
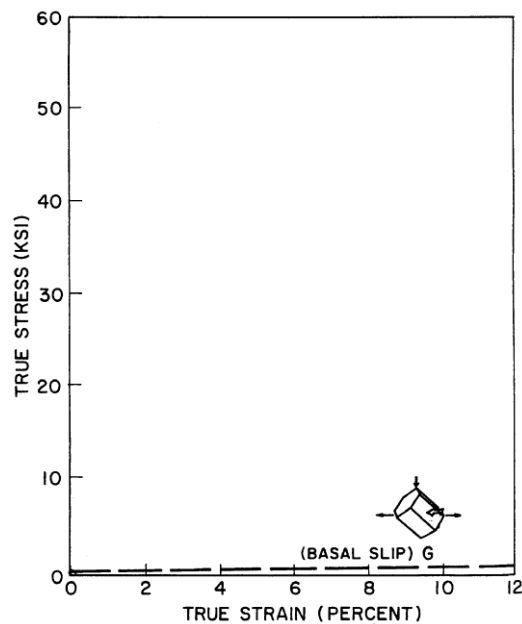Figure 3-5 Stress-strain curves in different loading conditions for pure/alloyed Mg single crystals [16]

Figure 3-6 Stress-strain curve for a loaded pure Mg single crystal [16]

Recently, Bhattacharya [1] performed uniaxial tension tests on single crystals of pure magnesium in five different loading directions (Figure 3-7), at the temperatures of 4.2 K, 78 K, and 300 K. In his work, similar to the works of Wonsiewicz and Backofen [15], and Kelley and Hosford [16], the plastic deformation mechanisms (slip and twinning) in each loading direction for the single crystals of pure magnesium specimens were identified.
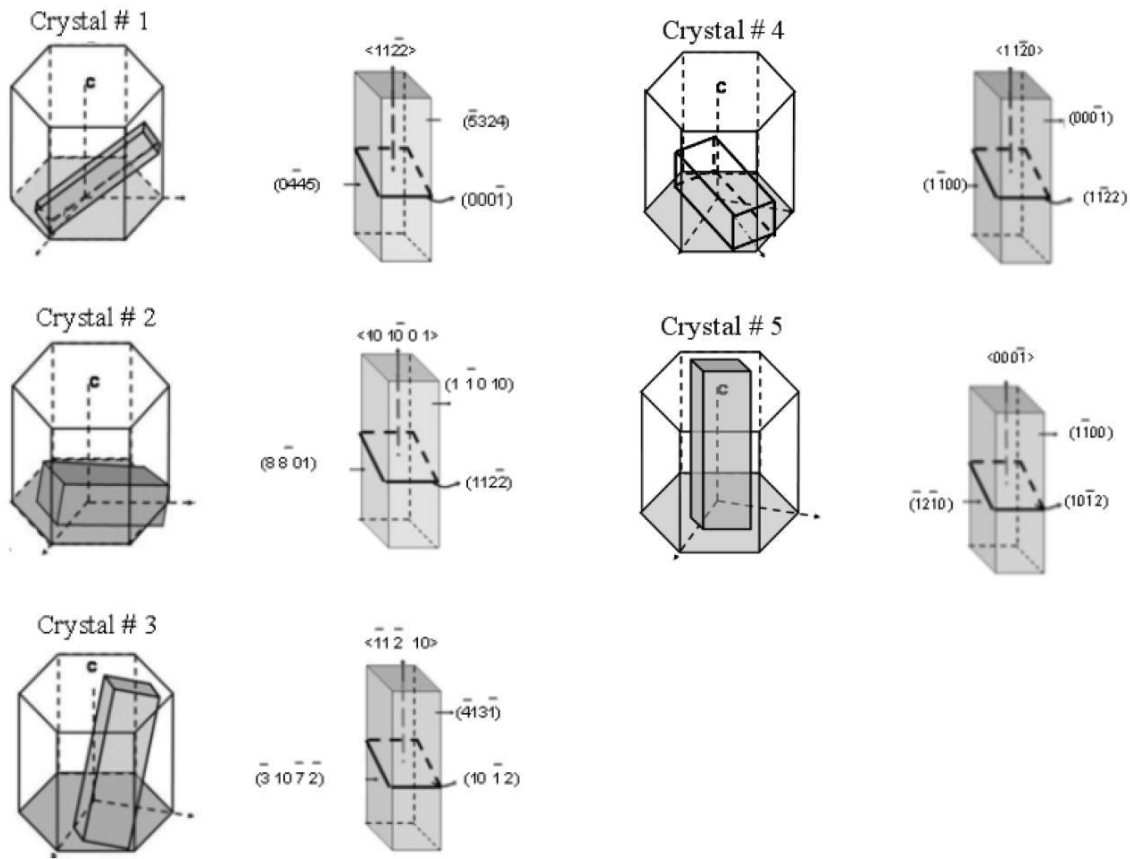
47

Figure 3-7 Orientation of the specimens with respect to the unit cell of the HCP lattice [1]

3.2 Model calibration

The experimental data of Bhattacharya [1] was used to calibrate the parameters of the resistance functions in the proposed CPCM at room temperature. This data was used because specimens in his work were under uniaxial tension loading, and the boundary conditions applied on the specimens had less complexity compared to the works of Wonsiewicz and Backofen [15] or that of Kelley and Hosford [16]. In these two works the loading was plane strain compression and the boundary conditions were rather complex.

The measured stress-strain curves by Bhattacharya [1] in the five different orientations at room temperature are presented in Figure 3-8. Based on the orientation of the specimen with respect to the tensile axis, as shown in Figure 3-7, the dominant plastic deformation mechanisms in orientation 1 are the primary slip systems. In orientations 2 and 4 they are the primary slip and contraction twinning systems. In orientations 3 and 5 they are the primary slip and extension twinning systems.

The slip and twinning systems listed in Table C-1 (Appendix C) are considered as the active plastic deformation mechanisms at room temperature. The CPCM was integrated at one material point, representing the entire specimen in the uniaxial tension.
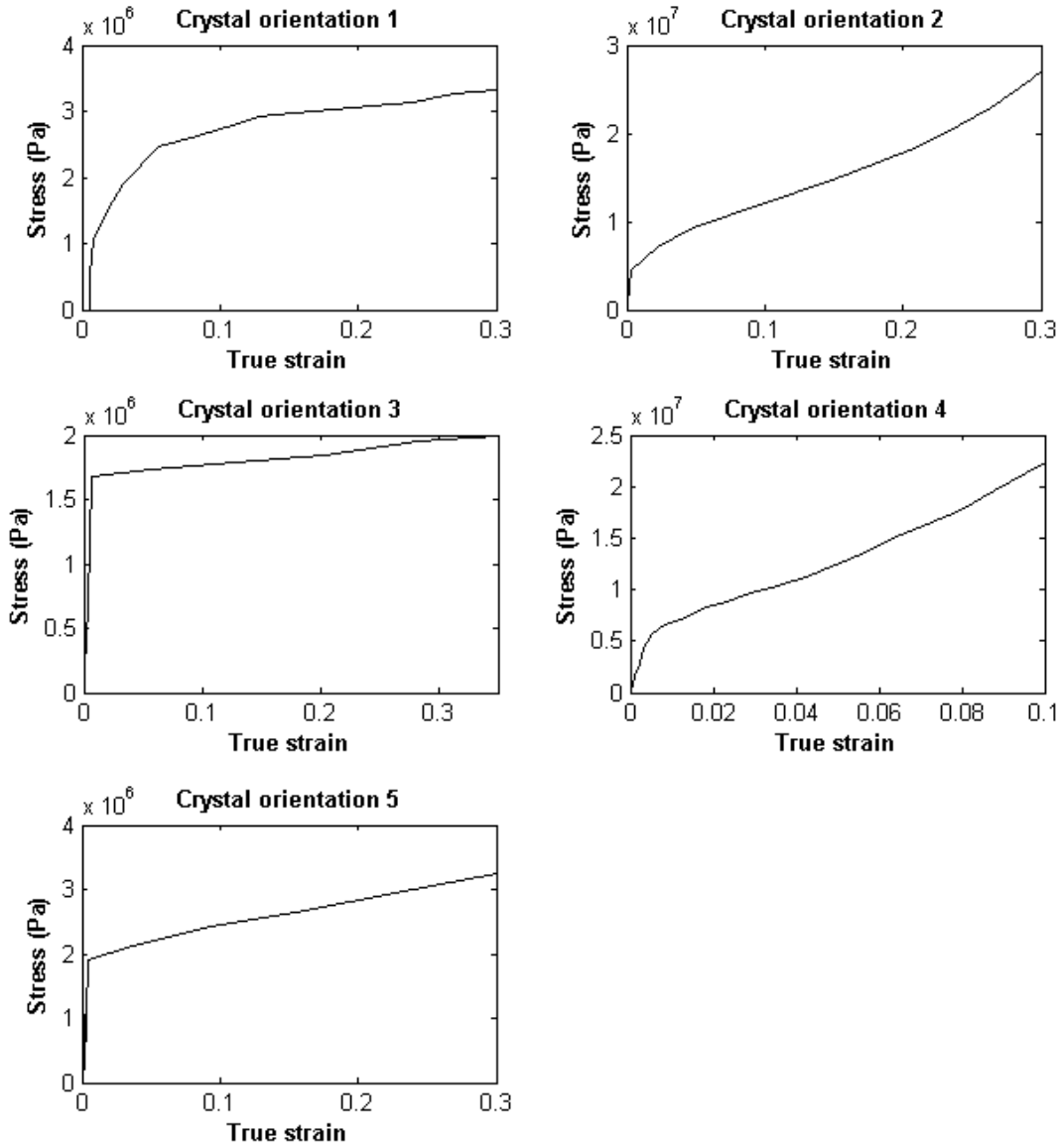
Figure 3-8 Stress-strain curves measured in uniaxial tension tests of the specimens shown in Figure 3-7 at room temperature [1]

A common resistance evolution function used for the FCC materials [53] has been used for the various plastic deformation mechanisms. The h_x^{ij} functions (for example in Equations (2-24), (2-46), (2-53), (2-64), (2-68), (2-75) etc.) have the following identical form:

$$h_x^{ij} = h_0 \sec h^2 \left(\frac{h_0 \gamma_k}{\tau_s} \right)$$

(3-1)

(e.g. in Equations (2-24), (2-46), (2-64), (2-75) etc.) or

$$h_x^{ij} = h_0 \sec h^2 \left(\frac{h_0 f_k}{\tau_s} \right) \tag{3-2}$$

(e.g. in Equations (2-53), (2-68) etc.)

This resistance evolution function has the same behaviour as a power-law type evolution function in the form of:

$$h_x^{ij} = h_0 \left(\frac{h_0 \gamma_{tot}}{\tau_0 n} + 1 \right)^{n-1} \quad \text{or} \quad h_x^{ij} = h_0 \left(\frac{h_0 f_{tot}}{\tau_0 n} + 1 \right)^{n-1} \tag{3-3}$$

i.e. by increasing the value of γ_{tot} or f_{tot} both of these two types of functions saturate.

Since the latent hardening effect for the slip systems in magnesium is not experimentally quantified yet, it is assumed that the self-hardening effect equals latent hardening. The value of m was chosen to be 0.02 to simulate the behavior of metals at room temperature (for instance in Equations (2-21), (2-49), (2-71), (2-104), (2-137) etc.). The reference slip rate and volume fraction rate ($\dot{a}^{(\alpha p)}$ in Equation (2-21), $\dot{a}^{(\alpha s)}$ in Equation (2-71), $\dot{a}^{(\beta p)}$ in Equation (2-49), and $\dot{a}^{(\beta s)}$ in Equation (2-104)) were arbitrarily set to 1×10^{-3} (similar to the value Wu et al. selected in [25]).

The calibration procedure is as follows. The stress-strain curve in loading orientation 1, where there is no twinning, was used to calibrate the parameters of the resistance evolution function for the primary slip systems in step 1 of the CPCM (i.e. Equation (2-24)). The stress-strain curves in loading orientations 3 and 5, where the extension twinning systems are active, were used to calibrate the parameters of the resistance evolution functions for the primary and secondary slip, as well as the primary twinning systems in steps 2 and 3-4 of the CPCM (i.e. Equations (2-47), (2-48), (2-52), (2-53), (2-64), (2-65), (2-67)-(2-69), (2-74), and (2-75)). The stress-strain curves in loading orientations 2 and 4, where the contraction twinning systems are active, were used to calibrate the parameters of the resistance evolution functions for the primary, secondary, and tertiary slip, as well as the primary and secondary twinning systems in steps 2, 3-4, 5, and 6 of the CPCM, i.e. Equations (2-47), (2-48), (2-52), (2-53), (2-64), (2-65), (2-67)-(2-69), (2-74), (2-75), (2-93), (2-94), (2-96)-(2-99), (2-101)-(2-103), (2-107)-(2-109), (2-121), (2-122), (2-124)-(2-127), (2-129)-(2-131), (2-133)-(2-136), (2-140), and (2-141). As it will be explained later in Subsection 3.2.5, with the available experimental data (Figure 3-8) it was only possible to calibrate the resistance evolution functions for the primary slip and twinning systems. The following subsections describe the calibration procedure.

3.2.1 Calibration of the resistance evolution function of primary slip systems

The stress-strain curve in loading orientation 1, reported by Bhattacharya in [1], was used to calibrate the parameters of the resistance of primary slip systems in step 1 of the proposed CPCM. As it was mentioned in the previous section, the dominant plastic deformation mechanisms in this loading orientation were primary slip systems. The CRSS for the primary basal slip systems is taken as 0.8 MPa [61], 2 MPa for the primary pyramidal $<c+a>$ slip systems [1], and 39.2 MPa for the primary prismatic slip systems [62]. In our formulation the CRSS for a given plastic deformation mechanism corresponds to the initial value for the resistance of that plastic deformation mechanism.
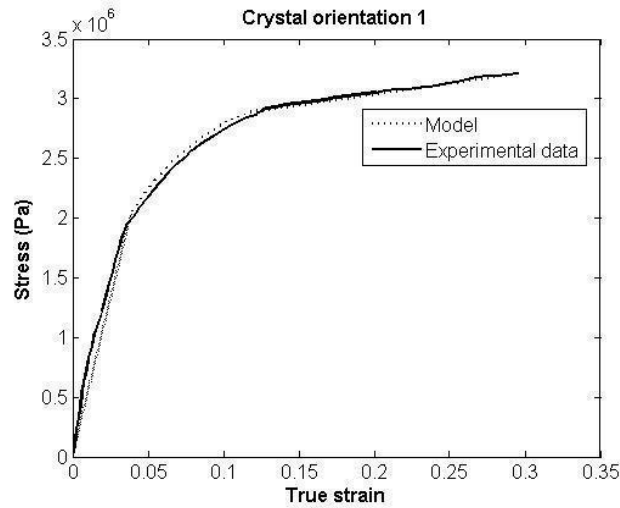

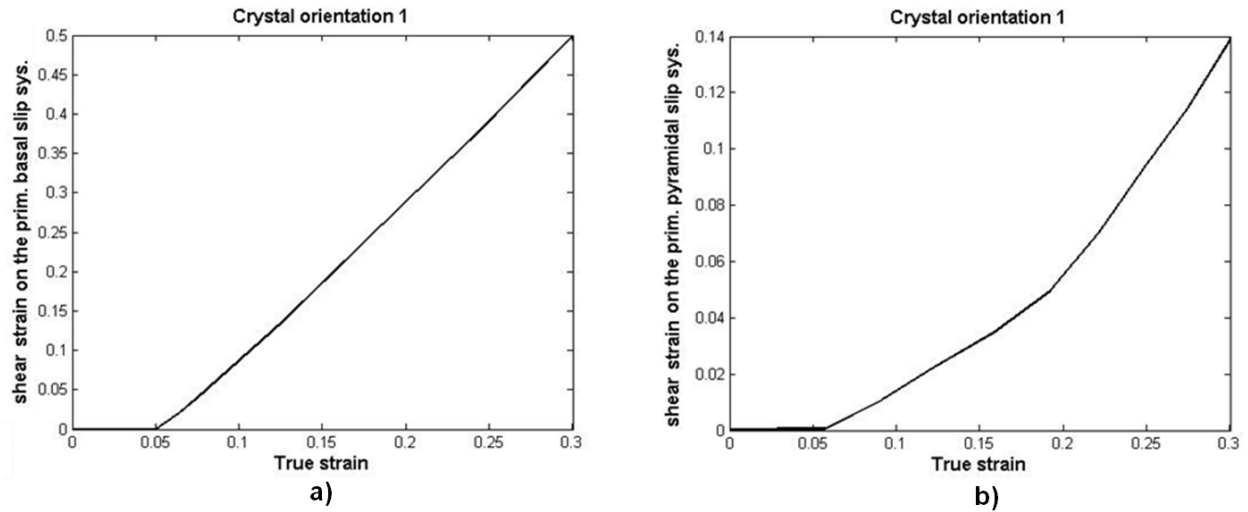Figure 3-9 Curve fit results when only primary slip systems were considered (orientation 1)

Figure 3-10 Total shear strain on a) the primary basal slip systems and b) the pyramidal $<c+a>$ slip systems (orientation 1)

51

In the next step, the experimental stress-strain curve provided by Bhattacharya [1] in loading orientation 1, was matched by calibrating $h_0^{1A(\alpha p)}$ and $\tau_s^{1A(\alpha p)}$ (Equation (3-1)) for the resistance function of the primary slip systems (Equation (2-24)). The best calibration result obtained is shown in Figure 3-9. The total shear strain on all primary basal and pyramidal $<c+a>$ slip systems are presented in Figure 3-10 (in this loading orientation, the prismatic slip systems do not take up any shear strain). The parameter values for this calibration are: in Equation (2-24), $h_0^{1A(\alpha p)} = 1.22 \times 10^6$ Pa, $\tau_s^{1A(\alpha p)} = 2.7 \times 10^5$ Pa.

3.2.2 Calibration of the resistance evolution function of the primary extension twinning systems (orientations 3 and 5)

An attempt was made to curve fit the stress-strain curves in orientations 3 and 5 with the primary slip systems alone, primary extension twinning systems alone, a combination of primary slip and extension twinning systems, and a combination of primary and secondary slip and primary twinning systems. Also, nucleating the primary and secondary twinning systems at different plastic work levels, and the secondary slip systems at different deformation stages were tried.

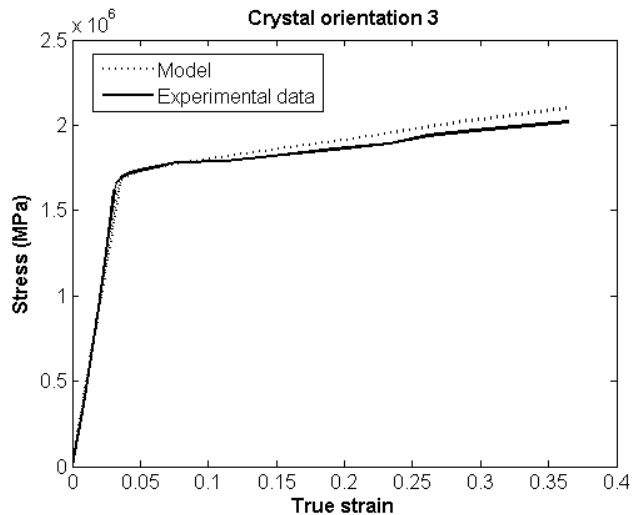Figure 3-11 Curve fit results when primary slip and extension twinning systems were considered (orientation 3)

The best curve fits for loading orientations 3 and 5 were obtained by considering primary slip systems and primary extension twinning systems where nucleation of the primary extension twinning systems was allowed at the very beginning of simulation (i.e. required plastic work for their nucleation

was set to zero). The curve fit results are shown in Figures 3-11 and 3-13. The total shear strain on all the primary slip, and primary extension twinning systems for both loading orientations are presented in Figures 3-12 and 3-14. The CRSS for the primary extension twinning systems is considered 1 MPa [63].

Figure 3-12 a) Total accumulated shear strain by the primary pyramidal $<c+a>$ slip systems, and b) by the primary extension twinning systems (orientation 3)

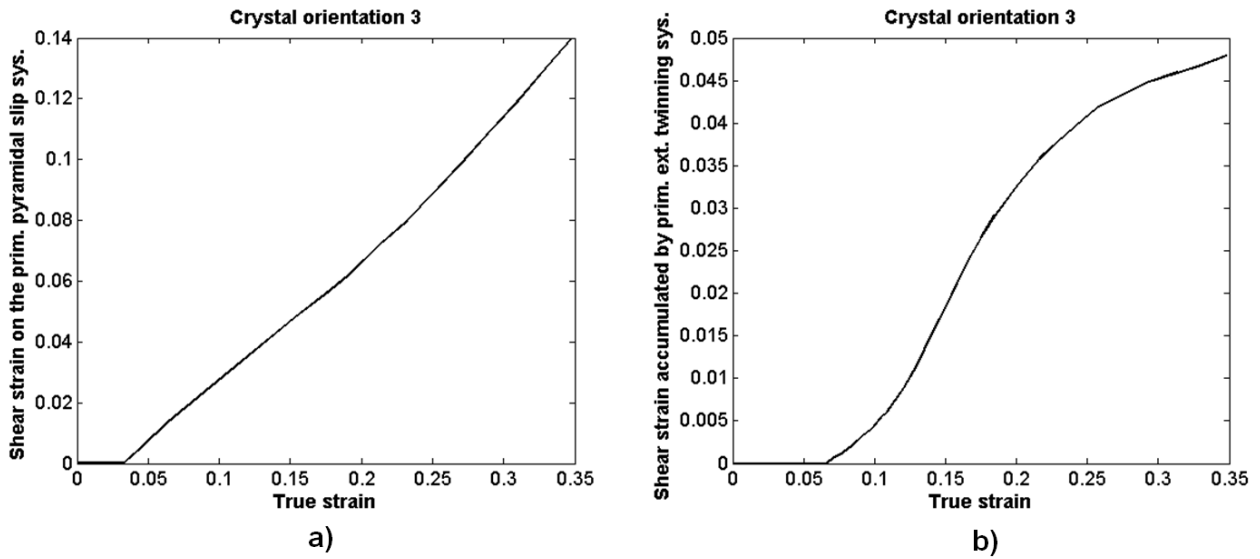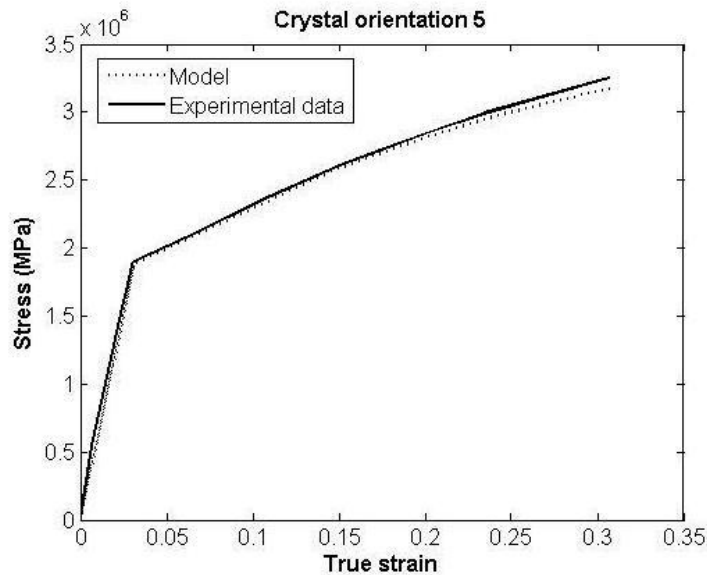Figure 3-13 Curve fit results when primary slip and extension twinning systems were considered (orientation 5)
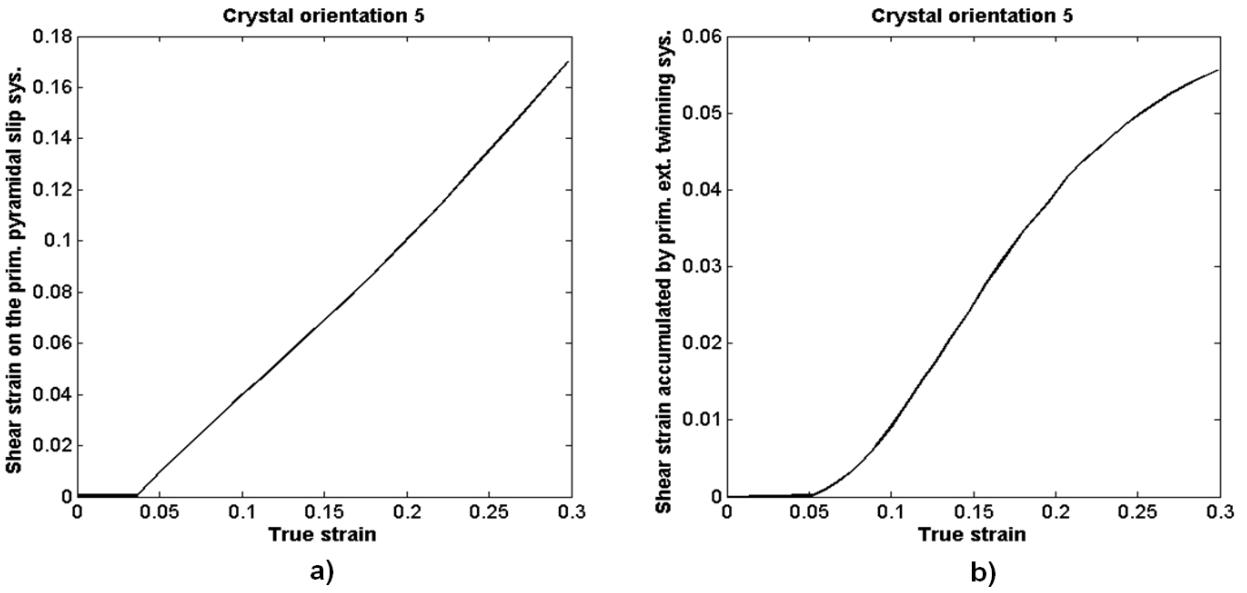
Figure 3-14 a) Total accumulated shear strain by the primary pyramidal $<c+a>$ slip systems, and b) by the primary extension twinning systems (orientation 5)

Table 3-1 contains the parameter values for the resistance of the slip ($h_{\alpha p}^{2A}$ in Equation (2-47) and $h_{\beta p}^{\prime 2A}$ in Equation (2-48)) and extension twinning systems ($h_{\alpha p}^{2B}$ in Equation (2-52) and $h_{\beta p}^{\prime 2B}$ in Equation (2-53)) obtained by calibration.

Equation (2-47)	$h_0^{2A(\alpha p)}$	4.1×10^6 Pa
	$\tau_s^{2A(\alpha p)}$	4.0×10^5 Pa
Equation (2-48)	$h_0^{\prime 2A(\beta p)}$	7.3×10^6 Pa
	$\tau_s^{\prime 2A(\beta p)5}$	1×10^5 Pa
Equation (2-52)	$h_0^{2B(\alpha p)}$	0 Pa
	$\tau_s^{2B(\alpha p)}$	1×10^5 Pa
Equation (2-53)	$h_0^{\prime 2B(\beta p)}$	4.2×10^6 Pa
	$\tau_s^{\prime 2B(\beta p)}$	3.3×10^5 Pa

Table 3-1 The parameter values for the resistance of the primary slip and extension twinning systems

3.2.3 Calibration of the resistance evolution function of primary contraction twinning systems (orientation 2 and 4)

Attempts were made to curve fit the stress-strain curves in loading orientations 2 and 4, with primary slip systems alone, primary contraction twinning systems alone, a combination of primary slip and contraction twinning systems, a combination of primary and secondary slip and primary contraction twinning systems, and a combination of primary and secondary slip as well as primary contraction and secondary extension twinning systems. Also, nucleating the primary contraction and secondary extension twinning systems at different plastic work levels, and secondary slip systems at different deformation stages were tried. In order to keep the number of state variables at a minimum, the effect of considering tertiary slip systems (36x12=432 state variables associated with the shear strain on the tertiary slip systems) on the stress-strain response of the material in loading orientations 2 and 4 was not investigated.

The best curve fits for loading orientations 2 and 4 were obtained by considering the primary slip and contraction twinning systems.

Figure 3-15 Stress-strain curve fit results when primary pyramidal $<c+a>$ slip and contraction twinning systems were considered (orientation 2)

For loading orientation 2, the result is shown in Figure 3-15. In this case, the nucleation of the primary contraction twinning systems was allowed at the plastic work of 3.54×10^4 Pa. The shear strain on the primary pyramidal $<c+a>$ slip, and primary twinning systems are shown in Figures 3-16a and 3-16b, respectively (the primary basal and prismatic slip systems do not take up shear strain). While the results in Figure 3-15 represent the best match between the model and experimental results found, there is

55

a noticeable discrepancy between the two curves in this figure. The only way to improve the model results is to use more elaborate resistance evolution functions for the primary slip and twinning systems.

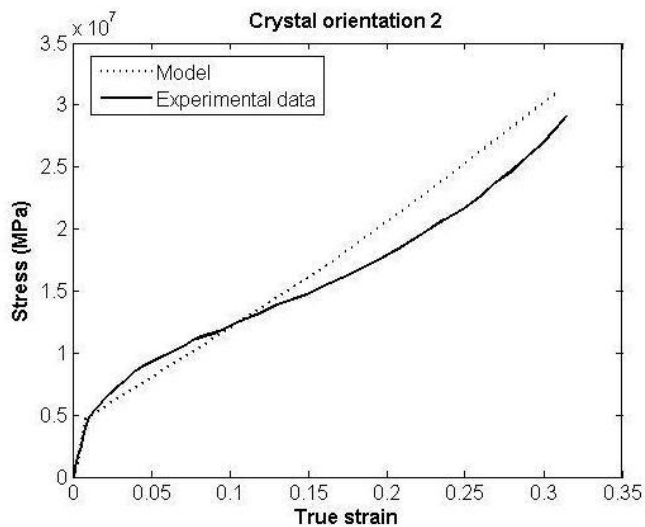Figure 3-16 a) Total accumulated shear strain by the primary pyramidal $<c+a>$ slip systems, and b) by the primary contraction twinning systems (orientation 2)

Figure 3-17 Stress-strain curve fit results when primary slip and contraction twinning systems were considered (orientation 4)

The curve fit result in loading orientation 4 is shown in Figure 3-17. Nucleation of the primary contraction twinning systems was allowed at the beginning of loading (i.e. the required plastic work for

their nucleation was set to zero). The shear strain on the primary pyramidal $<c+a>$ slip, and primary twinning systems are shown in Figures 3-18a and 3-18b, respectively (the primary basal and prismatic slip systems do not take up shear strain).
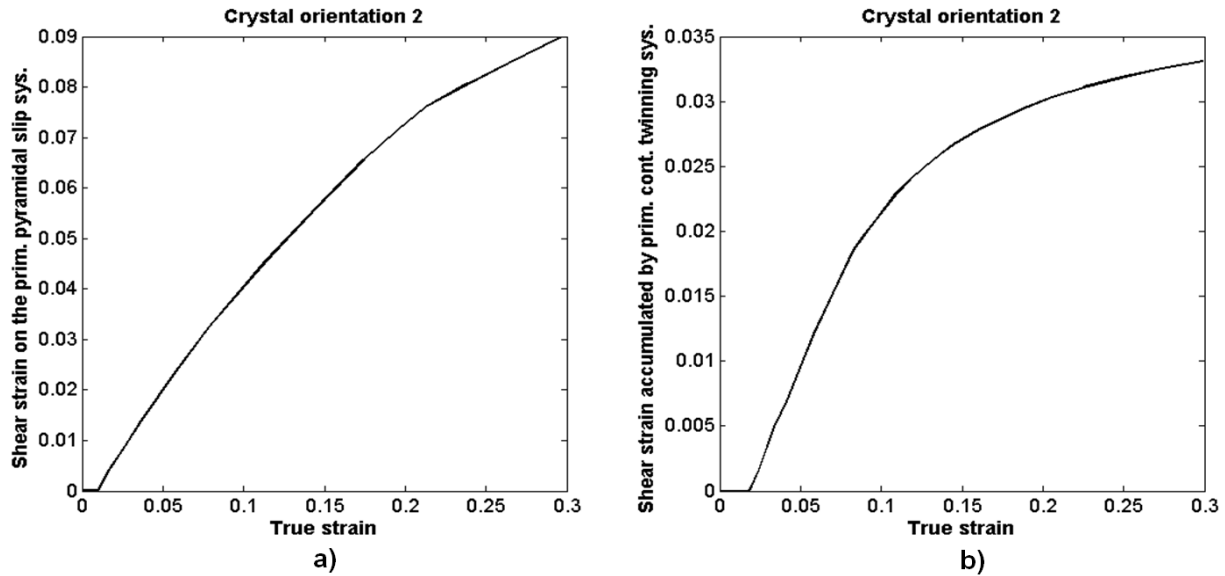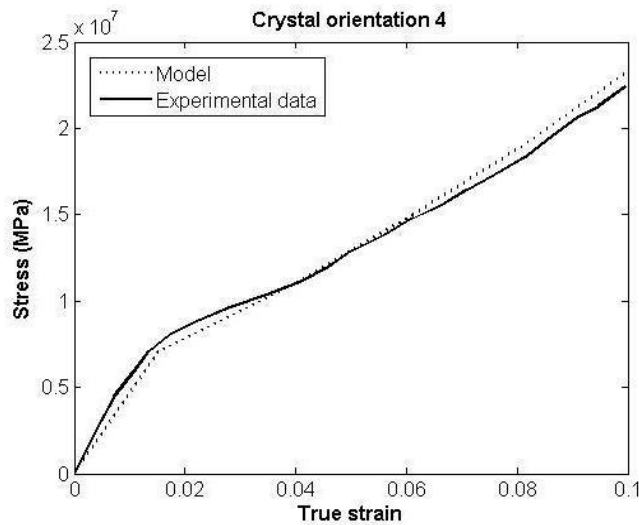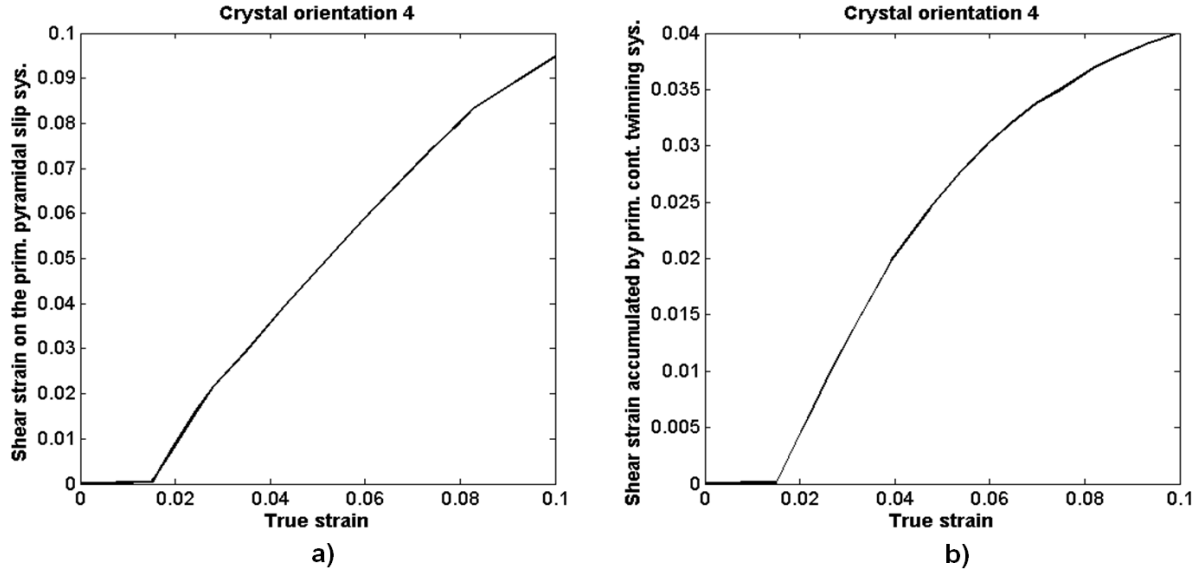

Figure 3-18 Total accumulated shear strain by the primary pyramidal $<c+a>$ slip systems, and b) by the primary contraction twinning systems (orientation 4)

Equation (2-47)	$h_0^{2A(\alpha p)}$	4.1×10^6 Pa
	$\tau_s^{2A(\alpha p)}$	4.0×10^5 Pa
Equation (2-48)	$h_0'^{2A(\beta p)}$	0 Pa
	$\tau_s'^{2A(\beta p)5}$	1×10^5 Pa
Equation (2-52)	$h_0^{2B(\alpha p)}$	2.0×10^7 Pa
	$\tau_s^{2B(\alpha p)}$	0.3×10^5 Pa
Equation (2-53)	$h_0'^{2B(\beta p)}$	4.7×10^6 Pa
	$\tau_s'^{2B(\beta p)}$	6.7×10^5 Pa

Table 3-2 The parameter values for the resistance of the primary slip and contraction twinning systems

The CRSS for the primary contraction twinning systems in magnesium was not reported in literature. From calibration it was discovered that the choice of 2 MPa results in the best prediction of the experimental stress-strain curve in loading orientations 2 and 4.

The parameter values for the resistance of slip ($h_{\alpha p}^{2A}$ in Equation (2-47) and $h_{\beta p}'^{2A}$ in Equation (2-48)) and contraction twinning systems ($h_{\alpha p}^{2B}$ in Equation (2-52) and $h_{\beta p}'^{2B}$ in Equation (2-53)) obtained by calibration are shown in Table 3-2.

3.2.4 Texture evolution

As previously mentioned, the CPCM was integrated at one material point, representing the entire specimen in the uniaxial tension, and with this scheme any size effect (e.g. specimen aspect ratio) cannot be accounted for [71,72,77]. The calibration was done within a small range of deformation of the loaded specimens in five orientations (according to the Figure 3-8 the maximum strain in all the loaded specimens was only 35%), where the deformation can be assumed homogeneous. At this level of deformation, no experimental data regarding evolved grain orientation for the loaded specimens is available in [1], and so it was not possible to compare the simulated evolution of the grain with experimental data.

For very large deformations (e.g. 250% strain in orientation 1, 60% strain in orientation 2, and 150% strain in orientation 3, etc.), the experimental data regarding the evolved grain orientation for the loaded specimens is available in [1], however, at these high levels of deformation, it is very unlikely that the deformation in the specimens was homogeneous. Therefore, since the implemented integration scheme is only valid for homogeneous deformation throughout the specimen, it was not logical to compare the model prediction of grain orientation at these high levels of deformation (where the deformation is unlikely homogeneous) with the available experimental data in the five loaded specimens.

3.2.5 Calibration conclusions

The results of calibration for various plastic deformation mechanisms are summarized below:

When the primary slip systems are the only active plastic deformation mechanisms (i.e. step 1 of the model), the parameters of their resistance were calibrated with good accuracy in Sections 3.2.1. In step 2 of the model where, in addition to the primary slip systems, primary twinning systems are active, the parameters of the resistance of the primary slip systems were calibrated with good accuracy as well. In this case, one set of parameter values for the resistance of primary slip systems was obtained for the case

where the primary slip systems interacted with primary extension twinning systems (orientations 3 and 5), and another set was obtained for the case where the primary slip systems interacted with primary contraction twinning systems (orientations 2 and 4). Since the nature of interaction between the primary slip and primary extension twinning systems differs from that between the primary slip and primary contraction twinning systems, the sets of parameter values for the resistance of primary slip systems differ in these two cases.

Since the primary prismatic slip systems have a very high CRSS at room temperature, 39.2 MPa [62], regardless of the parameter values selected for their resistance evolution function, they did not take up any shear strain in all the loading orientations of the single crystals considered. The relatively low CRSS values for the slip and twinning systems, of the order of 1 MPa, which were used in the model, were obtained in deformation experiments on magnesium single crystals under the condition of uniaxial tension (as shown in Figure 3-8). On the other hand, experimental results on magnesium polycrystals [1] and on magnesium alloys [64,65], show that the yield stress of these materials is one order of magnitude larger than the yield stress observed in single crystals. The reason for this difference is the grain boundaries. These results suggest that to simulate the deformation behaviour of polycrystalline aggregate, much higher values for the CRSSs of the slip and twinning systems than those used for single crystals have to be considered.

It was possible to determine one set of parameter values for the primary extension twinning systems in orientations 3 and 5, such that the experimental stress-strain curves were predicted with good accuracy in these two orientations. Also, one set of parameter values for the primary contraction twinning systems in orientations 2 and 4 was determined, such that the experimental stress-strain curves were predicted with good accuracy in these two orientations.

The calibration of the CRSSs and resistance evolution function parameters of the secondary slip and twinning systems was not possible; this is only possible when there are more experimental stress-strain curves in loading orientations where these plastic deformation mechanisms are active.

3.3 Model application: importance of accounting for various plastic deformation mechanisms

A numerical experiment was designed in which the proposed CPCM was used to simulate the simple shear loading of a magnesium single crystal to show the significance of accounting for the kinematics of various slip and twinning systems. 50% shear strain is applied to the single crystal, and the response of the material was calculated with steps 1, 2, 3-4, and 5 of the proposed CPCM. In this study, the nucleation of the primary twinning systems was allowed from the very beginning of the simulation (i.e. when the

shear strain was 0). Also, nucleation of the secondary slip systems was allowed around a shear strain of 0.045. Finally, nucleation of the secondary twinning systems was allowed around a shear strain of 0.055.

Through this strategy, it was possible to individually examine the effect of various plastic deformation mechanisms on the macroscopic stress-strain response of the material. For the reason mentioned previously in the Subsection 3.2.3, the effect of tertiary slip systems in the model was not investigated.

Figure 3-19 shows the simple shear loading of a single crystal of magnesium. {X,Y,Z} corresponds to the global coordinate system, and $\{e_1, e_2, e_3\}$ corresponds to the orthonormal local coordinate system attached to the crystal. The c-axis of the crystal is aligned with the e_3 axis. The orientation of the orthonormal coordinate system $\{e_1, e_2, e_3\}$ with respect to the crystal is shown in Figure C-1, Appendix C.

Based on Figure 3-19, for $0° < \alpha < 90°$, the contraction twinning systems, and for $270° < \alpha < 360°$, the extension twinning systems, get activated. The results of the simulations show that for $\alpha = 17.5°$, a secondary extension twinning systems inside a primary contraction twinned region has a favourable orientation for nucleation and growth. Also, inside the primary contraction twinned region, four secondary pyramidal $<c+a>$ slip systems have a favourable orientation for nucleation and growth. So, all the plastic deformation mechanisms have favourable orientation for nucleation and growth in this orientation, and therefore this crystal orientation was selected for simulation. In terms of Bunge angles [59], the crystal orientation is as follows:

$$\varphi_1 = -162.5°, \varphi = 90°, \varphi_2 = 0 \tag{3-4}$$
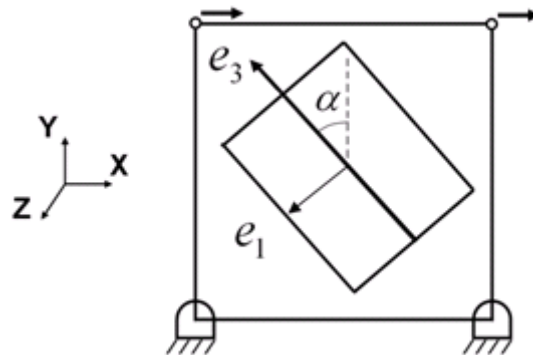

Figure 3-19 Simple shear loading of a single crystal of magnesium

60

The relationship between the orientation matrix and Bunge angles is given in Equations (2-178)-(2-187). The slip and twinning systems considered in the simulation are presented in Table C-1 in Appendix C. The elasticity modulus for a single crystal of magnesium and the values of its components are given in Appendix D.

The choice of resistance evolution functions for the various slip and twinning systems was the same as in Section 3.2 (Equations (3-1) and (3-2)).

In step 1, the CRSS and resistance evolution function parameter values of the primary slip systems obtained by calibration in Subsection 3.2.1 were used.

In step 2, the CRSS and resistance evolution function parameter values of the primary slip and contraction twinning systems obtained by calibration in Subsection 3.2.3 were used (Table 3-2).

In steps 3-4, the CRSS and resistance evolution function parameter values of the primary slip and contraction twinning systems obtained by calibration in Section 3.2.3 were used (Table 3-2). For the resistance evolution function of the secondary slip systems, the same values as the ones obtained for the primary slip systems in Section 3.2.3 were used, i.e. in Equation (2-74), $h_0^{3-4C(\beta p)} = 0$, $\tau_s^{3-4C(\beta p)} = 1 \times 10^5$ Pa; and in Equation (2-75), $h_0'^{3-4C(\alpha s)} = 4.1 \times 10^6$ Pa, $\tau_s'^{3-4C(\alpha s)} = 4.0 \times 10^5$ Pa. The simple shear loading for three different conditions were simulated:

$$\text{CRSSs}_{\text{second. slip sys.}} = c_3 \times \text{CRSSs}_{\text{prim. slip sys.}} \tag{3-5}$$

where c_3 = 1, 2.5, and 6.

Lastly, in step 5, the CRSS and resistance evolution function parameter values of the primary slip and contraction twinning systems obtained by calibration in Section 3.2.3 were used (Table 3-2). For the resistance evolution function of the secondary slip systems, the same values as the ones obtained for the primary slip systems in Section 3.2.3 were used, i.e. in Equation (2-101), $h_0^{5C(\beta p)} = 0$, $\tau_s^{5C(\beta p)} = 1 \times 10^5$ Pa; in Equation (2-102), $h_0'^{5C(\alpha s)} = 4.1 \times 10^6$ Pa, $\tau_s'^{5C(\alpha s)} = 4.0 \times 10^5$ Pa; and in Equation (2-103), $h_0''^{5C(\beta s)} = 0$, $\tau_s''^{5C(\beta s)} = 1 \times 10^5$ Pa. For the resistance evolution function of the secondary extension twinning systems, the same values as the ones obtained for the primary extension twinning systems in Section 3.2.2 were used, i.e. in Equation (2-107), $h_0^{5D(\beta p)} = 0$, $\tau_s^{5D(\beta p)} = 1 \times 10^5$ Pa; in Equation (2-108), $h_0'^{5D(\alpha s)} = 0$, $\tau_s'^{5D(\alpha s)} = 1 \times 10^5$ Pa; and in Equation (2-109), $h_0''^{5D(\beta s)} = 4.2 \times 10^6$ Pa, $\tau_s''^{5D(\beta s)} = 3.3 \times 10^5$ Pa. We have simulated the simple shear loading for three different conditions:

$$\text{CRSSs}_{\text{second. slip sys.}} = c_3 \times \text{CRSSs}_{\text{prim. slip sys.}} \qquad (3\text{-}6)$$

$$\text{CRSSs}_{\text{second. twinning sys.}} = c_3 \times \text{CRSSs}_{\text{prim. twinning sys.}} \qquad (3\text{-}7)$$

where $c_3 = 1, 2.5,$ and 6.

The CPCM was integrated at one material point, representing the entire specimen in the simple shear loading.

Figure 3-20 shows the global stress-strain curves for the four steps (when $c_3 = 1$). It can be seen that the macroscopic stress response of the material in steps 1, 2, 3-5, and 5 are different. The maximum difference between the stresses in steps 1 and 2 is 26.1%. This shows that if a part of plastic deformation is taken up by primary slip and twinning systems, the macroscopic stress-strain curve will be different compared to step 1 where the entire plastic deformation is taken up by the primary slip systems alone. The maximum difference between the stresses in steps 2 and 3-4 is 6.5% which indicates the effect of considering secondary slip systems as additional plastic deformation mechanisms. Finally, the difference between the stress responses in steps 3-4 and 5 is 3.5% which indicates that the accommodated shear strain by the secondary twinning systems did not increase enough to make a significant difference.
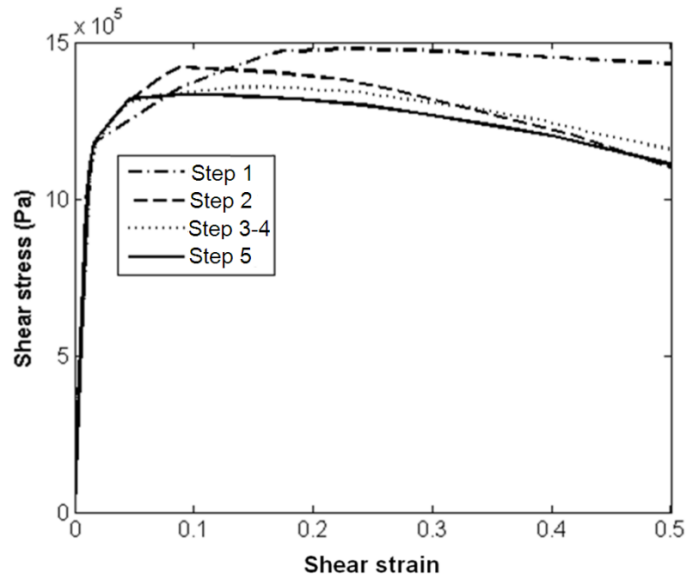

Figure 3-20 Simulation results of simple shear loading of a magnesium single crystal, $c_3 = 1$

Figure 3-21 shows the global stress-strain curves for the five steps when $c_3 = 2.5$. The macroscopic stress response of the material in steps 3-4 and 5 are slightly different (1.3%), and their difference with the stress-strain curve in step 2 decreased. The maximum difference between the stresses

in steps 2 and 3-4 is 4.1% which is less than the corresponding value for when $c_3 = 1$. This is because the CRSS for the secondary slip systems is higher in this step which results in less accumulation of shear strain on the secondary slip systems.
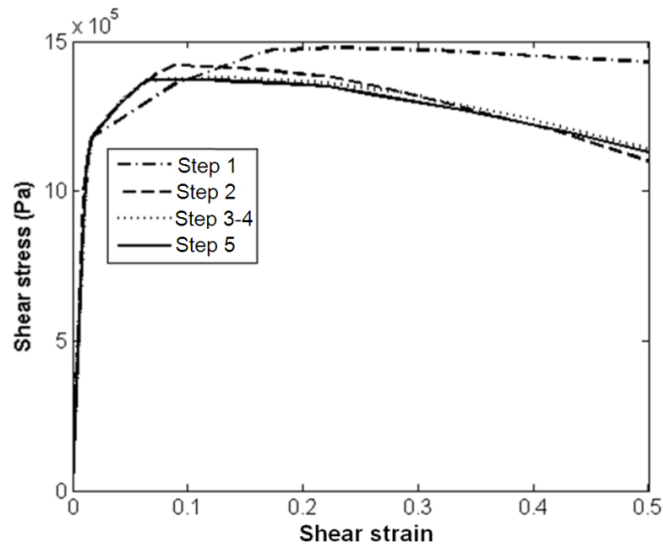
Figure 3-21 Simulation results of simple shear loading of a magnesium single crystal, $c_3 = 2.5$

Figure 3-22 shows the global stress-strain curves for the five steps when $c_3 = 6$. Note that the macroscopic stress response of the material in steps 2, 3-4, and 5 are all the same. This means that for $c_3 = 6$ the secondary slip and twinning systems do not take up any plastic strain.

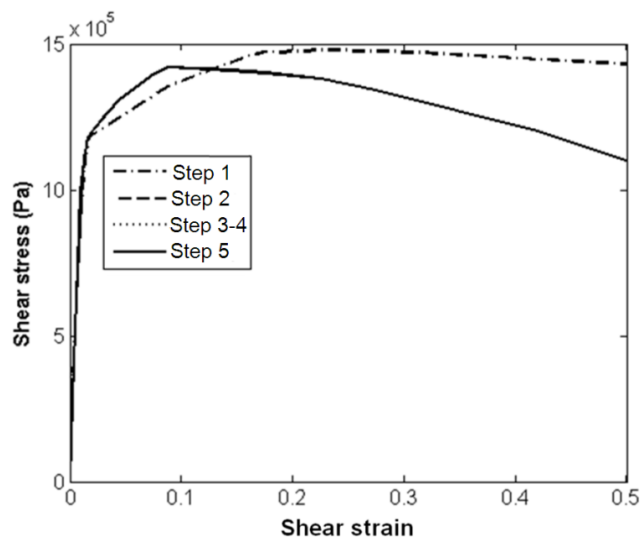

Figure 3-22 Simulation results of simple shear loading of a magnesium single crystal, $c_3 = 6$

The distribution of plastic deformation on the various slip and twinning systems in the five steps are discussed next. For the presented grain orientation, in steps 2, 3-4, and 5 only one primary contraction twinning system was activated. In step 5 one secondary extension twinning system was activated inside the primary twinned region.

Figure 3-23 shows the shear strain on the primary basal, prismatic, and pyramidal $<c+a>$ slip systems in the loading step 1.
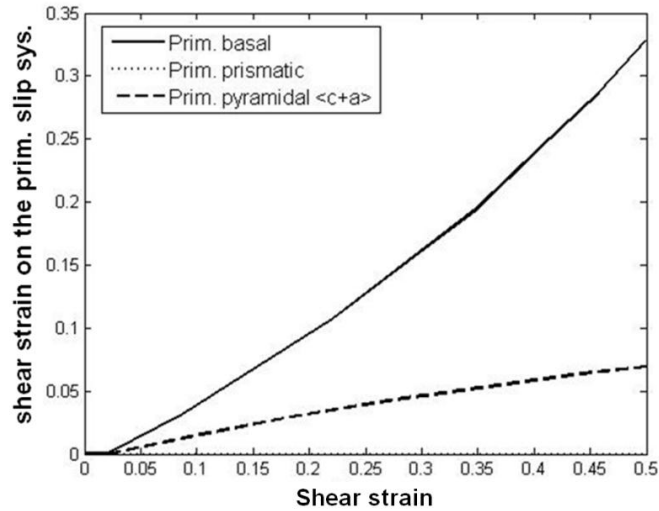

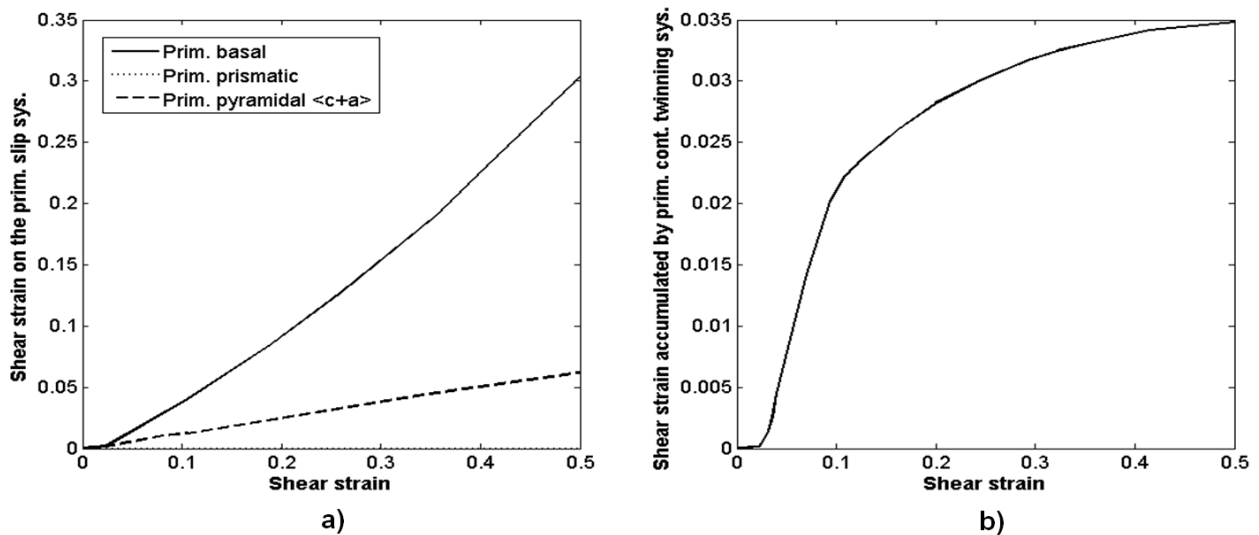Figure 3-23 Distribution of shear strain on the primary slip systems, step 1

Figure 3-24 a) Distribution of shear strain on the primary slip systems, and b) primary twinning systems, step 2

The shear strain distribution over the primary slip and twinning systems in step 2 are shown in Figures 3-24a and 3-24b, respectively. Compared with step 1, while the pattern of shear strain on the primary basal and prismatic slip systems did not change (Figure 3-23), the pattern of shear strain on the primary $<c+a>$ slip systems changed in step 2. This is because in step 2, strain along the c-axis of the HCP crystal can be taken up either by primary pyramidal $<c+a>$ slip systems or by primary twinning systems, and whichever has a greater resolved shear stress and lesser resistance takes up more strain. The accumulated shear strain by the only primary contraction twinning system is shown in Figure 3-24b.

In steps 3-4, the accumulated shear strain by the primary slip systems is shown in Figure 3-25. The accumulated shear strain by the primary twinning the secondary pyramidal $<c+a>$ slip systems is shown in Figure 3-26 for three cases of c_3 = 1, 2.5, and 6. For c_3 = 1 and 2.5, the trend of shear strain on the primary slip primary twinning systems is very similar to step 2 (Figure 3-24). Around a shear strain of 0.045, nucleation of the secondary slip systems was allowed and Figure 3-26b shows that the shear strain on the secondary pyramidal $<c+a>$ slip systems (other secondary slip systems did not have favourable orientation for growth). For, c_3 = 6 the distribution of shear strain on the primary slip and primary twinning systems are identical to step 2 (Figure 3-24). Furthermore, there is no shear strain on the secondary slip systems.
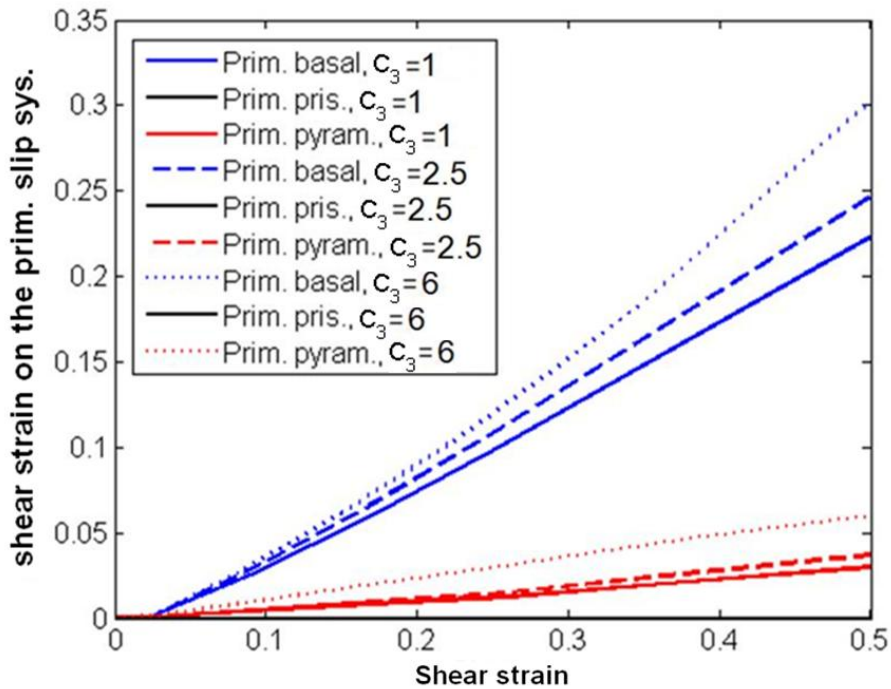

Figure 3-25 Distribution of shear strain on the primary slip systems, steps 3-4

Figure 3-26 a) Distribution of shear strain on the primary twinning systems, and b) secondary slip systems, steps 3-4

Figure 3-27 Distribution of shear strain on the primary slip systems, step 5

In step 5, the distribution of shear strain on the primary slip systems is shown in Figure 3-27. The distribution of shear strain on the primary twinning and secondary pyramidal $<c+a>$ slip systems are shown in Figure 3-28. The shear strain accumulated by the secondary twinning systems is shown in Figure 3-29 for three cases of c_3 = 1, 2.5, and 6. For c_3 = 1 and 2.5, the distribution of shear strain on the primary slip and primary twinning systems are very similar to step 2 (Figure 3-24). Around a shear of 0.045, nucleation of the secondary slip systems was allowed. Around a shear of 0.055 nucleation of the secondary twinning systems was allowed. Figure 3-26b shows the shear strain on the secondary

66

pyramidal $<c+a>$ slip systems, and Figure 3-29 shows the shear strain accumulated by the secondary twinning systems. For $c_3 = 6$, the distribution of shear strain on the primary slip systems and primary twinning systems are identical to step 2 (Figure 3-24). Furthermore, there is no shear strain on the secondary slip and twinning systems.

a)

b)
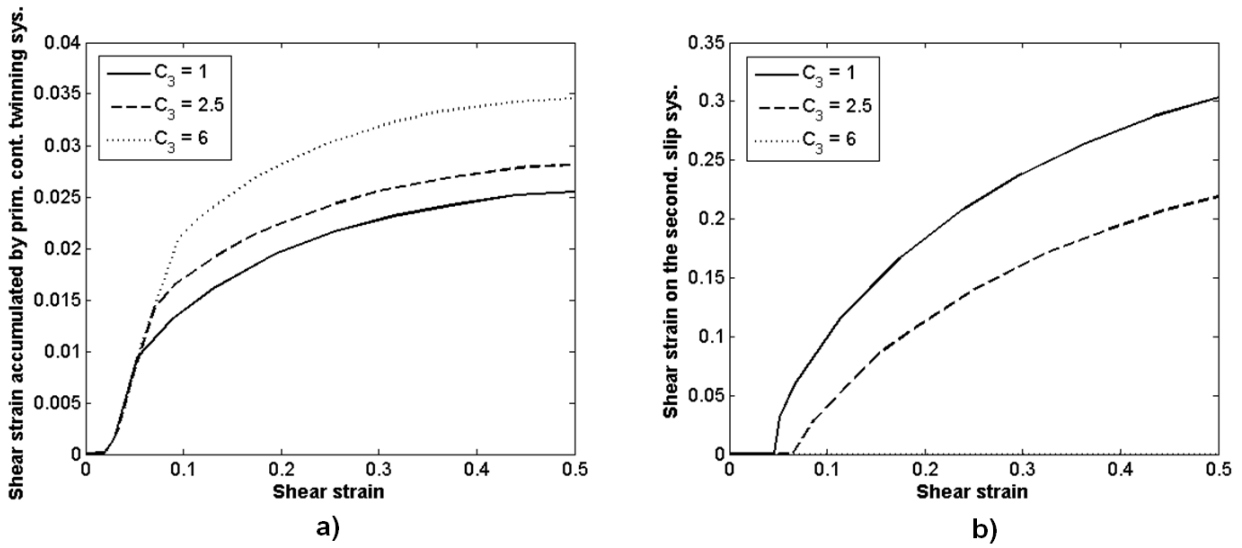
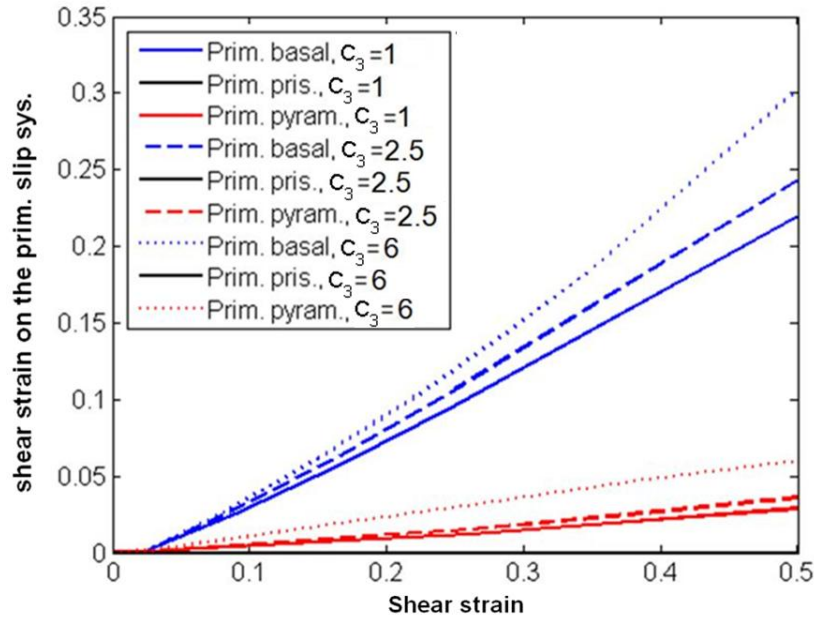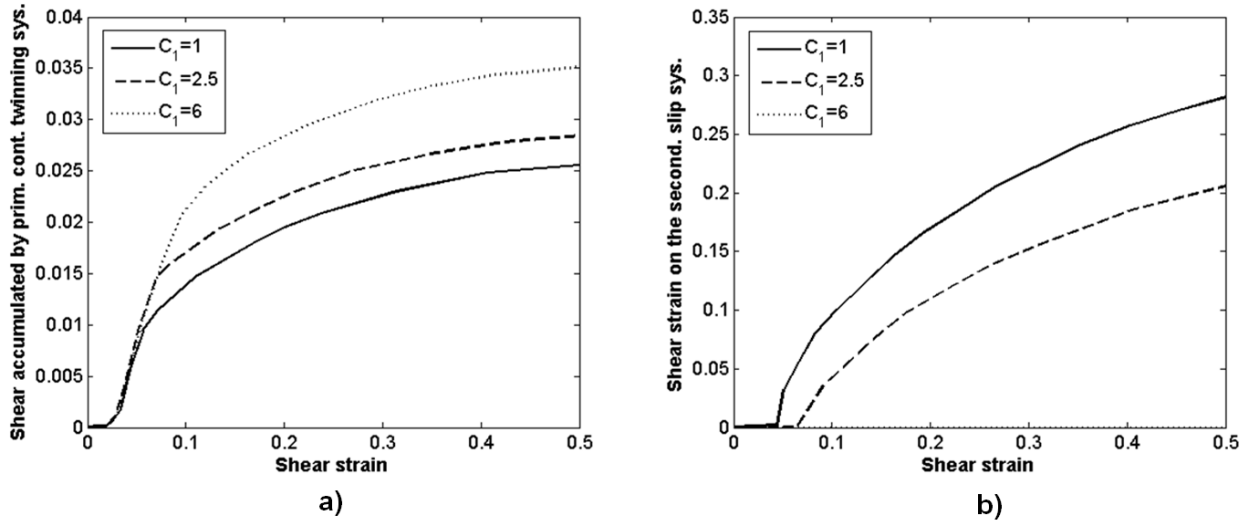Figure 3-28 a) Distribution of shear strain on the primary twinning systems, and b) secondary slip systems, step 5
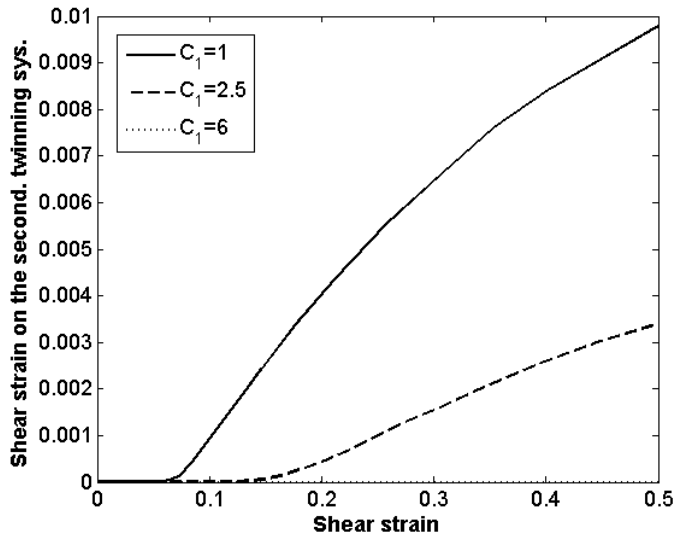
Figure 3-29 Shear strain accumulated by the secondary twinning systems, step 5

While the c_3 value was kept constant in the above simulations, it is trivial to see how an evolving c_3 value from low to high, and/or high to low can affect the material response. Therefore, one can

conclude that the partially calibrated CPCM predicts that, depending upon the plastic deformation mechanisms taken into account and the resistance considered for them, the large strain deformation of the material can be different. This, in other words, indicates that neglecting secondary slip and twinning systems can reduce the accuracy of the predicted microscopic (texture) and macroscopic properties (stress-strain response) of magnesium alloys by the crystal plasticity modelling scheme. It is clear from the above that contraction twinning must not be neglected in any simulation of magnesium deformation.

Chapter 4

Predicting the forming limit diagram for a single crystal of magnesium

4.1 Introduction

Assessing the FLDs of metals is integral to the study of their formability capabilities. In a practical sense, Keeler [66] introduced the concept of an FLD from his experimental investigations on plastic instability and fracture in sheets stretched over steel punches. His idea was proven to be very useful in representing the flow localization during sheet stretching. In a theoretical sense, there are two main approaches to compute FLDs in sheet metals. The first approach is the perturbation method based on the stability of deformation [67,68]. In this method, one deformation mode is considered in the entire sheet. Tóth et al. [68] computed FLDs where they accounted for the texture development. The second approach, which is the focus of this thesis, is based on the Marciniak–Kuczynski (M–K) analysis [69]. In the M–K analysis, thickness imperfections are introduced to simulate pre-existing defects in the sheet material. Unlike the perturbation method, the deformation mode in the groove is different from the mode outside the groove. Necking is considered to occur when the ratio of the thickness in the groove to the nominal thickness is below a critical value. Marciniak and Kuczynski [69] showed that the presence of even slight intrinsic inhomogeneities in load bearing capacity throughout a deforming sheet can lead to unstable growth of strain in the weaker regions, and subsequently can cause localized necking and failure [70,71].

By using the phenomenological plasticity models within the M–K framework, the influence of yield surface vertices, anisotropy, and material rate sensitivity on FLDs were explored [72-74]. A detailed discussion about the development of phenomenological-plasticity-based models for FLD computation can be found in [70]. The initial texture and its evolution are two important factors in the formability of anisotropic materials. Tóth et al. [75,76] used the M–K framework and, by accounting for texture evolution, computed the FLDs for aluminum sheets. Wu et al. [70,77] and Inal et al. [71] used the rate-dependent Crystal Plasticity Constitutive Model (CPCM) of Peirce et al. [30] to calculate FLDs for FCC and BCC polycrystals, respectively. The effects of initial imperfection intensity and orientation, initial distribution of grain orientations, crystal elasticity, strain-rate sensitivity, single slip hardening, and latent hardening on the predicted FLDs were discussed in detail in the works by Wu et al. [70,77] and Inal et al. [71]. Neil and Agnew [33] used a Viscoplastic Self-Consistent (VPSC) polycrystal plasticity model [78] in conjunction with the M-K framework to predict the FLDs for magnesium alloy, AZ31B, sheets. While they had considerable success, Lévesque et al. [29] addressed the requirement of a CPCM to generate FLDs for magnesium alloys (within the M-K framework) that would account for the strain rate effects. They used a rate-dependent elastic-viscoplastic CPCM with Taylor [8] assumptions in conjunction with the M-K framework to predict the formability of AM30 magnesium alloy at $200^\circ C$ at the strain rates of 0.1/s, 0.01/s, and 0.001/s.

In this thesis, as an application of the proposed CPCM, the effect of intragranular plastic deformation mechanisms of primary slip and twinning systems on the formability of a magnesium single crystal at room temperature is studied. This was done by simulating the FLDs using the proposed CPCM together with the M–K framework. The parameter values of the resistance functions for the primary slip and twinning systems obtained by calibration in Chapter 3 were used to simulate the FLDs. The significance of this investigation is that by studying the formability in magnesium single crystals, where the grain boundary effects do not have any contribution in the plastic deformation, the exclusive effect of intragranular plastic deformation mechanisms on the formability of magnesium can be assessed.

According to the available literature to date, the effects of intragranular plastic deformation mechanisms in magnesium on its formability has not been exclusively studied. When more experimental data is available, assessing the effect of secondary twinning systems, as well as secondary and tertiary slip systems on formability of magnesium single crystals in different crystal orientations and loading paths, will be possible.

The FLDs were computed for two different crystal orientations. In the first orientation, primary slip systems and extension twinning systems have favourable orientation for activation. In the second orientation, primary slip systems, as well as contraction twinning systems have favourable orientation for activation. Aside from the effect of primary slip and twinning systems on the FLDs, the effects of rate

sensitivity, c/a ratio, and shear strain (D_{12}) outside the necking band on the simulated FLDs for the two orientations were investigated.

Sheet necking was initiated from an initial imperfection in terms of a narrow band. The deformations inside and outside the band were assumed to be homogeneous and conditions of compatibility and equilibrium were enforced across the band interfaces. Thus, the CPCM needs to be applied to only two regions, one inside and one outside the band.

The problem formulation and the method of solution are presented in Section 4.2. In section 4.3, the predicted FLDs for two grain orientations under various conditions are presented.

4.2 Formulation for the computation of the forming limit diagram

In Figure 4-1, x_1 and x_2 are the global coordinate system. A sheet having a non-uniformity in the form of a band (or groove) which is initially inclined at an angle ψ with respect to the x_2 direction is considered in the analysis.
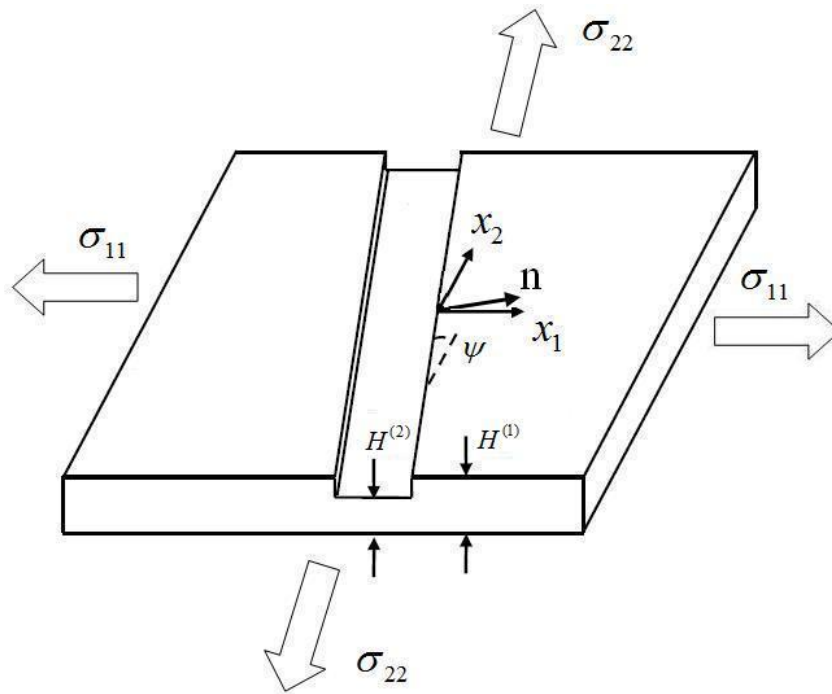

Figure 4-1 The geometry and convention used in the FLD analysis [33]

Quantities outside and inside the band are denoted by (1) and (2), respectively. The thickness along the minimum section in the band is denoted by $H^{(2)}(t)$ with an initial value of $H^{(2)}(0)$. The initial geometric non-uniformity is defined by:

$$f = \frac{H^{(2)}(0)}{H^{(1)}(0)} \tag{4-1}$$

where $H^{(1)}(0)$ is the initial thickness outside the band. The typical value of f is between 0.95 and 0.995 [71,77].

The imposed boundary conditions on the edges of the sheet are as follows:

$$\frac{D_{22}^{(1)}}{D_{11}^{(1)}} = \rho = \text{const.} \tag{4-2}$$

$$\dot{\sigma}_{33}^{(1)} = 0, \ \dot{\sigma}_{12}^{(1)} = 0 \tag{4-3}$$

where $D_{11}^{(1)}$ and $D_{22}^{(1)}$ are the (principal) logarithmic strain rates and $\sigma^{(1)}$ is the total Cauchy stress outside the band. In step 1 of the model, where the plastic deformation mechanisms are primary slip systems alone and there is no twinned region, the total Cauchy stress is equal to the stress in the parent (matrix) and is given by Equation (2-26). In step 2 of the model, where the plastic deformation mechanisms are primary slip and twinning systems, a homogeneous deformation field is assumed in the parent and twinned regions of the grain (Taylor [8] assumptions), and the total Cauchy stress is a weighted average of the stresses in the parent and twinned regions of the grain given by Equation (2-55).

Following the works in [29,70,71,77] the following conditions are imposed:

$$D_{13}^{(1)} = D_{23}^{(1)} = 0, \Omega_{12}^{(1)} = \Omega_{13}^{(1)} = \Omega_{23}^{(1)} = 0 \tag{4-4}$$

where Ω is the spin tensor. These are simplifying assumptions to reduce the numerical calculations.

In the papers by Wu et al. [70,77] and Inal et al. [71] the effect of shear strain $D_{12}^{(1)}$ in the formulation was ignored, i.e. it was assumed $D_{12}^{(1)} = 0$. This was done to avoid the required numerical computations to calculate the shear strain $D_{12}^{(1)}$ outside the band. Because of the anisotropic relationship between the Jaumann rate of stress and strain rate (Equations (2-19), (2-42), and (2-43)), the condition of $D_{12}^{(1)} = 0$ may or may not result in a zero value for $\sigma_{12}^{(1)}$ (in brief, this depends on the relative orientation of the grain with respect to the global coordinate system shown in Figures 4-1 and 4-2; more details are available in [79]).

In the current work we account for $D_{12}^{(1)}$ for more accuracy. $D_{12}^{(1)}$ and $D_{33}^{(1)}$ are simultaneously calculated in each simulation time step by the boundary conditions in Equation (4-3) (in this case, $\sigma_{12}^{(1)}$ is zero throughout the entire deformation).

The simulation results corresponding to these two different boundary conditions are compared in Subsection 4.4.1.

Under this deformation condition, the groove orientation ψ is updated by [72]:

$$\tan(\psi_{n+1}) = e^{((1-\rho)\varepsilon_{11}^{(1)})} \tan(\psi_n) \tag{4-5}$$

Since uniform deformations are assumed both inside and outside the band, equilibrium and compatibility inside and outside the band are automatically satisfied, apart from the necessary conditions at the band interface. Following Hutchinson and Neale [72], the compatibility condition at the band interface is given in terms of the differences in the velocity gradients inside and outside the band as follows:

$$L_{\alpha\beta}^{(2)} = L_{\alpha\beta}^{(1)} + g_\alpha n_\beta \tag{4-6}$$

or

$$D_{\alpha\beta}^{(2)} = D_{\alpha\beta}^{(1)} + \frac{1}{2}\left(g_\alpha n_\beta + g_\beta n_\alpha\right), \ \Omega_{\alpha\beta}^{(2)} = \Omega_{\alpha\beta}^{(1)} + \frac{1}{2}\left(g_\alpha n_\beta - g_\beta n_\alpha\right) \tag{4-7}$$

here, $n_1 = \cos(\psi)$ and $n_2 = \sin(\psi)$ are the components of the unit normal to the band in the current configuration (Figure 4-1). The g_α values are the parameters to be determined. Equilibrium on each side of the interface requires that:

$$\left(n_1\sigma_{11}^{(2)} + n_2\sigma_{21}^{(2)}\right) H^{(2)} = \left(n_1\sigma_{11}^{(1)} + n_2\sigma_{21}^{(1)}\right) H^{(1)} \tag{4-8}$$

$$\left(n_1\sigma_{12}^{(2)} + n_2\sigma_{22}^{(2)}\right) H^{(2)} = \left(n_1\sigma_{12}^{(1)} + n_2\sigma_{22}^{(1)}\right) H^{(1)} \tag{4-9}$$

Again, σ is the total Cauchy stress. The sheet thicknesses outside the band $H^{(1)}$ and inside the band $H^{(2)}$ are updated with the following evolution functions:

$$\dot{H}^{(1)} = D_{33}^{(1)} H^{(1)} \text{ and } \dot{H}^{(2)} = D_{33}^{(2)} H^{(2)} \tag{4-10}$$

The same instability criterion used by Inal [71] and Wu [70] was implemented in this research, i.e. the onset of sheet necking is defined by the occurrence of a much higher maximum principal logarithmic strain rate inside the band rather than outside the band: $\dfrac{D_{33}^{(2)}}{D_{11}^{(1)}} \geq 10^5$.

4.3 The integration procedure used to simulate the forming limit diagrams using step 2 of the crystal plasticity constitutive model and M-K framework

The integration procedure of the CPCM when primary slip and twinning systems are the plastic deformation mechanisms (i.e. step 2 of the CPCM) within the M-K approach is presented in this subsection. This is a more complicated scenario than the case where the plastic deformation mechanisms are primary slip systems alone (i.e. step 1 of the CPCM). For the sake of simplicity, the forward Euler integration algorithm was used to integrate the constitutive equations within the updated Lagrangian setting. The idea behind this algorithm is to use the slip rates per slip system, and the volume fraction rates per twinning system at time $t_{(n)}$ to compute quantities for time $t_{(n+1)}$. For forward Euler integration scheme to give valid results, a rather small time step has to be used.

- Subroutine passes $D_{11(n)}^{(1)}$, $\gamma_{(n)}^{(ip)\alpha p}$, $g_{(n)}^{(ip)\alpha p}$, $f_{(n)}^{(ip)\beta p}$, $g_{(n)}^{(ip)\beta p}$, $\sigma_{(n)}^{(ip)mat}$, $\sigma_{(n)}^{(ip)\beta p}$, $\varphi_{1(n)}^{(ip)}$, $\varphi_{(n)}^{(ip)}$, $\varphi_{2(n)}^{(ip)}$, $\Delta F_{(n)}^{*(ip)}$,

$\varepsilon_{11(n)}^{(1)}$, $\psi_{(n)}$, $n_{1(n)}$, $n_{2(n)}$, $H_{(n)}^{(1)}$, $H_{(n)}^{(2)}$, Δt

- Updating the lattice vectors and P and W inside and outside the band:

$$s_{(n)}^{*(ip)(\alpha p)} = \Delta F_{(n)}^{*(ip)} Q_{(n)}^{(ip)} s_{(1)}^{(ip)(\alpha p)} \tag{4-11}$$

$$s_{(n)}^{*(ip)(\beta p)} = \Delta F_{(n)}^{*(ip)} Q_{(n)}^{(ip)} s_{(1)}^{(ip)(\beta p)} \tag{4-12}$$

$$m_{(n)}^{*(ip)(\alpha p)} = Q_{(n)}^{(ip)} m_{(1)}^{(ip)(\alpha p)} \Delta F_{(n)}^{*(ip)-1} \tag{4-13}$$

$$m_{(n)}^{*(ip)(\beta p)} = Q_{(n)}^{(ip)} m_{(1)}^{(ip)(\beta p)} \Delta F_{(n)}^{*(ip)-1} \tag{4-14}$$

$$P_{(n)}^{(ip)(\alpha p)} = \frac{1}{2}(s_{(n)}^{*(ip)(\alpha p)} \otimes m_{(n)}^{*(ip)(\alpha p)} + m_{(n)}^{*(ip)(\alpha p)} \otimes s_{(n)}^{*(ip)(\alpha p)}) \tag{4-15}$$

$$W_{(n)}^{(ip)(\alpha p)} = \frac{1}{2}(s_{(n)}^{*(ip)(\alpha p)} \otimes m_{(n)}^{*(ip)(\alpha p)} - m_{(n)}^{*(ip)(\alpha p)} \otimes s_{(n)}^{*(ip)(\alpha p)}) \tag{4-16}$$

$$P_{(n)}^{(ip)(\beta p)} = \frac{1}{2}(s_{(n)}^{*(ip)(\beta p)} \otimes m_{(n)}^{*(ip)(\beta p)} + m_{(n)}^{*(ip)(\beta p)} \otimes s_{(n)}^{*(ip)(\beta p)}) \tag{4-17}$$

$$W_{(n)}^{(ip)(\beta p)} = \frac{1}{2}(s_{(n)}^{*(ip)(\beta p)} \otimes m_{(n)}^{*(ip)(\beta p)} - m_{(n)}^{*(ip)(\beta p)} \otimes s_{(n)}^{*(ip)(\beta p)})$$

(4-18)

- Updating the elasticity modulus:

$$C_{mat(n)}^{(ip)} = Q_{(n)}^{(ip)}Q_{(n)}^{(ip)} \overset{\circ}{C} Q_{(n)}^{(ip)}Q_{(n)}^{(ip)T}$$

(4-19)

$$Q_{(n)}^{(ip)tw1} = Q_{(n)}^{(ip)} \times (X^{(ip)-1}RX^{(ip)})^{-1}$$

(4-20)

$$C_{tw1(n)}^{(ip)} = Q_{(n)}^{(ip)tw1}Q_{(n)}^{(ip)tw1} \overset{\circ}{C} Q_{(n)}^{(ip)tw1T}Q_{(n)}^{(ip)tw1T}$$

(4-21)

- Calculating the slip shear strain rates at time $t_{(n)}$ using the stress state and $P_{(n)}^{(ip)\alpha p}$, and the volume fraction rates at time $t_{(n)}$ using the stress state and $P_{(n)}^{(ip)\beta p}$:

$$\sigma_{(n)}^{(ip)(\alpha p)} = P_{(n)}^{(ip)(\alpha p)} : \sigma_{(n)}^{(ip)mat}$$

(4-22)

$$\dot{\gamma}_{(n)}^{(ip)(\alpha p)} = \dot{\gamma}_\circ \operatorname{sgn}(\sigma_{(n)}^{(ip)(\alpha p)}) \left| \frac{\sigma_{(n)}^{(ip)(\alpha p)}}{g_{(n)}^{(ip)(\alpha p)}} \right|^{\left(\frac{1}{m}\right)-1}$$

(4-23)

$$\sigma_{(n)}^{ave((ip)mat,(ip)\beta p)} = (1 - f_{(n)}^{(ip)\beta p})\sigma_{(n)}^{(ip)mat} + f_{(n)}^{(ip)\beta p}\sigma_{(n)}^{(ip)\beta p}$$

(4-24)

$$\sigma_{(n)}^{(ip)(\beta p)} = P_{(n)}^{(ip)(\beta p)} : \sigma_{(n)}^{ave((ip)mat,(ip)\beta p)}$$

(4-25)

$$\dot{f}_{(n)}^{(ip)(\beta p)} = \frac{\dot{f}_\circ}{\gamma_{tw}^{(\beta p)}} \operatorname{sgn}(\sigma_{(n)}^{(ip)(\beta p)}) \left| \frac{\sigma_{(n)}^{(ip)(\beta p)}}{g_{(n)}^{(ip)(\beta p)}} \right|^{\left(\frac{1}{m}\right)-1}$$

(4-26)

- Computing total slip, resistance and update the shear strengths of the slip systems:

$$\gamma_{(n+1)}^{(ip)(\alpha p)} = \gamma_{(n)}^{(ip)(\alpha p)} + \sum_{(ip)\alpha p} \left| \dot{\gamma}_{(n)}^{(ip)(\alpha p)} \right| \Delta t$$

(4-27)

$$f_{(n+1)}^{(ip)(\beta p)} = f_{(n)}^{(ip)(\beta p)} + \sum_{(ip)\beta p} \left| \dot{f}_{(n)}^{(ip)(\beta p)} \right| \Delta t$$

(4-28)

75

$$g_{(n+1)}^{(ip)(\alpha p)} = g_{(n)}^{(ip)(\alpha p)} + \sum_{(ip)\alpha p} h_{(ip)\alpha p(n)}^{2A} \left| \dot{\gamma}_{(n)}^{(ip)(\alpha p)} \right| \Delta t + \sum_{(ip)\beta p} h_{(ip)\beta p(n)}'^{2A} \left| \dot{f}_{(n)}^{(ip)(\beta p)} \right| \Delta t \qquad (4\text{-}29)$$

$$g_{(n+1)}^{(ip)(\beta p)} = g_{(n)}^{(ip)(\beta p)} + \sum_{(ip)\alpha p} h_{(ip)\alpha p(n)}^{2B} \left| \dot{\gamma}_{(n)}^{(ip)(\alpha p)} \right| \Delta t + \sum_{(ip)\beta p} h_{(ip)\beta p(n)}'^{2B} \left| \dot{f}_{(n)}^{(ip)(\beta p)} \right| \Delta t \qquad (4\text{-}30)$$

- Update $D_{22}^{(1)}$

$$D_{22(n)}^{(1)} = \rho D_{11(n)}^{(1)} \qquad (4\text{-}31)$$

- Calculating $D_{33(n)}^{(1)}$ and $D_{12(n)}^{(1)}$ outside the band by simultaneously solving the following two equations:

$$\dot{\sigma}_{33(n)}^{(1)tot} = \frac{d}{dt}\left(\left(1 - \sum_{\beta p} f_{(n)}^{(1)\beta p} \right) \sigma_{33(n)}^{(1)mat} + \sum_{\beta p} f_{(n)}^{(1)\beta p} \sigma_{33(n)}^{(1)\beta p} \right) = 0 \qquad (4\text{-}32)$$

$$\dot{\sigma}_{12(n)}^{(1)tot} = \frac{d}{dt}\left(\left(1 - \sum_{\beta p} f_{(n)}^{(1)\beta p} \right) \sigma_{12(n)}^{(1)mat} + \sum_{\beta p} f_{(n)}^{(1)\beta p} \sigma_{12(n)}^{(1)\beta p} \right) = 0 \qquad (4\text{-}33)$$

- Calculating g_1, g_2, and $D_{33(n)}^{(2)}$ inside the band by simultaneously solving the following three equations:

$$\left(n_{1(n)}\sigma_{11(n)}^{(2)tot} + n_{2(n)}\sigma_{21(n)}^{(2)tot} \right) H_{(n)}^{(2)} = \left(n_{1(n)}\sigma_{11(n)}^{(1)tot} + n_{2(n)}\sigma_{21(n)}^{(1)tot} \right) H_{(n)}^{(1)} \qquad (4\text{-}34)$$

$$\left(n_{1(n)}\sigma_{12(n)}^{(2)tot} + n_{2(n)}\sigma_{22(n)}^{(2)tot} \right) H_{(n)}^{(2)} = \left(n_{1(n)}\sigma_{12(n)}^{(1)tot} + n_{2(n)}\sigma_{22(n)}^{(1)tot} \right) H_{(n)}^{(1)} \qquad (4\text{-}35)$$

$$\dot{\sigma}_{33(n)}^{(2)tot} = \frac{d}{dt}\left(\left(1 - \sum_{\beta p} f_{(n)}^{(2)\beta p} \right) \sigma_{33(n)}^{(2)mat} + \sum_{\beta p} f_{(n)}^{(2)\beta p} \sigma_{33(n)}^{(2)\beta p} \right) = 0 \qquad (4\text{-}36)$$

- Updating $H^{(1)}$, $H^{(2)}$, ψ, n_1, and n_2:

$$H_{(n+1)}^{(1)} = H_{(n)}^{(1)} e^{(D_{33(n)}^{(1)} dt)} \qquad (4\text{-}37)$$

$$H_{(n+1)}^{(2)} = H_{(n)}^{(2)} e^{(D_{33(n)}^{(2)} dt)} \qquad (4\text{-}38)$$

$$\psi_{(n+1)} = \tan^{-1}(e^{((1-\rho)\varepsilon_{11(n)}^{(1)})} \tan(\psi_{(1)})) \tag{4-39}$$

$$n_{1(n+1)} = \cos(\psi_{(n+1)}) \tag{4-40}$$

$$n_{2(n+1)} = \sin(\psi_{(n+1)}) \tag{4-41}$$

$$\varepsilon_{11(n+1)}^{(1)} = \varepsilon_{11(n)}^{(1)} + D_{11(n)}^{(1)} dt \tag{4-42}$$

- Updating the deformation rate and spin inside the band:

$$D_{11(n)}^{(2)} = D_{11(n)}^{(1)} + g_1 n_{1(n)} \tag{4-43}$$

$$D_{22(n)}^{(2)} = D_{22(n)}^{(1)} + g_2 n_{2(n)} \tag{4-44}$$

$$D_{12(n)}^{(2)} = D_{12(n)}^{(1)} + \frac{1}{2}(g_1 n_{2(n)} + g_2 n_{1(n)}) \tag{4-45}$$

$$D_{13(n)}^{(2)} = \frac{1}{2}(g_1 n_{3(n)} + g_3 n_{1(n)}) \tag{4-46}$$

$$D_{23(n)}^{(2)} = \frac{1}{2}(g_2 n_{3(n)} + g_3 n_{2(n)}) \tag{4-47}$$

$$\Omega_{12(n)}^{(2)} = \frac{1}{2}(g_1 n_{2(n)} - g_2 n_{1(n)}) \tag{4-48}$$

$$\Omega_{13(n)}^{(2)} = \frac{1}{2}(g_1 n_{3(n)} - g_3 n_{1(n)}) \tag{4-49}$$

$$\Omega_{23(n)}^{(2)} = \frac{1}{2}(g_2 n_{3(n)} - g_3 n_{2(n)}) \tag{4-50}$$

- Updating the stress in the parent, primary twinned region, and the whole grain:

$$
\overset{\triangledown\,(ip)(mat)}{\sigma_{(n)}} = C^{(ip)}_{mat(n)} D^{(ip)}_{(n)} - \sum_{(ip)\alpha p}\left(C^{(ip)}_{mat(n)} P^{(ip)(\alpha p)}_{(n)} + W^{(ip)(\alpha p)}_{(n)}\sigma^{(ip)mat}_{(n)} - \sigma^{(ip)mat}_{(n)} W^{(ip)(\alpha p)}_{(n)} \right)\dot{\gamma}^{(ip)(\alpha p)}_{(n)}
$$
$$
- \sum_{(ip)\beta p}\left(C^{(ip)}_{mat(n)} P^{(ip)(\beta p)}_{(n)} + W^{(ip)(\beta p)}_{(n)}\sigma^{(ip)mat}_{(n)} - \sigma^{(ip)mat}_{(n)} W^{(ip)(\beta p)}_{(n)} \right)\dot{f}^{(ip)(\beta p)}_{(n)}\gamma^{(\beta p)}_{tw}
$$
$$
- \sigma^{(ip)mat}_{(n)}\left(D^{(ip)}_{11(n)} + D^{(ip)}_{22(n)} + D^{(ip)}_{33(n)} \right)
$$

(4-51)

$$
\overset{\triangledown\,(ip)(tw1)}{\sigma_{(n)}} = C^{(ip)}_{tw1(n)} D^{(ip)}_{(n)} - \sum_{(ip)\alpha p}\left(C^{(ip)}_{tw1(n)} P^{(ip)(\alpha p)}_{(n)} + W^{(ip)(\alpha p)}_{(n)}\sigma^{(ip)tw1}_{(n)} - \sigma^{(ip)tw1}_{(n)} W^{(ip)(\alpha p)}_{(n)} \right)\dot{\gamma}^{(ip)(\alpha p)}_{(n)}
$$
$$
- \sum_{(ip)\beta p}\left(C^{(ip)}_{tw1(n)} P^{(ip)(\beta p)}_{(n)} + W^{(ip)(\beta p)}_{(n)}\sigma^{(ip)tw1}_{(n)} - \sigma^{(ip)tw1}_{(n)} W^{(ip)(\beta p)}_{(n)} \right)\dot{f}^{(ip)(\beta p)}_{(n)}\gamma^{(\beta p)}_{tw}
$$
$$
- \sigma^{(ip)tw1}_{(n)}\left(D^{(ip)}_{11(n)} + D^{(ip)}_{22(n)} + D^{(ip)}_{33(n)} \right)
$$

(4-52)

$$
\sigma^{(ip)mat}_{(n+1)} = \sigma^{(ip)mat}_{(n)} + \left(\overset{\triangledown\,(ip)(mat)}{\sigma_{(n)}} + \Omega^{(ip)}_{(n)}\sigma^{(ip)mat}_{(n)} - \sigma^{(ip)mat}_{(n)}\Omega^{(ip)}_{(n)} \right)\Delta t
$$

(4-53)

$$
\sigma^{(ip)tw1}_{(n+1)} = \sigma^{(ip)tw1}_{(n)} + \left(\overset{\triangledown\,(ip)tw1}{\sigma_{(n)}} + \Omega^{(ip)}_{(n)}\sigma^{(ip)tw1}_{(n)} - \sigma^{(ip)tw1}_{(n)}\Omega^{(ip)}_{(n)} \right)\Delta t
$$

(4-54)

$$
\sigma^{(ip)tot}_{(n+1)} = \left(1 - \sum_{(ip)\beta p} f^{(ip)\beta p}_{(n+1)} \right)\sigma^{(ip)mat}_{(n+1)} + \sum_{(ip)\beta p} f^{(ip)\beta p}_{(n+1)}\sigma^{(ip)\beta p}_{(n+1)}
$$

(4-55)

- Updating the orientation matrix $Q^{(ip)}_{(n)}$ and the Bunge angles [59]:

$$
\Omega^{(ip)p}_{(n)} = \sum_{(ip)\alpha p} W^{(ip)(\alpha p)}_{(n)}\dot{\gamma}^{(ip)(\alpha p)}_{(n)} + \sum_{(ip)\beta p} W^{(ip)(\beta p)}_{(n)}\dot{f}^{(ip)(\beta p)}_{(n)}\gamma^{(\beta p)}_{tw}
$$

(4-56)

$$
\Omega^{(ip)*}_{(n)} = \Omega^{(ip)}_{(n)} - \Omega^{(ip)p}_{(n)}
$$

(4-57)

$$
Q^{(ip)}_{(n+1)} = e^{\left(\Omega^{*(ip)}_{(n)}\cdot\Delta t \right)} Q^{(ip)}_{(n)}
$$

(4-58)

$$Q_{(n+1)}^{(ip)} = \begin{bmatrix} Q_{11(n+1)}^{(ip)} & Q_{12(n+1)}^{(ip)} & Q_{13(n+1)}^{(ip)} \\ Q_{21(n+1)}^{(ip)} & Q_{22(n+1)}^{(ip)} & Q_{23(n+1)}^{(ip)} \\ Q_{31(n+1)}^{(ip)} & Q_{32(n+1)}^{(ip)} & Q_{33(n+1)}^{(ip)} \end{bmatrix} \tag{4-59}$$

where from Bunge [59]:

$$Q_{11(n+1)}^{(ip)} = \cos(\varphi_{2(n+1)}^{(ip)})\cos(\varphi_{1(n+1)}^{(ip)}) - \sin(\varphi_{2(n+1)}^{(ip)})\sin(\varphi_{1(n+1)}^{(ip)})\cos(\varphi_{(n+1)}^{(ip)}) \tag{4-60}$$

$$Q_{12(n+1)}^{(ip)} = -\sin(\varphi_{2(n+1)}^{(ip)})\cos(\varphi_{1(n+1)}^{(ip)}) - \cos(\varphi_{2(n+1)}^{(ip)})\sin(\varphi_{1(n+1)}^{(ip)})\cos(\varphi_{(n+1)}^{(ip)}) \tag{4-61}$$

$$Q_{13(n+1)}^{(ip)} = \sin(\varphi_{1(n+1)}^{(ip)})\sin(\varphi_{(n+1)}^{(ip)}) \tag{4-62}$$

$$Q_{21(n+1)}^{(ip)} = \cos(\varphi_{2(n+1)}^{(ip)})\sin(\varphi_{1(n+1)}^{(ip)}) + \sin(\varphi_{2(n+1)}^{(ip)})\cos(\varphi_{1(n+1)}^{(ip)})\cos(\varphi_{(n+1)}^{(ip)}) \tag{4-63}$$

$$Q_{22(n+1)}^{(ip)} = -\sin(\varphi_{2(n+1)}^{(ip)})\sin(\varphi_{1(n+1)}^{(ip)}) + \cos(\varphi_{2(n+1)}^{(ip)})\cos(\varphi_{1(n+1)}^{(ip)})\cos(\varphi_{(n+1)}^{(ip)}) \tag{4-64}$$

$$Q_{23(n+1)}^{(ip)} = -\cos(\varphi_{1(n+1)}^{(ip)})\sin(\varphi_{(n+1)}^{(ip)}) \tag{4-65}$$

$$Q_{31(n+1)}^{(ip)} = \sin(\varphi_{2(n+1)}^{(ip)})\sin(\varphi_{(n+1)}^{(ip)}) \tag{4-66}$$

$$Q_{32(n+1)}^{(ip)} = \cos(\varphi_{2(n+1)}^{(ip)})\sin(\varphi_{(n+1)}^{(ip)}) \tag{4-67}$$

$$Q_{33(n+1)}^{(ip)} = \cos(\varphi_{(n+1)}^{(ip)}) \tag{4-68}$$

$$Q_{(n+1)}^{(ip)} \rightarrow \varphi_{1(n+1)}^{(ip)}, \varphi_{(n+1)}^{(ip)}, \varphi_{2(n+1)}^{(ip)} \tag{4-69}$$

- Calculating $\Delta F^{*(ip)}$:

$$\Delta L_{(n)}^{(ip)P} = \left(\sum_{(ip)\alpha p} s_{(n)}^{*(ip)(\alpha p)} \otimes m_{(n)}^{*(ip)(\alpha p)} \dot{\gamma}_{(n)}^{(ip)(\alpha p)} + \sum_{(ip)\beta p} s_{(n)}^{*(ip)(\beta p)} \otimes m_{(n)}^{*(ip)(\beta p)} \dot{f}_{(n)}^{(ip)(\beta p)} \gamma_{tw}^{(\beta p)} \right) \Delta t \tag{4-70}$$

$$L_{(n)}^{(ip)} = D_{(n)}^{(ip)} + \Omega_{(n)}^{(ip)} \tag{4-71}$$

$$\Delta F_{(n+1)}^{*(ip)} = I + L_{(n)}^{(ip)} \Delta t - \Delta L_{(n)}^{(ip)P} \qquad (4\text{-}72)$$

- Condition to exit the subroutine:

$$D_{33(n)}^{(2)} > 10^5 D_{33(n)}^{(1)} \qquad (4\text{-}73)$$

4.4 Forming limit diagram results and discussion

The FLDs were simulated for two orientations (Figure 4-2). In orientation A, primary slip systems and extension twinning systems have favourable orientation for activation. In orientation B, primary slip systems and contraction twinning systems have favourable orientation for activation. The Bunge angles [59] corresponding to these two orientations are as follows:

Orientation A:

$$\varphi_1 = \frac{\pi}{2}, \ \varphi = \frac{\pi}{2}, \ \varphi_2 = -\frac{\pi}{2} \qquad (4\text{-}74)$$

Orientation B:

$$\varphi_1 = \pi, \ \varphi = \frac{\pi}{2}, \ \varphi_2 = \frac{\pi}{2} \qquad (4\text{-}75)$$

The relationship between the Bunge angles and orientation matrix is given in Equations (2-178)-(2-187).
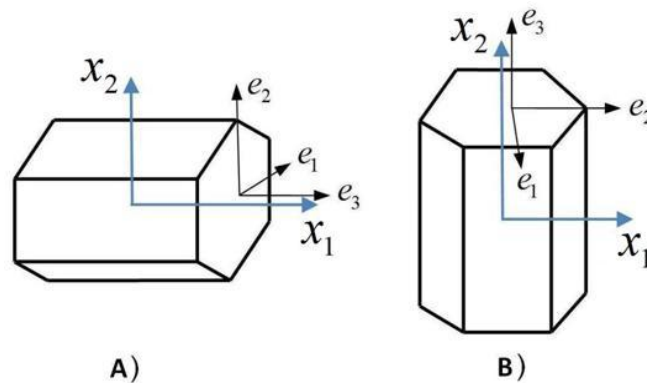

Figure 4-2 Grain orientations along with the lattice and global coordinate systems: a) orientation A, and b) orientation B

There are two reasons for choosing these two orientations. First, in each orientation only one twinning kind (extension or contraction) has favourable orientation for activation; the effect of each

twinning kind can be assessed individually. Second, because the required loadings in orientations A and B in Figure 4-2 to compute the FLDs are similar to the loadings in crystal orientations 2, 3, 4, and 5 (Figure 3-7), it is expected that the predicted FLDs in these two orientations have the most accuracy, compared with other grain orientations. The similarity here is that the prediction of a non-linear model around the operating point at which it was calibrated is much more accurate, compared with its prediction at other operating points.

For the above two orientations, the effects of shear strain ($D_{12}^{(1)}$) outside the necking band, slip and twinning systems, rate sensitivity parameter (m), and c/a ratio on the FLDs have been investigated. In these studies, the groove angle was changed from 0 to $40°$ at increments of $5°$ (similar to the work of Neil and Agnew [33] and Inal et al. [71]) to find the critical groove orientation at which the model predicts minimum formability. The initial imperfection parameter f in Equation (4-1) was taken as 0.992 in all the calculations. To simulate the FLDs, the strain rate ratio, ρ in Equation (4-2), was varied from 0 to 1. Because the constitutive model was not calibrated for compressive loading parallel and perpendicular to the c-axis of the magnesium single crystal (Figure 3-7), ρ was not assigned negative values when computing the FLDs. Negative values for ρ would be equivalent to using the model to simulate something outside its calibration domain and prediction capabilities.

The slip and twinning systems considered in this work are listed in Table C-1 in Appendix C.

4.4.1. Effect of the shear strain outside the band ($D_{12}^{(1)}$)

The effect of shear strain ($D_{12}^{(1)}$) on the simulated FLDs was investigated. Figure 4-3 shows that neglecting or accounting for the shear strain ($D_{12}^{(1)}$) in the FLD computation in step 1 of the model for orientation A does not have any effect on the predicted formability. However, in step 1 for orientation B (Figure 4-4) as well as in step 2 for both orientations A and B (Figures 4-5 and 4-6, respectively), accounting for $D_{12}^{(1)}$ in the FLD computation results in improved formability prediction. This suggests that in simulating the FLD of magnesium single crystals using crystal plasticity and M-K analysis, neglecting the shear strain ($D_{12}^{(1)}$) results in a more conservative formability prediction.
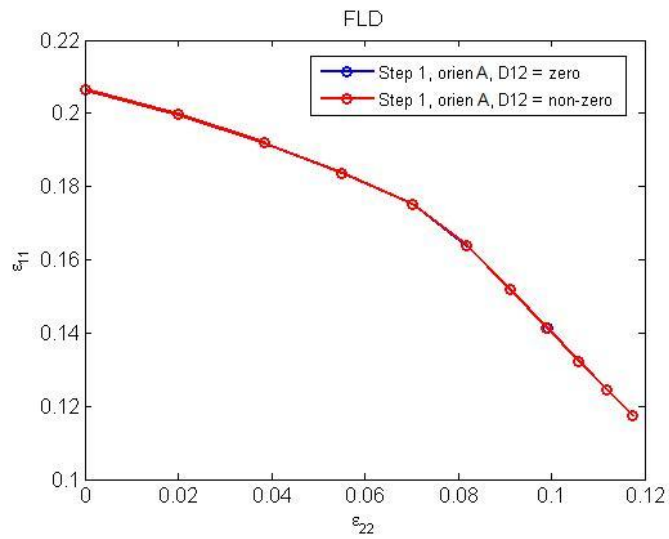
Figure 4-3 FLDs computed with step 1 of the CPCM for orientation A with $D_{12}^{(1)} = 0$ and $D_{12}^{(1)} \neq 0$
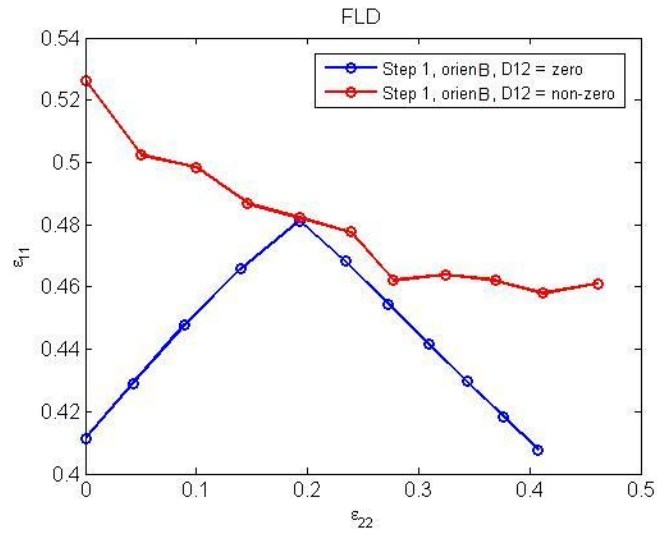

Figure 4-4 FLDs computed with step 1 of the CPCM for orientation B with $D_{12}^{(1)} = 0$ and $D_{12}^{(1)} \neq 0$
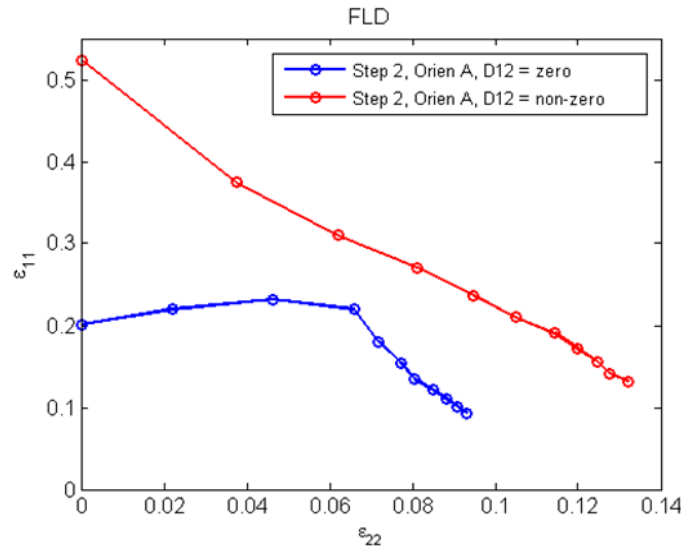
Figure 4-5 FLDs computed with step 2 of the CPCM for orientation A with $D_{12}^{(1)} = 0$ and $D_{12}^{(1)} \neq 0$
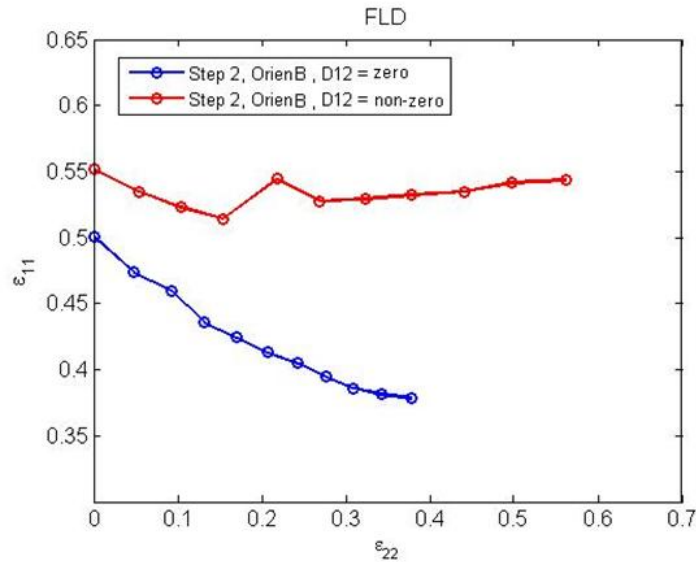

Figure 4-6 FLDs computed with step 2 of the CPCM for orientation B with $D_{12}^{(1)} = 0$ and $D_{12}^{(1)} \neq 0$

4.4.2. Effect of twinning on formability

Figure 4-7 shows the FLDs computed by steps 1 and 2 of the model for orientation A, where extension twinning systems have favourable orientation for activation. This figure shows that extension twinning systems improve the formability of the magnesium single crystal. The same conclusion was drawn by Lévesque et al. [29], as well as Neil and Agnew [33] for the AZ31 magnesium alloy (polycrystal with a rolling texture but at high temperature) which are in agreement with experimental results presented by Yukutake et al. [80] and Chino et al [81] at high temperature.
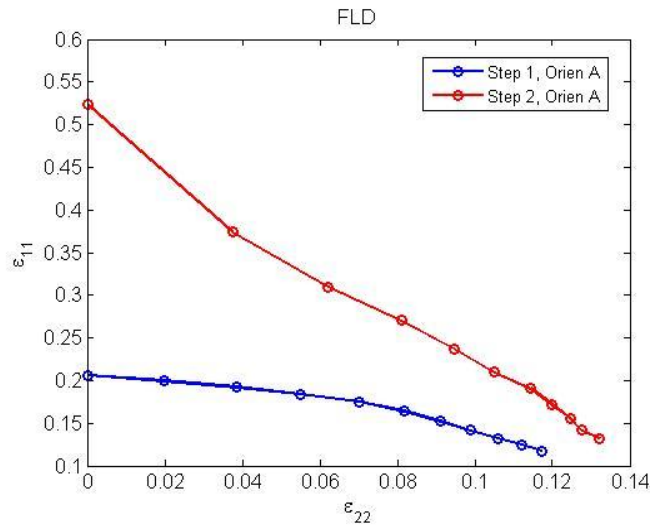
Figure 4-7 Comparing the FLDs computed with steps 1 and 2 of the CPCM for orientation A
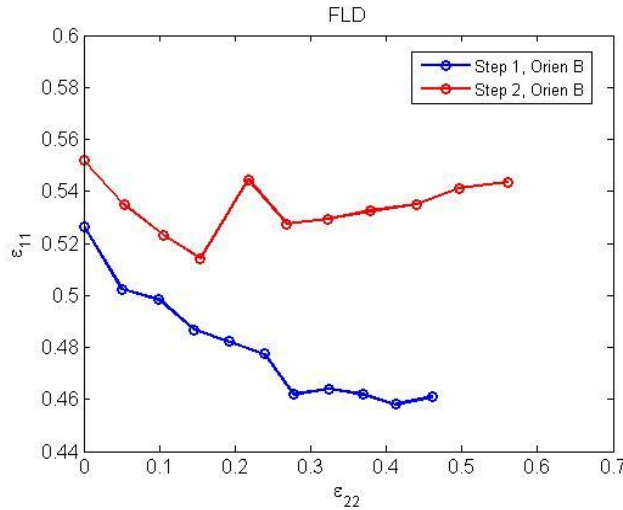

Figure 4-8 Comparing the FLDs computed with steps 1 and 2 of the CPCM for orientation B

Figure 4-8 presents the FLDs predicted by steps 1 and 2 of the model for orientation B where contraction twinning systems have favourable orientation for activation. Simulations show that similar to the extension twinning systems, contraction twinning systems improve the formability of the magnesium single crystal, as well.

Figure 4-9a presents the FLD computed by step 1 of the CPCM for orientation A and the shear strain on the pyramidal $\langle c+a \rangle$ slip systems. The FLD follows the trend of shear strain on the pyramidal $\langle c+a \rangle$ slip systems. Figure 4-9b shows the FLD computed by step 2 of the CPCM for orientation A, the shear strain on the pyramidal $\langle c+a \rangle$ slip systems, and the volume fraction of the extension twinned

regions. It is apparent that the activity of the extension twinning systems drastically changes the magnitude of the shear strain on the pyramidal $\langle c+a \rangle$ slip systems, but the FLD still follows the trend of shear strain on the pyramidal $\langle c+a \rangle$ slip systems. Furthermore, to check the validity of this conclusion with respect to the grain orientation, the crystal in orientation A (Figure 4-2a) was tilted individually around the X_2 and X_3 axes. It was found that up to the tilt angle of $\pm 7.5°$ around the X_2 and X_3 axes, the FLD still follows the trend of the shear strain on the pyramidal $\langle c+a \rangle$ slip systems, in both steps 1 and 2 of the CPCM in orientation A.
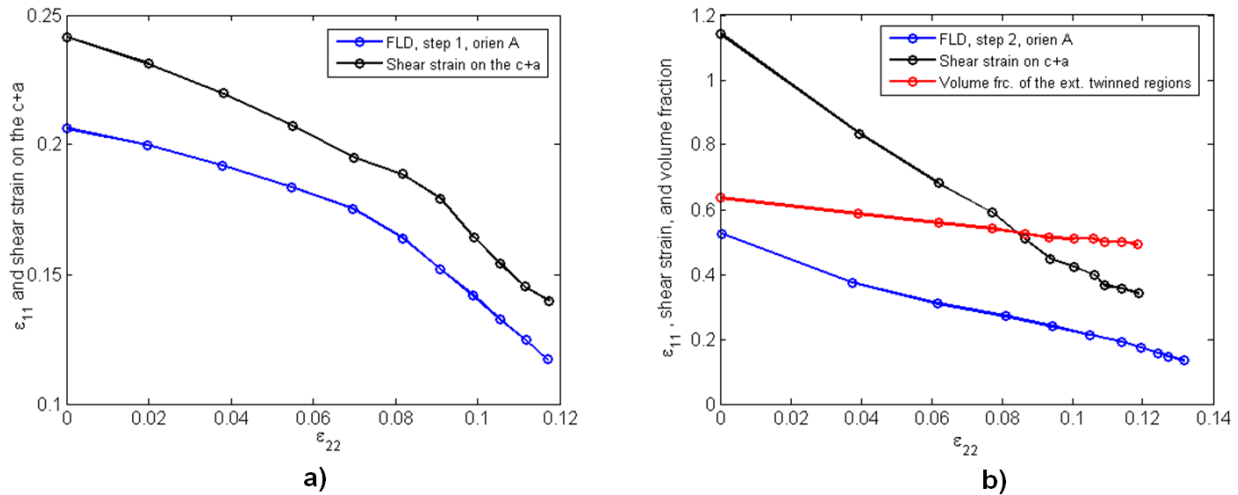

Figure 4-9 Comparing the break-down of shear corresponding to the FLDs computed with steps 1 and 2 for orientation A. a) shear strain on the slip systems, b) shear strain and volume fraction of the twinned regions

The FLD computed by step 1 of the CPCM for orientation B and the relative shear strain on the basal and pyramidal $\langle c+a \rangle$ slip systems are presented in Figure 4-10a. Predictions show that the FLD follows the trend of shear strain on the basal slip systems curve. Figure 4-10b shows the FLD computed by step 2 of the CPCM for orientation B, the shear strain on the basal and pyramidal $\langle c+a \rangle$ slip systems, and the volume fraction of the contraction twinned regions. It is apparent that the activity of the contraction twinning systems slightly changes the magnitude of the shear strain on the basal systems, but the FLD still follows the trend of shear strain on the basal slip systems. Furthermore, to check the validity of this conclusion with respect to the grain orientation, the crystal in orientation B (Figure 4-2b) was tilted individually around the X_1 and X_3 axes. Simulations show that up to the tilt angle of $\pm 5°$ around the X_1

and X_3 axes, the FLD still follows the shear strain on the basal slip systems, in both steps 1 and 2 of the CPCM in orientation B.

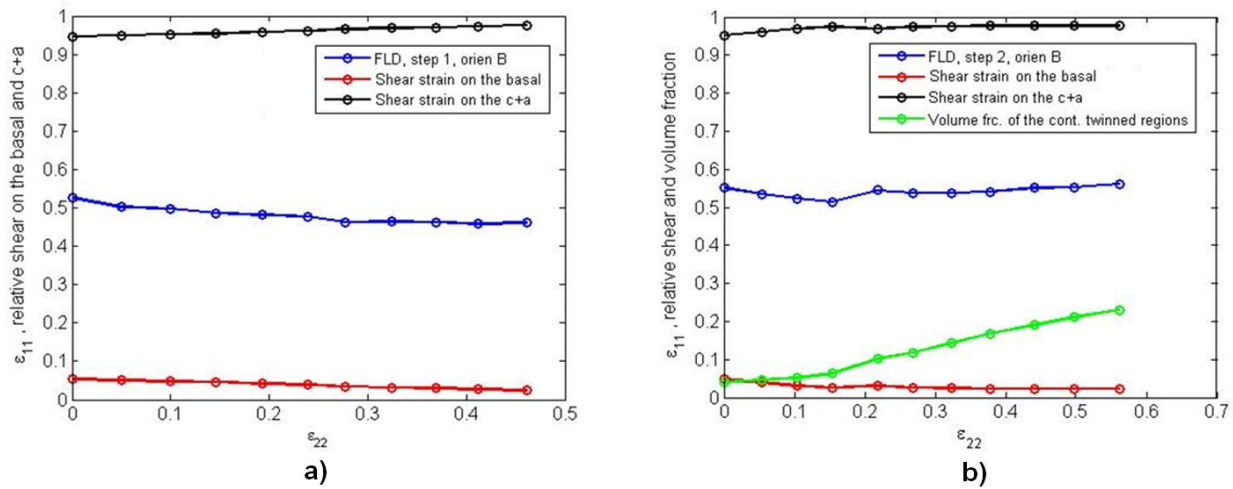a)   b)

Figure 4-10 Comparing the break-down of shear corresponding to the FLDs computed with steps 1 and 2 for orientation B. a) relative shear strain on the slip systems, b) relative shear strain and volume fraction of the twinned regions

4.4.3. Effect of rate sensitivity (*m*)

The effect of the strain rate sensitivity parameter (*m* in Equation (2-21) for primary slip systems, and in Equation (2-49) for primary twinning systems) on the FLDs was investigated in this subsection. The predicted FLDs by step 1 of the CPCM, for orientation A, corresponding to the *m* values (in Equation (2-21)) of 0.005, 0.02, and 0.05 are presented in Figure 4-11. Simulations show that an increase in the *m* value corresponds to an increase in formability.
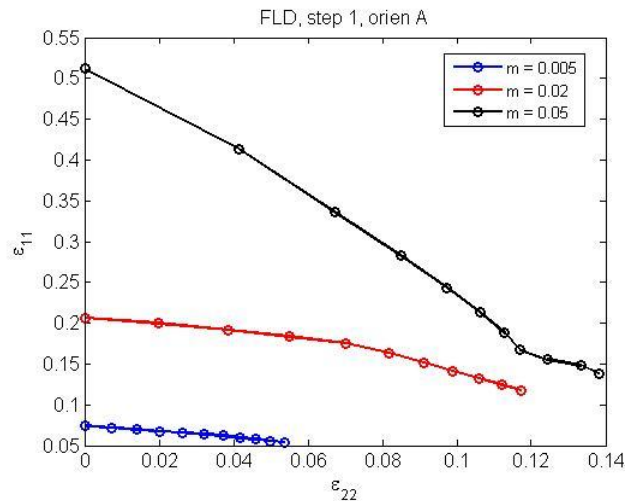

Figure 4-11 Effect of rate sensitivity parameter, *m*, on the FLDs in step 1 of the CPCM (orientation A)

86

Figure 4-12 shows the predicted FLDs by step 1 of the CPCM, for orientation B, corresponding to the *m* values (in Equation (2-21)) of 0.005, 0.02, and 0.05. Once again, increasing the *m* value results in improved formability.
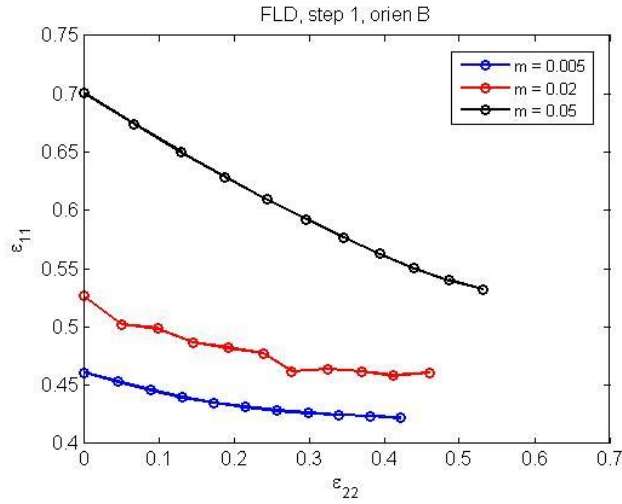

Figure 4-12. Effect of rate sensitivity parameter, *m*, on the FLDs in step 1 of the CPCM (orientation B)

Increasing the strain rate sensitivity parameter also leads to improved formability predictions by step 2 of the CPCM, for both orientations A and B (Figures 4-13 and 4-14).
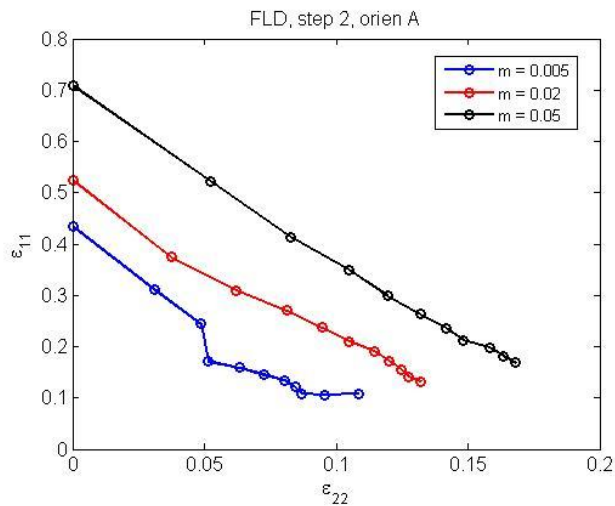

Figure 4-13 Effect of rate sensitivity parameter, *m*, on the FLDs in step 2 of the CPCM (orientation A)
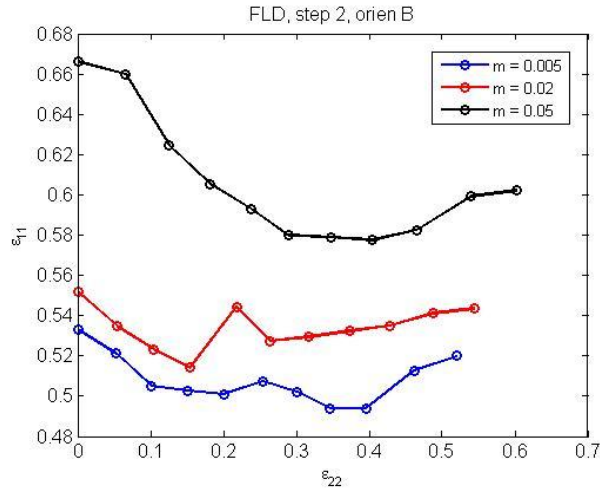
Figure 4-14 Effect of rate sensitivity parameter, *m*, on the FLDs in step 2 of the CPCM (orientation B)

Looking at the Equation (2-21), it is apparent that an increase in *m* corresponds to an increase in $\dot{\gamma}^{(\alpha p)}$ (because the $\left[\dfrac{\sigma^{(\alpha p)}}{g^{(\alpha p)}}\right]$ ratio is always a number less than one). This means that a material can take up more plastic deformation, and thus has more formability. A similar argument is made from Equation (2-49), where it shows that an increase in *m* corresponds to an increase in $\dot{f}^{(\beta p)}$. Therefore, the results in this subsection (an increase in *m* leads to improved formability in both steps of the model) are expected.

4.4.4. Effect of c/a ratio

One of the effects of alloying on magnesium is the ability to change the c/a ratio. The c/a ratio directly affects the plane normal and shear direction of slip and twinning systems (Equations (C-3) and (C-6), respectively). Thus, it changes the accumulated shear strain on the slip systems and volume fraction of the twinned regions. To assess this effect of alloying on magnesium, the sensitivity of FLDs with respect to the change in the c/a ratio was studied.

Figures 4-15 and 4-16 present the predicted FLDs by step 1 of the CPCM, for orientations A and B, corresponding to the c/a values of 1.6, 1.624, and 1.65. By increasing the c/a value, formability improves slightly in both orientations.
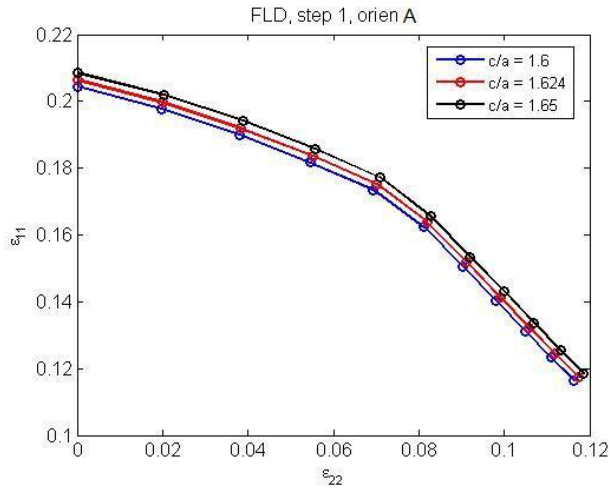
Figure 4-15 Effect of c/a ratio on the FLDs in step 1 of the CPCM (orientation A)

,
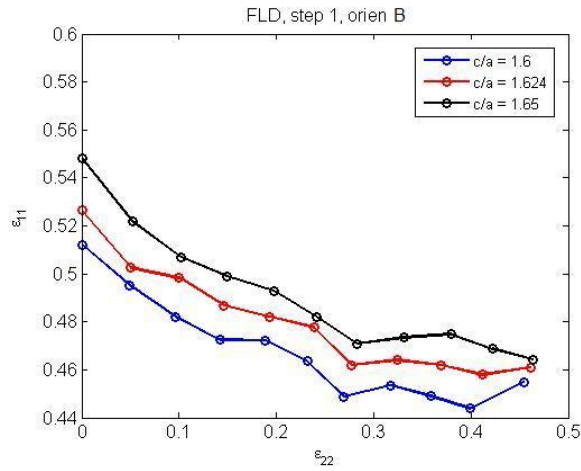
Figure 4-16 Effect of c/a ratio on the FLDs in step 1 of the CPCM (orientation B)
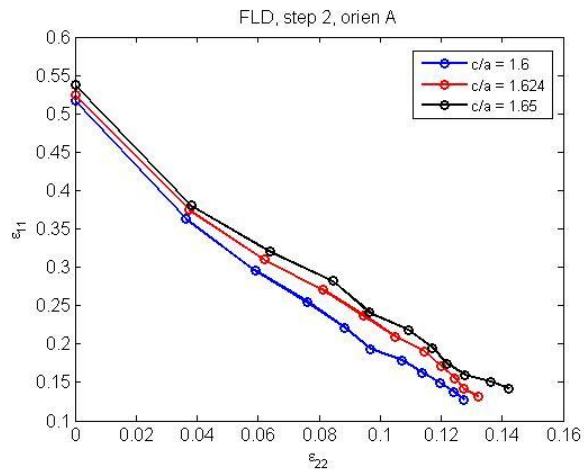
Figure 4-17 Effect of c/a ratio on the FLDs in step 2 of the CPCM (orientation A)
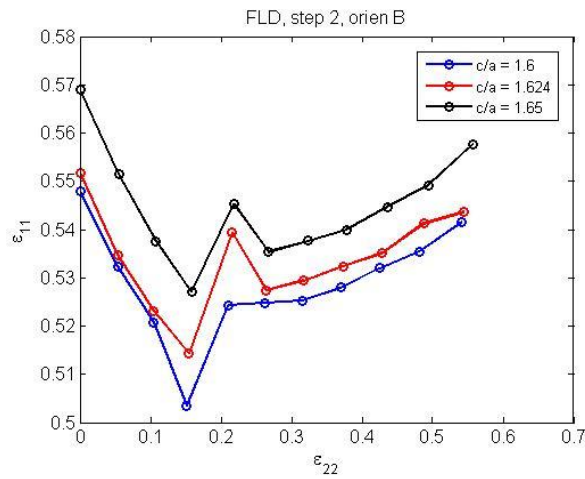
Figure 4-18 Effect of c/a ratio on the FLDs in step 2 of the CPCM (orientation B)

Figures 4-17 and 4-18 present the predicted FLDs by step 2 of the CPCM for orientations A and B, corresponding to the c/a values of 1.6, 1.624, and 1.65. Once again, by increasing the c/a value, formability improves slightly.

Besides changing the c/a ratio, alloying changes the CRSS values and deformation characteristics due to the solute effect. While the model predicts that change in the c/a ratio has a small effect on the FLD, changes in the other properties may have significant effects.

Chapter 5

Conclusions and future research

5.1 Conclusions

A new rate-dependent elastic-viscoplastic Crystal Plasticity Constitutive Model (CPCM) for magnesium single crystals was proposed. The model accounts for the plastic deformation mechanisms of primary, secondary, and tertiary slip systems, as well as primary and secondary twinning systems observed in magnesium at room temperature. The model tracks the texture evolution in the parent, primary and secondary twinned regions. Separate resistance evolution functions for the primary, secondary, and tertiary slip systems, as well as the primary and secondary twinning systems were considered in the formulation.

The major goal of this research was to investigate the contributions of various plastic deformation mechanisms in the macroscopic plastic deformation of a single crystal of magnesium. Therefore, using the available experimental data on plastic deformation of pure magnesium single crystals in literature, the parameters of a classic and common resistance evolution function for the primary slip and twinning systems were calibrated for the proposed CPCM. Simulations with the proposed CPCM (though due to the lack of quantitative experimental data certain assumptions were made, e.g. self-hardening equals the latent hardening effect) clearly indicated that accounting for the kinematics of various plastic deformation mechanisms is very important. For instance, depending upon loading path, neglecting secondary slip and twinning systems can lead to erroneous results while simulating plastic deformation of magnesium alloys

by crystal plasticity modelling approach. It is concluded that to model the plastic deformation in magnesium alloys accounting for all not just a few of the plastic deformation mechanisms is necessary. Upon availability of more quantitative experimental data it is possible to precisely account for the latent hardening effect in the proposed CPCM through the resistance evolution functions for the various slip systems.

The proposed CPCM together with the M–K approach were used to simulate the FLDs for a sheet of magnesium single crystal. The FLDs were simulated under two conditions: a) the plastic deformation mechanisms are primary slip systems alone, and b) the plastic deformation mechanisms are primary slip and twinning systems. Based on the simulation results obtained with the steps 1 and 2 of the CPCM for both crystal orientations, it was concluded that neglecting the shear strain in the formulation results in a more conservative formability prediction. Also, both extension and contraction twinning systems improve formability. Finally, increasing the value of rate sensitivity parameter (m) improves the formability, and the same is valid for the c/a ratio. These numerical studies help in understanding the sensitivity of the model on its key parameter values.

5.2 Future research

The following tasks are suggested for future research.

- Development and calibration of the resistance evolution functions for the secondary slip and twinning systems for the proposed CPCM is recommended. This will be possible if the contributions of these plastic deformation mechanisms in the macroscopic plastic deformation of magnesium in a few loading paths are experimentally available. After developing and calibrating these resistance evolution functions using the required experimental data, the contributions of these deformation mechanisms in the macroscopic plastic deformation of magnesium in any other loading path can be identified. Also, their effects on the formability through simulating the FLDs can be assessed.

- In terms of number of equations and computational time, the proposed CPCM is probably the least complex one for modelling the plastic deformation in magnesium. It assumes the same deformation field over the parent and twinned regions, and the locations of the parent and twinned regions in the grain are not determined. Upon availability of more experimental data, it is logical to develop more accurate CPCM along with finite element implementation where the matrix, primary twinned, and secondary twinned regions are included in different elements. This way, different deformation fields are considered in the parent and twinned regions, and the

locations of the parent and twinned regions in the grain can be determined. In order to develop such a model, quantified metallurgical information on the twin nucleation sites and their growth pattern is necessary. Clearly, the number of equations, computational time, and complexity of such a model will exceed that of the proposed model in this thesis.

- The latent hardening effect for various slip systems in the model is the other phenomenon that has to be precisely accounted for. Upon availability of experimental data, including this effect is quite straightforward.

- The proposed CPCM accounts for the intragranular plastic deformation mechanisms in magnesium single crystals alone. Employing this model to simulate the plastic deformation in magnesium polycrystals could require an additional model accounting for the Grain Boundary (GB) sliding effect (i.e. intergranular plastic deformation mechanism, reported by Hauser et al. [28]). Development of such a model for the GB effect is a feasible task once more quantitative experimental data on plastic deformation of magnesium bi-crystals becomes available.

Appendix A.

Calculation of plastic work in the parent and primary twinned regions

Plastic work is calculated from the following general relationship:

$$w^P = \int_0^t \sigma : D^P dt \tag{A-1}$$

where $\sigma : D^P = \sigma_{ji} D_{ij}^P$ is a scalar.

The plastic work in the matrix is calculated by the following values for σ and D^P:

$$\sigma = \sigma^{mat} \tag{A-2}$$

$$D^P = \sum_{\alpha p} P^{(\alpha p)} \dot{\gamma}^{(\alpha p)} \tag{A-3}$$

The plastic work in a given primary twinned region resulting from the activity of secondary slip systems inside of it, is calculated by the following values for σ and D^P:

$$\sigma = \sigma^{\beta p} \tag{A-4}$$

$$D^P = \left(\sum_{\alpha s} P^{(\alpha s)} \dot{\gamma}^{(\alpha s)} \right) f^{(\beta p)} \tag{A-5}$$

From Equations (A-3) and (A-5), it is apparent that because D^P is a function of activity of slip systems, the plastic work is a good indicator to describe the activity of slip systems.

Appendix B.

Total possible number of state variables for shear strain (slip systems), volume fraction of twinned regions (twinning systems), and Cauchy stress

The total possible number of state variables associated with the shear strain on the slip systems, the volume fraction of the twinned regions, and the stress in the parent and twinned regions are presented in Table B-1. In this thesis the secondary twinning systems considered are the extension ones that form in the primary contraction twinned regions (this is the common secondary twinning that happens in magnesium alloys). Therefore, the maximum number is 6x6=36.

	Shear strain on the slip systems	Volume fraction of the twinned regions	Cauchy stress
Parent	12	0	6
Prim. ext. twins	6x12	6	6x6
Prim. cont. twins	6x12	6	6x6
Secon. ext. twins	6x6x12	6x6	6x6x6
Sub total	**588**	**48**	**294**
Total	**588+48+294 = 930**		

Table B-1 Total possible number of state variables for shear strain, volume fraction of the twinned regions, and Cauchy stress in the model

Appendix C.

Conversion of the Miller-Bravais coordinate system into an orthonormal

The slip and twinning systems listed in Table C-1[2] are considered in the proposed Crystal Plasticity Constitutive Model (CPCM). The four-index Miller-Bravais coordinate system $\{a_1, a_2, a_3, c\}$ is not convenient for numerical modelling, since the coordinates in this system are not linearly independent in three-dimensional space. Therefore, an orthonormal coordinate system $\{e_1, e_2, e_3\}$ as shown in Figure C-1 is constructed.

The following equations relate the Miller-Bravais indices to the orthonormal indices for a plane normal:

$$e_1 = \frac{1}{\sqrt{3}}\left(2a_1 + a_2\right) \tag{C-1}$$

$$e_2 = a_2 \tag{C-2}$$

$$e_3 = \frac{a_4}{\left(\dfrac{c}{a}\right)} \tag{C-3}$$

---

[2] Pyramidal $\langle a \rangle$ slip systems have been reported to be almost non-active at room temperature [82], and therefore are not accounted for.

Slip Systems	Basal $\langle a \rangle$ slip systems	$\{0001\} < 1\bar{2}10 >$
	Prismatic $\langle a \rangle$ slip systems	$\{10\bar{1}0\} < 1\bar{2}10 >$
	Pyramidal $\langle c+a \rangle$ slip systems	$\{1\bar{2}12\} < 1\bar{2}1\bar{3} >$
Twinning Systems	Extension twinning systems	$\{10\bar{1}2\} < \bar{1}011 >$
	Contraction twinning systems	$\{1\bar{1}01\} < \bar{1}102 >$

Table C-1 The slip and twinning systems considered in the simulation
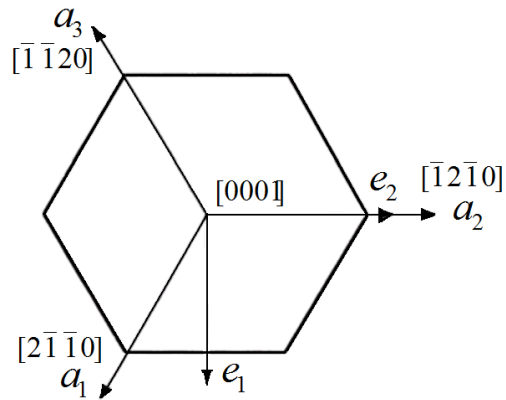

Figure C-1 Miller-Bravais indices and orthonormal indices

The following equations relate the Miller-Bravais indices to the orthonormal indices for a shear direction:

$$e_1 = \frac{\sqrt{3}}{2}(a_1 - a_3) \tag{C-4}$$

$$e_2 = \frac{3}{2}a_2 \tag{C-5}$$

$$e_3 = a_4 \left(\frac{c}{a} \right) \tag{C-6}$$

Orthonormal indices above should be normalized, as well.

Appendix D.

Metallurgical information about magnesium

In magnesium, the specific shear strain associated with the contraction twinning systems is [3]:

$$\gamma_{cont.} = \frac{\left(\dfrac{c}{a}\right)}{\sqrt{3}} - \frac{\left(\dfrac{9}{4}\right)}{\sqrt{3}\left(\dfrac{c}{a}\right)} = 0.1377 \tag{D-1}$$

The specific shear strain associated with the extension twinning systems is [3]:

$$\gamma_{ext.} = \frac{\left(\dfrac{c}{a}\right)}{\sqrt{3}} - \frac{\sqrt{3}}{\left(\dfrac{c}{a}\right)} = 0.1289 \tag{D-2}$$

The elasticity modulus for a single crystal of an HCP metal, with respect to the orthonormal coordinate system shown in Figure D-1, is as follows [3]:

$$C = \begin{bmatrix} C_{11} & C_{12} & C_{13} & 0 & 0 & 0 \\ C_{12} & C_{11} & C_{13} & 0 & 0 & 0 \\ C_{13} & C_{13} & C_{33} & 0 & 0 & 0 \\ 0 & 0 & 0 & C_{44} & 0 & 0 \\ 0 & 0 & 0 & 0 & C_{44} & 0 \\ 0 & 0 & 0 & 0 & 0 & C_{66} \end{bmatrix}$$ (D-3)

with:

$$C_{11} = \frac{\left(s_{33}s_{11} - s_{13}^2\right)}{\left(s_{11} - s_{12}\right)\left(s_{33}s_{11} + s_{33}s_{12} - 2s_{13}^2\right)}$$ (D-4)

$$C_{12} = \frac{-\left(s_{33}s_{12} - s_{13}^2\right)}{\left(s_{11} - s_{12}\right)\left(s_{33}s_{11} + s_{33}s_{12} - 2s_{13}^2\right)}$$ (D-5)

$$C_{13} = \frac{-s_{13}}{\left(s_{33}s_{11} + s_{33}s_{12} - 2s_{13}^2\right)}$$ (D-6)

$$C_{33} = \frac{\left(s_{11} + s_{12}\right)}{\left(s_{33}s_{11} + s_{33}s_{12} - 2s_{13}^2\right)}$$ (D-7)

$$C_{44} = \frac{1}{s_{44}}$$ (D-8)

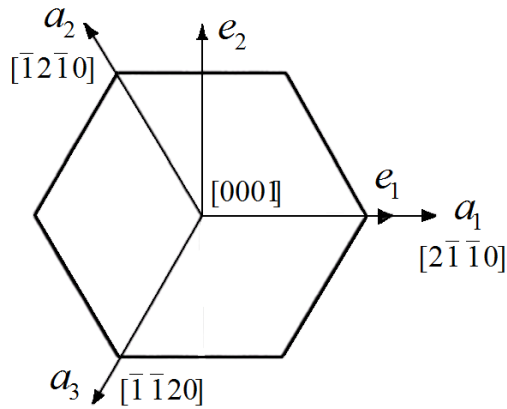$$C_{66} = \frac{1}{2\left(s_{11} - s_{12}\right)}$$ (D-9)

Figure D-1 The orthonormal coordinate system corresponding to the elasticity modulus in Equation (D-3)

For magnesium, the values of the parameters are as follows [83]:

$$s_{11} = 2.210 \times 10^{-9} \, Pa^{-1} \tag{D-10}$$

$$s_{12} = -0.770 \times 10^{-9} \, Pa^{-1} \tag{D-11}$$

$$s_{13} = -0.490 \times 10^{-9} \, Pa^{-1} \tag{D-12}$$

$$s_{33} = 1.970 \times 10^{-9} \, Pa^{-1} \tag{D-13}$$

$$s_{44} = 6.030 \times 10^{-9} \, Pa^{-1} \tag{D-14}$$

The angle between the basal planes in the parent and a primary extension twinned region is [18]:

$$2\tan^{-1}\left(\frac{\left(\frac{c}{a}\right)}{\sqrt{3}}\right) = 86° \tag{D-15}$$

The angle between the basal planes in the parent and a primary contraction twinned region is [18]:

$$180 - 2\tan^{-1}\left(\frac{\left(\frac{c}{a}\right)}{\left(\frac{\sqrt{3}}{2}\right)}\right) = 56° \tag{D-16}$$

The angle between the basal planes in the parent and a secondary extension twinned region is [18]:

$$2\tan^{-1}\left(\frac{\left(\frac{c}{a}\right)}{\left(\frac{\sqrt{3}}{2}\right)}\right) - 2\tan^{-1}\left(\frac{\left(\frac{c}{a}\right)}{\sqrt{3}}\right) = 38° \tag{D-17}$$

References

[1] Bhattacharya, B., "Plastic deformation behavior of pure magnesium in the temperature range 4.2 K - 300 K", PhD Dissertation, 2006, McMaster University, Ontario, Canada.

[2] Partridge, P.G., "Crystallography and deformation modes of hexagonal closepacked metals", Metallurgical Review, Vol. 12, 1967, pp. 169-194.

[3] Hosford, W.F., "The mechanics of crystals and texture polycrystals", 1993, Oxford University Press.

[4] Christian, J.W., Mahajan, S., "Deformation twinning", Progress in Materials Science, Vol. 39, 1995, pp. 1–157.

[5] Niewczas, M., "Lattice correspondence during twinning in hexagonal close-packed crystals", Acta Materialia, Vol. 58, 2010, 5848-5857.

[6] Christian, J.W., "The theory of transformations of metals and alloys", 1965, Pergamon Press, UK.

[7] Von Mises, R., "Plastic deformation of crystals". Zeitschrift fur Angewandte Mathematik und Mechanik, Vol. 8, 1928, pp. 161–185.

[8] Taylor, G.I., "Plastic strain in metals", Institute of Metals, Vol. 62, 1938, pp. 307-324.

[9] Agnew, S.R., Yoo, M.H., Tomé, C.N., "Application of texture simulation to understanding mechanical behavior of Mg and solid solution alloys containing Li or Y", 2001, Acta Materialia., Vol. 49, pp. 4277-4289.

[10] Yoo, M.H., Morris, J.R., Ho, K.M., Agnew, S.R., "Nonbasal deformation modes of HCP metals and alloys: role of dislocation source and mobility", Metallurgical and Materials Transactions A: Physical Metallurgy and Materials Science, Vol. 33, 2002, pp. 813-822.

[11] Agnew, S.R., Duygulu, Ö., "Plastic anisotropy and the role of non-basal slip in magnesium alloy AZ31B", International Journal of Plasticity, Vol. 21, 2005, pp. 1161-1193.

[12] Mordike, B.L., Ebert, T., "Magnesium properties - applications – potential", Materials Science and Engineering A, Vol. 302, 2001, pp. 37-45.

[13] Kaiser, F., Bohlen, J., Letzig, D., Kainer, K.U., Styczynski, A., Hartig, C., "Influence of Rolling Conditions on the Microstructure and Mechanical Properties of Magnesium Sheet AZ31", 2003, Advanced Engineering Materials, Vol. 5, pp. 891–896

[14] Graff, S., Brocks, W., Steglich, D., "Yielding of magnesium: From single crystal to polycrystalline aggregates", International Journal of Plasticity, Vol. 23, 2007, pp. 1957-1978.

[15] Wonsiewicz, B.C., Backofen, W.A., "Plasticity of magnesium crystals", Transactions of the Metallurgical Society of AIME., Vol. 239, 1967, pp. 1422-1431.

[16] Kelley, E.W., Hosford, W.F., "Plain-strain compression of magnesium and magnesium alloy crystals", Metallurgical Society of American Institute of Mining, Metallurgical and Petroleum Engineers – Transactions, Vol. 242, 1968, pp. 5-13.

[17] Jiang, L., Jonas, J.J., Luo, A.A., Sachdev, A.K., Godet, S., "Twinning-induced softening in polycrystalline AM30 Mg alloy at moderate temperatures", Scripta Materialia, Vol. 54, 2006, pp. 771-775.

[18] Jiang, L., Jonas, J.J., Mishra, R.K., Luo, A.A., Sachdev, A.K., Godet, S., "Twinning and texture development in two Mg alloys subjected to loading along three different strain paths", Acta Materialia, Vol. 55, 2007, pp. 3899-3910.

[19] Barnett, M.R., Keshavarz, Z., Beer, A.G., Ma, X., "Non-Schmid behaviour during secondary twinning in a polycrystalline magnesium alloy", Acta Materialia, Vol. 56 , 2008, pp. 5-15.

[20] Van Houtte, P., "Simulation of the rolling and shear texture of brass by the Taylor theory adapted for mechanical twinning", Acta Metallurgica, Vol. 26, 1978, pp. 591-604.

[21] Tomé, C.N., Lebensohn, R.A., Kocks, U.F., "A model for texture development dominated by deformation twinning: Application to zirconium alloys", Acta Metallurgica, Vol. 39, 1991, pp. 2667-2680.

[22] Kalidindi, S.R., "Incorporation of deformation twinning in crystal plasticity models", Journal of the Mechanics and Physics of Solids, Vol. 46, 1998, pp. 267-271.

[23] Kalidindi, S.R., Bronkhorst, C.A., Anand, L., "Crystallographic texture evolution in bulk deformation processing of FCC metals", Journal of the Mechanics and Physics of Solids, Vol. 40, 1992, pp. 537-569.

[24] Salem, A.A., Kalidindi, S.R., Semiatin, S.L., "Strain hardening due to deformation twinning in α-titanium: Constitutive relations and crystal-plasticity modeling", Acta Materialia, Vol. 53, 2005, pp. 3495-3502.

[25] Wu, X., Kalidindi, S.R., Necker, C., Salem, A.A., "Prediction of crystallographic texture evolution and anisotropic stress–strain curves during large plastic strains in high purity α-titanium using a Taylor-type crystal plasticity model", Acta Materialia, Vol. 55, 2007, pp. 423-432.

[26] Staroselsky, A., Anand, L., "A constitutive model for hcp materials deforming by slip and twinning: application to magnesium alloy AZ31B", International Journal of Plasticity, Vol. 19, 2003, pp. 1843-1864.

[27] ABAQUS Reference Manuals, 2001, Pawtucket, R.I.

[28] Hauser, F.E., Starr, C.D., Tietz, L., Dorn, J.E., "Deformation mechanisms in polycrystalline aggregates of magnesium", American Society for Metals, 1954, Preprints.

[29] Lévesque, J., Inal, K., Neale, K.W., Mishra, R.K., "Numerical modeling of formability of extruded magnesium alloy tubes", International Journal of Plasticity, Vol. 26, 2010, pp. 65-83.

[30] Peirce, D., Asaro, R.J., Needleman, A., "Material rate dependence and localized deformation in crystalline solids", Acta Metallurgica, Vol. 31, 1983, pp. 1951-1976.

[31] Lebensohn, R.A., Tomé, C.N., "A self-consistent anisotropic approach for the simulation of plastic deformation and texture development of polycrystals: Application to zirconium alloys", Acta Metallurgica, Vol. 41, 1993, pp. 2611-2624.

[32] Jain, A., Agnew, S.R., "Modeling the temperature dependent effect of twinning on the behavior of magnesium alloy AZ31B sheet", Materials Science and Engineering A, Vol. 462, 2007, pp. 29-36.

[33] Neil, C.J., Agnew, S.R., "Crystal plasticity-based forming limit prediction for non-cubic metals: Application to Mg alloy AZ31B", International Journal of Plasticity, Vol. 25, 2009, pp. 379-398.

[34] Proust, G., Tomé, C.N., Kaschner, G.C., "Modeling texture, twinning and hardening evolution during deformation of hexagonal materials", Acta Materialia, Vol. 55, 2007, pp. 2137-2148.

[35] Proust, G., Tomé, C.N., Jain, A., Agnew, S.R., "Modeling the effect of twinning and detwinning during strain-path changes of magnesium alloy AZ31", International Journal of Plasticity, Vol. 25, 2009, pp. 861-880.

[36] Signorelli, J.W., Bertinetti, M.A., Turner, P.A., "Predictions of forming limit diagrams using a rate-dependent polycrystal self-consistent plasticity model", International Journal of Plasticity, Vol. 25, 2009, pp. 1-25.

[37] Wang, H., Wu, P.D., Tomé, C.N., Huang, Y., "A finite strain elastic–viscoplastic self-consistent model for polycrystalline materials", Journal of the Mechanics and Physics of Solids, Vol. 58, 2010, pp. 594-612.

[38] Hall, E.O., "The deformation and ageing of mild steel III. Discussion of results", Proceedings of the Physical Society B, Vol. 64, 1951, pp. 747-753.

[39] Petch, N.J., "Cleavage strength of polycrystals", Iron and Steel Institute, Vol. 174, 1953, pp. 25-28.

[40] Basinski, Z.S., Szczerba, M.S., Niewczas, M., Embury, J.D., Basinski, S.J., "The transformation of slip dislocations during twinning of copper-aluminum alloy crystals", Revue de Metallurgie, vol. 94, 1997, pp. 1037-1043.

[41] Serra, A., Bacon, D.J., "Computer simulation of screw dislocation interactions with twin boundaries in hcp metals", Acta Metallurgica, Vol. 43, 1995, pp. 4465–4481.

[42] Serra, A., Bacon, D.J., Pond, R.C., "Twins as barriers to basal slip in hexagonal-close-packed metals", Metallurgical and Materials Transactions A, Vol. 33, 2002, pp. 809–812.

[43] Lebensohn, R.A., Dawson, P.R., Kern, H.M., Wenk, H-R, "Heterogeneous deformation and texture development in halite polycrystals: comparison of different modeling approaches and experimental data", Tectonophysics, Vol. 370, 2003, pp. 287-311.

[44] Niewczas, M., Saada, G., "Twinning nucleation in Cu-8 at.% Al single crystals", Philosophical Magazine A, Vol. 82, 2002, pp. 167-191.

[45] Beyerlein, I.J., Capolungo, L., Marshall, P.E., McCabe, R.J., Tomé, C.N., "Statistical analyses of deformation twinning in magnesium", Philosophical Magazine A, Vol. 90, 2010, 2161-2190.

[46] Beyerlein, I.J., Tomé, C.N., "A probabilistic twin nucleation model for HCP polycrystalline metals", Proceedings of the Royal Society of London A, 2010, doi:10.1098/rspa.2009.0661.

[47] Wang, J., Beyerlein, I.J., Tomé, C.N., "An atomic and probabilistic perspective on twin nucleation in Mg", Scripta Materialia, 2010, doi:10.1016/j.scriptamat.2010.01.047.

[48] Pan, J., Rice, J.R., "Rate sensitivity of plastic flow and implications for yield surface vertices", International Journal of Solids and Structures, Vol. 19, 1983, pp. 973-987.

[49] Hutchinson, J.W., "Bounds and self-consistent estimates for creep of polycrystalline materials", Proceedings of the Royal Society of London A, Vol. 348, 1976, pp. 101-127.

[50] Niewczas, M., "Chapter 75: Dislocations and Twinning in Face Centred Cubic Crystals", Dislocations in Solids, Vol. 13, 2007, pp. 263-364.

[51] Chin, G.Y., Thurston, R.N., Nesbitt, E.A., "Finite plastic deformation due to crystallographic slip", Metallurgical Society of American Institute of Mining, Metallurgical and Petroleum Engineers -- Transactions, Vol. 236, 1966, pp. 69-78.

[52] Kelly, A., Groves, G.W., "Crystallography and crystal defects", 1970, Addison Wesley, USA.

[53] Peirce, D., Asaro, R.J., Needleman, A., "An analysis of nonuniform and localized deformation in ductile single crystals", Acta Metallurgica, Vol. 30, 1982, pp. 1087-1119.

[54] Ling, X., Horstemeyer, M.F., Potirniche, G.P., "On the numerical implementation of 3D rate-dependent single crystal plasticity formulations", International Journal for Numerical Methods in Engineering, Vol. 63, 2005, pp. 548-568.

[55] Li, H.W., Yang, H., Sun, Z.C., "A robust integration algorithm for implementing rate dependent crystal plasticity into explicit finite element method", International Journal of Plasticity, Vol. 24, 2008, pp. 267-288.

[56] Raphanel, J.L., Ravichandran, G., Leroy, Y.M., "Three-dimensional rate-dependent crystal plasticity based on Runge-Kutta algorithms for update and consistent linearization", International Journal of Solids and Structures, Vol. 41, 2004, pp. 5995-6021.

[57] Kuchnicki, S.N., Cuitino, A.M., Radovitzky, R.A., "Efficient and robust constitutive integrators for single-crystal plasticity modeling", International Journal of Plasticity, Vol. 22, 2006, pp. 1988-2011.

[58] Rossiter, J., Brahme, A., Simha, C.H.M., Inal, K., Mishra, R., "A new crystal plasticity scheme for explicit time integration codes to simulate deformation in 3D microstructures: Effects of strain path, strain rate and thermal softening on localized deformation in the aluminum alloy 5754 during simple shear", International Journal of Plasticity, 2010, In press.

[59] Bunge, H.J., "Texture analysis in materials science: mathematical methods", 1982, Butterworth, London.

[60] Simo, J.C., Hughes, T.J.R., "Computational inelasticity", 1998, Springer, New York.

[61] Bakarian, P.W., Mathewson, C.H., "Slip and twinning in magnesium single crystals at elevated temperatures", 1943, American Institute of Mining and Metallurgical Engineers - Technical Publications - Metals Technology, Vol. 152, 28p.

[62] Reed-Hill, R.E., Robertson, W.D., "Deformation of magnesium single crystals by nonbasal slip", Journal of Metals, Vol. 9, 1957b, pp. 496–502.

[63] Reed-Hill, R.E., Robertson, W.D., "Additional modes of deformation twinning in magnesium", Acta Metallurgica, Vol. 5, 1957a, pp. 717-727.

[64] Choi, S-H, Kim, D.H., Park, S.S., You, B.S., "Simulation of stress concentration in Mg alloys using the crystal plasticity finite element method", Acta Materialia, Vol. 58, 2010, 320-329.

[65] Choi, S-H, Kim, D.H., Lee, H.W., Shin, E.J., "Simulation of texture evolution and macroscopic properties in Mg alloys using the crystal plasticity finite element method", Materials Science and Engineering A, Vol. 527, 2010, 1151-1159.

[66] Keeler, S.P., "Plastic instability and fracture in sheets stretched over rigid punches", Ph.D Dissertation, 1961, Massachusetts Institute of Technology, Cambridge, MA.

[67] Dudzinski, D., Molinari, A., "Perturbation analysis of thermoviscoplastic instabilities in biaxial loading", International Journal of Solids and Structures, Vol. 27, 1991, pp. 601-628.

[68] Tóth, L.S., Dudzinski, D., Molinari, A., "Forming limit predictions with the perturbation method using stress potential functions of polycrystal viscoplasticity", International Journal of Mechanical Sciences, Vol. 38, 1996a, pp. 805-824.

[69] Marciniak, Z., Kuczynski, K., "Limit strains in processes of stretch-forming sheet metal", International Journal of Mechanical Sciences, Vol. 9, 1967, pp. 609–620.

[70] Wu, P.D., Neale, K.W., van der Giessen, E., Jain, M., Makinde, A., MacEwen, S.R., "Crystal plasticity forming limit diagram analysis of rolled aluminum sheet", Metallurgical and Materials Transactions A: Physical Metallurgy and Materials Science, Vol. 29A, 1998, pp. 527–535.

[71] Inal, K., Neale, K.W., Aboutajeddine, A., "Forming limit comparisons for FCC and BCC sheets", International Journal of Plasticity, Vol. 21, 2005, pp. 1255-1266.

[72] Hutchinson, J.W., Neale, K.W., "Sheet necking. II. Time independent behavior. III. Strain-rate effects", In: Koistinen, K.P., Wang, N-M. (Eds.), Mechanics of Sheet Metal Forming, 2002, Plenum, Ney York, NY, 1978, pp. 127–153 and pp. 269–285.

[73] Bassani, J.L., Hutchinson, J.W., Neale, K.W., "On the Prediction of Necking in Anisotropic Sheets in Metal Forming Plasticity", 1979, edited by Lippmann, H. Springer-Verlag.

[74] Stören, S., Rice, J. R., "Localized necking in thin sheets", Journal of the Mechanics and Physics of Solids, Vol. 23, 1975, pp. 421-441.

[75] Tóth, L.S., Hirsch, J., Van Houtte, P., "On the role of texture development in the forming limits of sheet metals", International Journal of Mechanical Scieneces, Vol. 38, 1996b, pp. 1117-1126.

[76] Van Houtte, P., Tóth, L.S., Proc. Asia-Pacific Symposium on Advances in Engineering Plasticity and its Application. W. B. Lee (Ed.), 15-17 December, 1992, Hong Kong. Elsevier Science, Amsterdam, 1993, p. 1013.

[77] Wu, P.D., Neale, K.W., Van der Giessen, E., "On crystal plasticity FLD analysis", Proceedings of the Royal Society of London, Vol. 453, 1997, pp. 1831–1848.

[78] Lebensohn, R.A., Tomé, C.N., "A self-consistent anisotropic approach for the simulation of plastic deformation and texture development of polycrystals: application to zirconium alloys", Acta Metallurgica, Vol. 41, 1993, pp. 2611–2624.

[79] Kuroda, M., Tvergaard, V., "Forming limit diagrams for anisotropic metal sheets with different yield criteria", International Journal of Solids and Structures, Vol. 37, 2000, pp. 5037-5059.

[80] Yukutake, E., Kaneko, J., Sugamata, M., "Anisotropy and non-uniformity in plastic behavior of AZ31 magnesium alloy plates", Materials Transactions, Vol. 44, 2003, pp. 452-457.

[81] Chino, Y., Lee, J-S., Kensuke, S., Kamiya, A., Mamoru, M., "Press formability of a rolled AZ31 Mg alloy sheet with controlled texture", 2006, Materials Letters, Vol. 60, pp. 173-176.

[82] Reed-Hill, R.E., Robertson, W.D., "Pyramidal slip in magnesium", Metallurgical Society of American Institute of Mining, Metallurgical and Petroleum Engineers - Transactions, Vol. 221, 1958, pp. 256–259.

[83] Simmons, G., Wang, H., "Single crystal elastic constants and calculated aggregate properties", 1971, The M.I.T. Press, Cambridge.